Ph.D. Thesis

Chemically Twisted Superlattices of Two-dimensional Assemblies of Copper Nanoclusters

Submitted by

Priya Das

Under the Supervision of

Prof. Arun Chattopadhyay

Department of Chemistry

Indian Institute of Technology Guwahati

Guwahati-781039, Assam, India

Chemically Twisted Superlattices of Two-dimensional Assemblies of Copper Nanoclusters

A thesis submitted by

Priya Das

Roll No. 186122026

to

Indian Institute of Technology Guwahati

for the award of the degree of

Doctor of Philosophy

Department of Chemistry

Indian Institute of Technology Guwahati

Guwahati-781039, Assam, India

December 2023

Abstract

The organization of molecules or atoms in a hierarchical manner leads to the formation of complex superstructures with enhanced properties and functionalities, resulting in superior performance when compared to mono-morphological units. Researchers have been motivated by the impact of these achievements to explore the design and fabrication of materials with hierarchical assembly at the nanoscale level. In this regard, research on the hierarchical assembly of two-dimensional (2D) nanomaterials has led to several exciting discoveries in various fields such as energy storage, optoelectronic devices, chemical sensors, catalytic performance, membranes, and solar cells.

Recently, the angular-dependent arrangement of 2D layers has become popular in the scientific community due to the discovery of exciting new phenomena that are greatly influenced by the twist angle between consecutive layers. However, the conventional physical methods to design these superlattices limit their application owing to the weak coupling between the layers. Here, we have proposed a chemical bonding-based approach for stacking 2D nanosheets that holds significant potential for creating numerous fascinating and tunable properties. Chapter 1 describes the introduction highlighting the significance of hierarchical superstructures in nanoscale science and technology. Chapter 2 presents the formation of 2D crystalline nanosheets with exceptional delayed photoluminescence quantum yield from small-ligand-stabilized luminescent copper nanoclusters (CuNCs), followed by surface modification with organic ligand to create a single-component dual-emitting nanocompound with near-white-light emission. Chapter 3 describes the achievement for the first time of the chemical bonding mediated stacking of 2D hexagonal crystalline assembly of CuNCs at a specific relative angle of 30° providing regional dodecagonal quasicrystalline lattice. The so-formed quasiperiodic nanosheets exhibited superior delayed photoluminescence properties and enhanced chemical stability compared to individual nanosheets. Chapter 4 reports the successful formation of chemical-guided moiré superlattices on low twist angle stacking of 2D hexagonal crystalline assembly of CuNCs in a liquid medium. The resulting superlattices generated an additional quantum emissive state in the blue region due to the inter-nanocluster coprophilic interactions. This state can be tuned based on the density of the moiré superlattices, leading to white light emission with a chromaticity index value of (0.32, 0.39). Finally, chapter 5 concludes the thesis by summarizing the findings and discussing the plausible future prospects.

Statement

This thesis entitled "**Chemically Twisted Superlattices of Two-dimensional Assemblies of Copper Nanoclusters**" is a work of research and investigation carried out by me under the supervision of Prof. Arun Chattopadhyay, Professor, Department of Chemistry, Indian Institute of Technology Guwahati. This thesis has been submitted by me to the Department of Chemistry, Indian Institute of Technology Guwahati for the award of the degree of Doctor of Philosophy. I further declare that this work has not been submitted anywhere else for any degree, diploma, associateship or membership etc. of any Institute or University to the best of my knowledge.

Priya Das

Department of Chemistry,

IIT Guwahati,

Guwahati-781039, Assam, India

Date: 04.12.2023

Place: Guwahati, Assam

Certificate

It is certified that the thesis entitled "**Chemically Twisted Superlattices of Two-dimensional Assemblies of Copper Nanoclusters**" being submitted to the Indian Institute of Technology Guwahati by Priya Das (Roll. No. 186122026) for the award of the degree of Doctor of Philosophy in Chemistry, is a bonafide record of research work carried out by her. The information and data reported by her are solely the results of her original findings. She has meticulously carried out the investigations and followed the guidelines of the laboratory. This work has not been submitted elsewhere for any degree or diploma.

Prof. Arun Chattopadhyay

Thesis Supervisor

Professor,

Department of Chemistry, IIT Guwahati,

Guwahati-781039, Assam, India.

Date: 04.12.2023

Place: Guwahati, Assam

Dedicated to my beloved Parents

Mr. Ratneswar Das

and

Mrs. Niyati Das

Acknowledgement

First and foremost, I am immensely grateful for the unwavering love, support, and faith of my family and friends who motivated me to embark on this doctoral journey. Their love, encouragement, and faith in me have been a blessing. I am truly fortunate to have them by my side as I take the first step towards achieving my ultimate goal.

I would like to express my sincere gratitude to my supervisor, Prof. Arun Chattopadhyay, for welcoming me into his research group and providing me with unwavering guidance and moral support throughout my research journey. His innovative ideas and perspectives on science have always inspired me to pursue my passion for research. I am grateful for the exceptional research environment under his guidance that allowed me to work freely and discover my full potential. During my PhD, his teachings of patience, resilience, and a positive attitude towards every challenge have aided my personal growth. It has been an honor to have such a kind and generous mentor.

I am also grateful to my M.Sc. project supervisor, Professor Anumita Paul, for imparting valuable knowledge and core values to me. I am grateful for her support and advice whenever I needed it during my doctoral journey. I sincerely acknowledge her contribution to my research work.

Furthermore, I would like to express my sincere gratitude to my doctoral committee chairman, Prof. Sumana Dutta, as well as the other committee members, Dr. Sunanda Chatterjee and Dr. Akshai Kumar Alape Seetharam, for their timely evaluation of my thesis work. Their valuable suggestions and comments played a significant role in improving the quality of my thesis.

I am grateful for my lab members, both past and present, who have been part of my research journey. Regardless of the duration of their time with me, each individual has contributed significantly to my personal growth and advancement.

I would also like to thank the Department of Chemistry, Centre for Nanotechnology, and CIF for providing me with research facilities.

I want to convey my heartfelt gratitude to my dear friends, Priyanka and Nikita for making my journey so much more enjoyable. Your support and presence throughout all the ups and downs, as well as celebrating all of my achievements, have been invaluable. The journey would not have been the same without you both. You have made the journey easy and unforgettable.

Last but not least, I would like to express my heartfelt gratitude to my parents for their endless support and unconditional love.

Thank you

Priya Das

Table of Contents

Chapter 1

Introduction

Hierarchical nanostructures are the long-range assembly of nanoscale building units such as nanowires, quantum dots, nanoparticles, nanoclusters, and nanosheets into higher dimensional superstructures. Such architectures with combined features of well-organized nanoscale units offer the advantage of utilizing the unique physical and chemical properties of nanomaterials in practical applications. Besides, obtaining high surface area and synergistic interactions, the hierarchy in nanostructures can also provide unique and new physical and chemical properties that are different from their component mono-morphological units. While self-assembly is considered a simple route to form the ensemble of nanostructures, the decades-old research shows that the directed assembly with proper control in the dimension and length scale of the nanostructures could provide more access to tune optical, electrical, and magnetic properties and thus provide a greater range of applications.

1.1 Two-dimensional (2D) materials and their assembly:

In material science, 2D materials have taken a significant step forward in implications of potential applications especially in energy and environmental applications due to chemical reactivity with large surface area, in-plane tunable electroconductivity, and out-of-plane flexibility. From the discovery of single-layer graphene in 2004, 2D materials of various materials such as Mxenes, transition metal dichalcogenides, phosphene, silicene and more have subsequently drawn attention owing to their fascinating in-plane properties. However, controlling restacking of 2D materials in synthesis medium and irreversible aggregation are the major challenges in large-scale synthesis of the 2D systems for practical applications. These problems have been found to be overcome by the directed organization of 2D materials.

1.1.1 Assembly of Graphene: Graphene, a single-layer 2D material with a covalently bonded sp^2 carbon network has emerged as a potential material owing to its high carrier

mobility, excellent mechanical strength, high thermal conductivity, and unique optical and mechanical properties.

It has been discovered that combining multiple layers of graphene can induce an electrical conductance band gap, making bilayer or multilayer graphene more accessible for specific properties due to the tuning of the band gap. Other 2D materials are also used in conjunction with graphene to improve its performance. For example, when assembling heterostructures such as graphene/h-BN, the novel Hofstadter Butterfly phenomenon and graphene quantum Hall Effect have been observed. [1-3] Additionally, graphene/MoS2/graphene and graphene/WSe2/graphene assembled heterostructures have demonstrated excellent optoelectronic properties, including broadband photoresponse from 405-2000 nm and high photodetection efficiency with picosecond photo response respectively.[4-5]

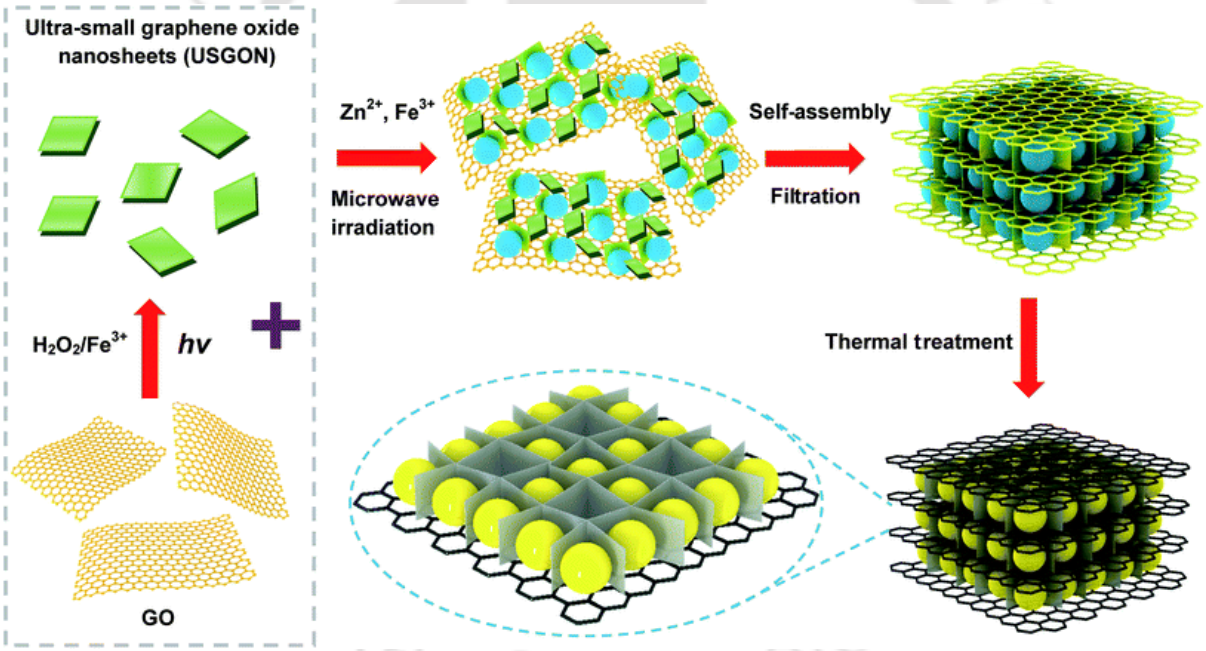

Fig 1.1 Schematic illustration of an assembly of graphene to confine $ZnFe_2O_4$ nanoparticles. Reprinted with permission *Journal of Materials Chemistry A* **2017,** *5* (22), 11188-11196.

1.1.2 Assembly of Mxenes: Mxenes, transition metal carbides or nitrides have also attracted attention as 2D layered structures since 2011 due to their unique properties. However, the tendency to restack results in poor processability in a range of applications, which was successfully overcome by proper assembly formation of the layers through surface modifications,[6] hetero atoms doping,[7] and incorporating interfacial spacers.[8] In most of the cases the strategy of assembly formation includes the introduction of intercalants (ions or small molecules) and spacers (nanomaterials or polymers) between the layers to increase the lattice parameter ranging from ≈0.3 to 4.8 nm. Metal ion intercalated Mxenes have been found to improve the stability of the structure where the lattice parameters are decreased due to the strong electrostatic interactions among the metal ions and the 2D layers resulting in improved electrical performances. For example, Li^+, Na^+, and Mg^{2+} cation intercalation were found to improve the chemical stability as well as flexibility in chemically unstable V_2CT_x and Ti_2CT_x MXenes.[8] 2D nanomaterials, on the other hand, also have been used as interlayer spacers in MXene sheets to improve their applications by suppressing aggregation. For example, RGO/$Ti_3C_2T_x$ hybrid films showed great volumetric performance in aqueous acidic electrolyte,[9] assemblies of Mxene with electrochemically exfoliated graphene showed excellent areal and volumetric capacitance,[10] and 2D Fe–N–C/MXene superlattice have been observed to exhibit enhanced oxygen reduction rlectrocatalysis.[11]

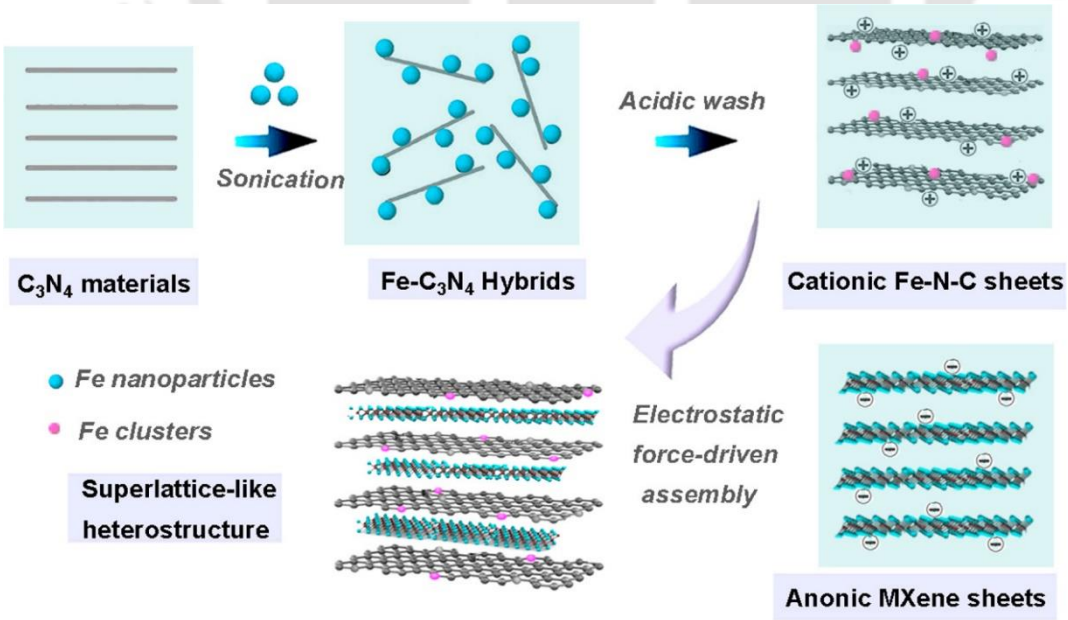

Fig 1.2. Schematic illustration of iron cluster mediated formation of 2D/2D Fe–N–C/MXene superlattice. (Reprinted with permission from Reference [11]. Copyright *ACS Nano*. 2020 American Chemical Society)

1.1.3 Assembly of 2D MOF: 2D nano metal-organic frameworks (MOF) comprising metal clusters and bridged organic ligands provide wide adsorption applications such as storage and separation of gases, chemical sensing, and catalysis due to their special functionalities and pore characteristics.[12-13] Bringing material anisotropy in chemical bonding and connectivity through the hierarchical layered assembly of MOFs could influence electronic band structure , chemical reactivity, surface interaction, catalytic activity, etc. For example, hierarchical assembly of 2D structured DUT-134(Cu)·DMF ($[Cu_2(dttc)_2(DMF)_2(L)_x]_n$, dttc: dithieno[3,2-*b* : 2′,3′-*d*]thiophene-2,6-dicarboxylate, L - solvent) MOF into carpet like meta crystals enhanced H_2S adsorption capacity in gas filtering tests showing excellent application in air-filtration process[14], polycationic polymers mediated assembly of 2D MOF of iron-porphyrin complex interconnected with Zn metal ion exhibited superior nanofiltration performances at low operating pressures,[15] assembly of 2D M-TCPP(Fe) (M = Co, Cu, or Zn) nanosheet on electrodes through Langmuir–Schäfer method provided an excellent sensitivity in electrochemical detection of H_2O_2.[16]

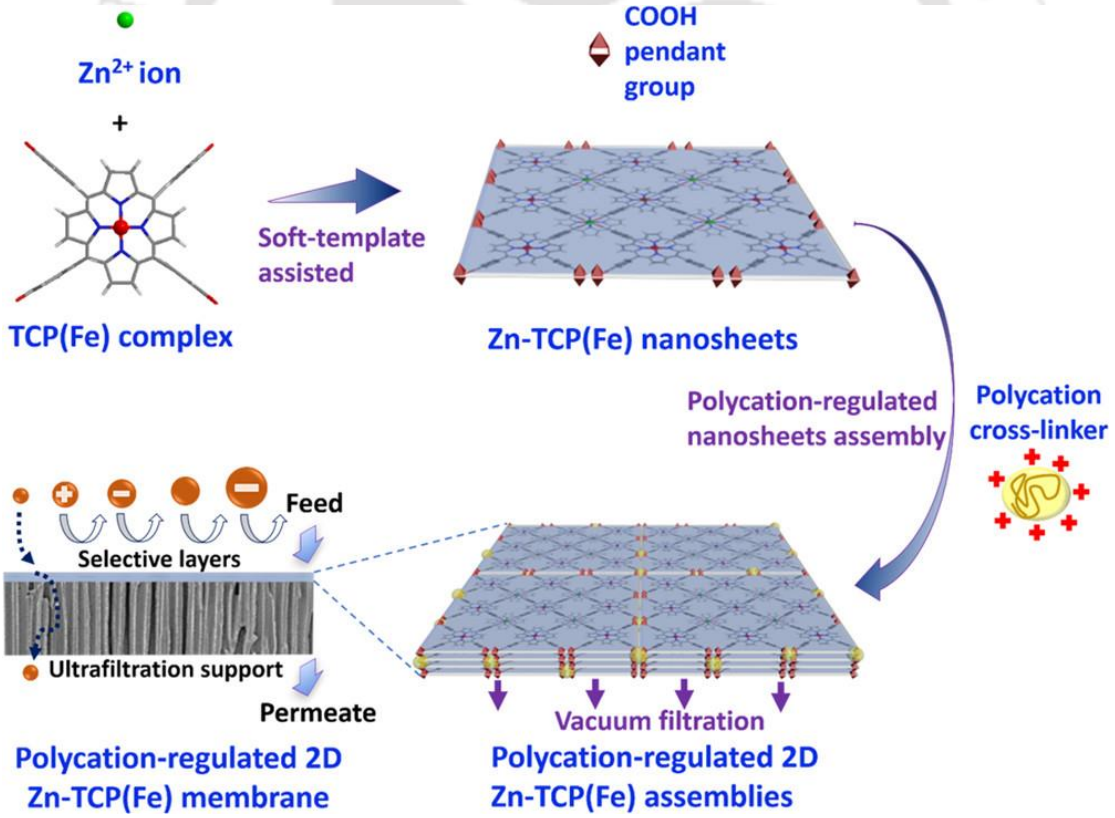

Fig 1.3. Schematic illustration for polycation-regulated assembly of 2D Zn-TCP(Fe) layers. (Reprinted with permission from Reference [15]. Copyright *ACS Appl. Mater. Interfaces* 2017 American Chemical Society)

1.1.4 Assembly of Metal Dichalcogenide Nanosheets: 2D transition metal dichalcogenides (TMDs) such as MoS_2, TiS_2, $MoSe_2$, WSe_2, and WS_2, etc are gaining significant attention as new generation photonic materials owing to intrinsic band gap tunability, high carrier mobility, and mechanical strength in designing electronics and optoelectronic devices. However, controlled assembled structures of similar or heterogenous 2D TMDs could bring more exotic properties to the system. Tunability in optical properties has been realized on superlattice formation with alternatively arranged MoS_2 and WSe_2.[17] Besides, the generation of strong localized photoluminescence intensity enhancement and intrinsic p-n junction in layer-by-layer assembly of MoS_2 / WSe_2,[18] $MoSe_2$ / WSe_2,[19] superior photovoltaic effect with high quantum efficiency in WSe_2/ $MoSe_2$ heterostructures,[20] tuning the carrier confinement in MoS_2/WS_2 heterostructures,[21] expand the application of 2D TMDs in optoelectronic devices.

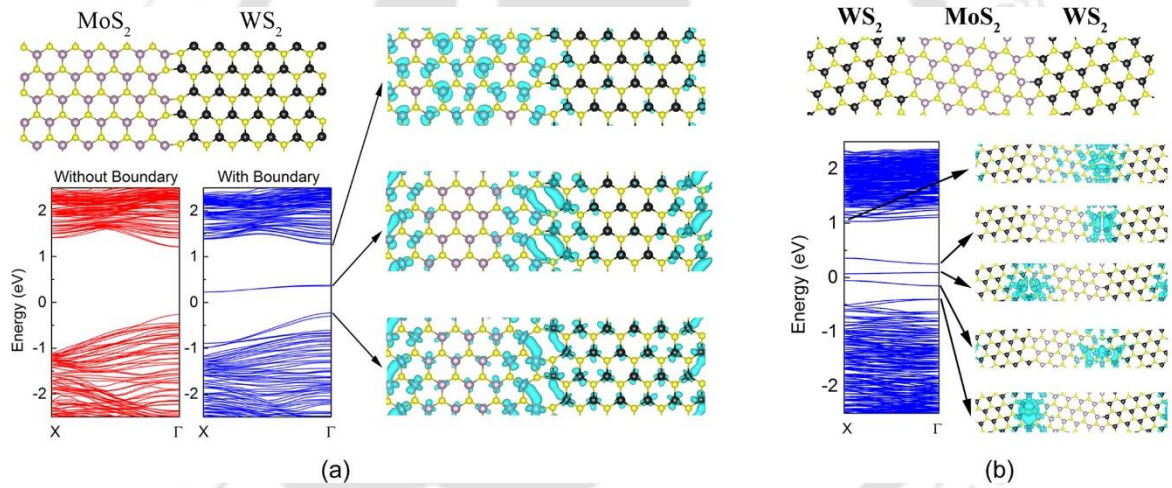

Fig 1.4. (a) Representation of structure and energy bands for a lateral heterostructure of MoS_2/WS_2 with grain boundary at the armchair interface along with the charge density of the conduction band minimum, valence band maximum, and in-gap states. (b) The same as (a) for a 5–7 boundary. (Reprinted with permission from Reference [21]. Copyright *J. Phys. Chem. C* 2015 American Chemical Society)

1.2. Twisted Superstructures of 2D Materials:

The discovery of superconductivity in magic-angle twisted graphene in 2018 has led to unprecedented interest in the twist angle as an emerging control of property in the super-assembly of 2D materials.[22] Twist angle significantly impacts the band gap of materials,

resulting in unique properties such as Hove singularities,[23] moiré superlattice-induced superconductivity,[24] insulating states,[25] and topological valley transport.[26] Twisted superstructures of 2D materials are generated by overlapping two or more layers on each other with a relative rotation- this rotational angle or twist angle provides additional degrees of freedom to control the interlayer interactions, allowing for a fine-tuning of the electronic properties. Depending on the twist angle a range of complex unique structures of layers can be created. The two most important structures that have brought revolution in physical as well as material sciences are- the quasicrystal which occurs at a definite twist angle and the moire superlattices which occur at smaller twist angles.

1.2.1 Quasicrystal: Quasicrystal, a new form of crystalline material with quasi-periodic orders (such as rotational symmetry) without translational periodicity, has gained extraordinary popularity since its discovery in 1984. Unlike traditional crystals, quasicrystals may have 5, 10 or 12-fold symmetries which are forbidden according to the conventional crystal definition. Even after so many years of its discovery, the development of such materials in the laboratory is still limited due to its synthetic challenges. During the initial period of discovery, it was believed that quasicrystals were only found in metal alloys, later on, it has been observed in a wide variety of materials including colloids, polymers, micelles, and nanoparticles.[27-30] So far quasicrystalline periodicity in nanomaterials has been reported as a serendipitous discovery resulting from chemically induced self-assembly, which is driven by the general entropy-driven nanomaterial packing phenomenon. Determining the strategy to chemically design quasicrystal alike conventional crystals is a big challenge for scientists.

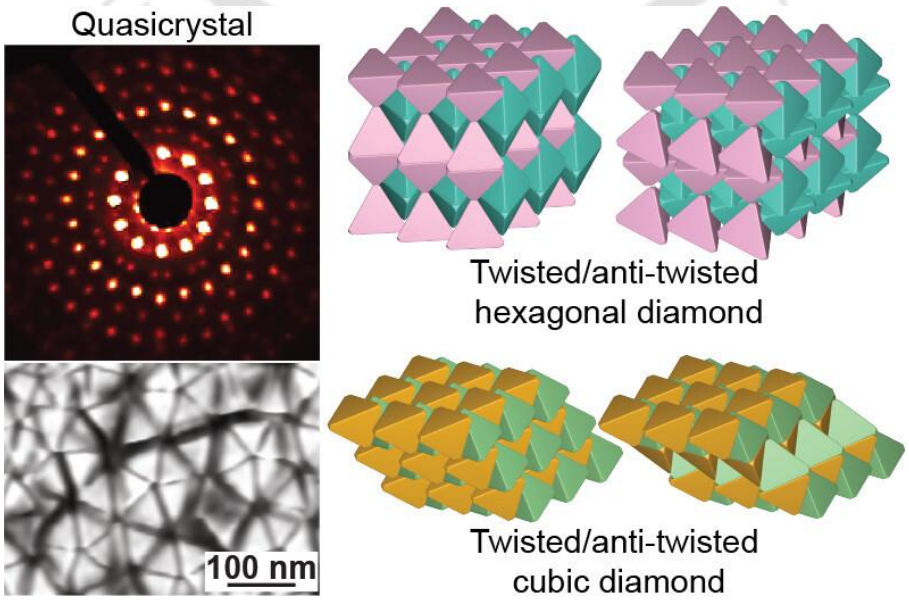

Fig 1.5. Schematic illustration of controlled self-assembly of gold nanotetrahedra into quasicrystal. (Reprinted with permission from Reference [30]. Copyright *J. Am. Chem. Soc.* 2023 American Chemical Society)

However, the recent result suggests that proper angular stacking of 2D materials could also be an option to generate quasicrystallinity with higher-ordered rotational symmetry.[31] Such as two graphene layers overlapped on each other with a twist angle of 30° gives dodecagonal quasicrystalline periodicity in the system which is termed as graphene quasicrystal.[32] This new form of quasicrystal has attracted immense interest as it brings a quasicrystalline nature to the graphene system with the simultaneous existence of its relativistic properties. For example, anomalous strong interlayer coupling with quasiperiodicity were observed in 30° twisted bilayer graphene quasicrystal.[33] This led to the emergence of mirror-symmetric Dirac cones inside the Brillouin zone of each graphene layer and a gap opening at the zone boundary.[33-35] Theoretical calculations also showed that the quasi-periodicity in the graphene quasicrystal could generate quantum oscillations and critical eigenstates.[36-38]

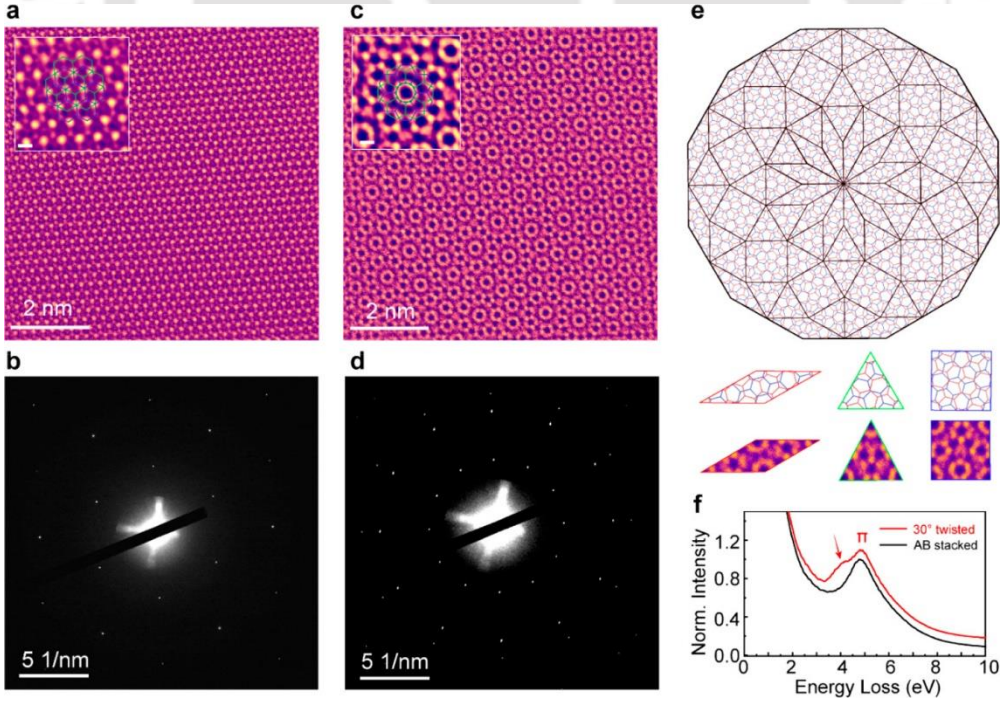

Fig 1.6. (a) High-angle annular dark-field scanning transmission electron microscopy (HAADF-STEM) image of bi-layer graphene (BLG) stacked in AB pattern. Inset: closer view of the same image. (b) selected area electron diffraction (SAED_of AB-stacked BLG. (c) HAADF-STEM image of 30° twisted bilayer graphene (tBLG). Inset: closer view of the same image. (d) SAED of 30°-tBLG. (e) illustrates the structure of 30°-tBLG as a dodecagonal quasicrystal pattern and its structure units, (f) the electron energy loss spectroscopy (EELS) of AB-stacked BLG and 30°-tBLG (Reprinted with permission from Reference [32]. Copyright *ACS Nano* 2020 American Chemical Society)

1.2.2 Moiré Superlattices: Moiré superlattices are another significant outcome of the super-assembly of 2D materials. A moiré superlattice or pattern occurs when there is a lattice mismatch between two identical 2D layers or different layers that overlap each other due to dissimilar lattices or twist angles between them.[39] Besides, providing additional periodicity to the system, it leads to the emergence of new physical properties due to the perturbation in electronic states of the intervening layers. A few examples are- observations of secondary Dirac points, [40,41] Hofstadter's butterfly and the fractal quantum Hall effect,[42,43] quantum oscillations at high temperature,[44] topological currents,[45] in graphene superlattices on hexagonal boron nitride. However, it has been observed that moiré superlattices formed due to smaller angle displacement of the layers (precisely at magic angle) give rise to the novel exotic phenomenon. At smaller twist angles, the hybridization of two Dirac cones of two respective layers occurs due to interlayer hopping, which leads to the formation of a flattened band and reduced Fermi velocity at Dirac cones.[46-50] The strong interlayer coupling generates insulating states at charge-neutral points even though the system comprises two high-quality conducting sheets. The latest surprising finding from moiré superlattices was unconventional superconductivity in twisted graphene bilayers and trilayers at magic angle.[22,51] Other important discoveries on electrical properties modified by moiré superlattices include interfacial ferroelectricity in bilayer transitional metal dichalcogenides and graphene/ boron nitride moiré system,[52,53] atomic and electronic reconstruction in graphene and MoS_2 moiré superlattices.[54,55]

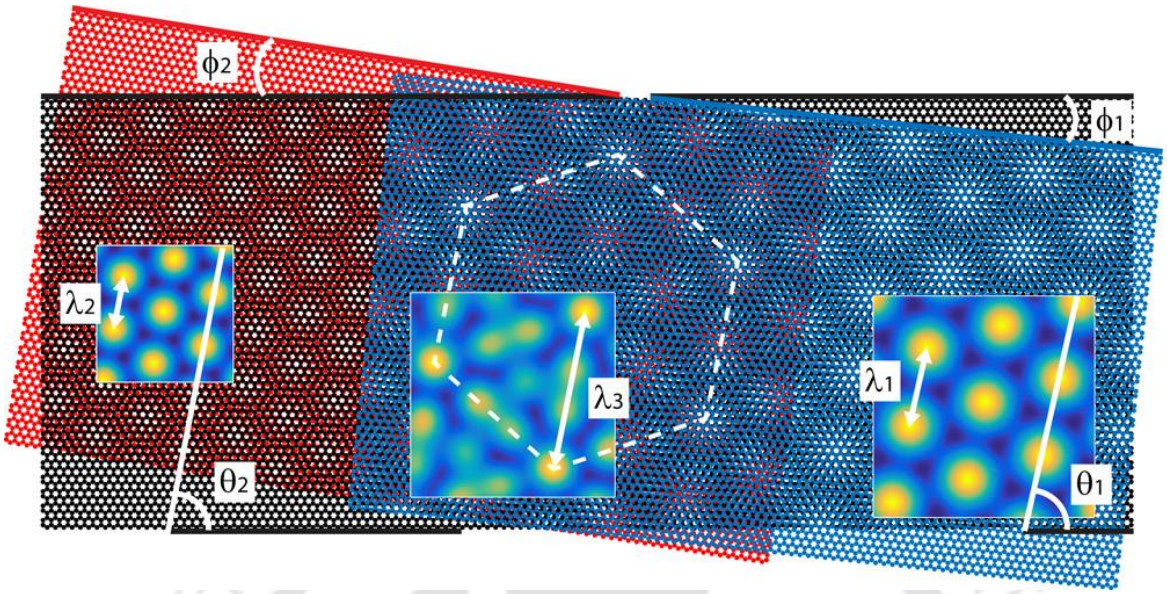

Fig 1.7. Schematic illustration of three different moire superlattices (MSLs) indicated with $\lambda_{1,2,3}$ formed in an hBN/graphene/hBN heterostructure. Blue, black, and red hexagonal lattices respectively represent top hBN, graphene, and bottom hBN lattices, . The twist angle between the top and bottom hBN and graphene is represented by ϕ1 (ϕ2), while θ1 (θ2) indicates the orientation of the corresponding MSL with respect to graphene. The three layer MSL (middle part) has a larger period than both two-layer MSLs (left and right parts). (Reference [39])

1.3. Physical Methods in the Synthesis of 2D Superlattices:

The three main popular techniques that have contributed to the development of 2D superlattices with improved features are -mechanical transfer, gas vapor growth, and liquid-assisted engineering, which combine both the advantages of top-down and bottom-up approaches.

1.3.1 Mechanical Transfer: This method involves two steps – first, exfoliation of the same type or different materials from its bulk to two pieces of Si/SiO_2 substrates, respectively. One material is chosen as the bottom layer, and the other as the upper layer. A transition film, composed of a water-soluble polymer and polymethyl methacrylate (PMMA) materials,

needs to be applied on top of the upper layer. Second, the film can be precisely transferred to another slice using a microscope operation system, ensuring the upper layer remains on top of the bottom layer. After dissolving the PMMA in acetone, the sample is annealed at a high temperature in a protective gas environment to establish close contact between the interfaces and successfully fabricate the van der Waal heterostructures.[56-58]

1.3.2 Gas Vapour Growth: There are two important methods in this category-

1.3.2.1 Chemical Vapor Deposition (CVD) Growth: In this technique, the solid or gaseous precursors are taken into a tube furnace. The precursors react chemically and nucleate at the reaction zones on a target substrate Then, with careful regulation of gas flow, temperature, and pressure the nucleation continues to form thin layers. Though the process seems to be easy, proper designing of superlattices needs demanding deposition methods including careful consideration of the chemical environment to duration time, and speed. [59-62]

1.3.2.2 Physical Vapor Deposition (PVD) Growth: This technique requires the same precursors and operations chambers as in the CVD method. However, PVD growth typically lacks chemical reactions and relies on bulk precursors. It's crucial to ensure lattice matching between 2D materials and substrates, with the aim of arranging atoms/molecules regularly on a specific substrate.[63-65]

1.3.3 Liquid-Assisted Engineering Method: Liquid-assisted layer-by-layer deposition and solution based self-assembly can be considered in this category-

1.3.3.1 Liquid-Assisted Layer-by-Layer Deposition (LLD): This is based on the charge adsorption where colloidal suspensions of nanosheets with opposite charges are generally used as different basic components of 2D substrates, and then the substrate is immersed into different liquids sequentially leading the superlattice formation at an air–liquid interface.[66,67]

1.3.3.2 Solution-Phase Self-Assembly (SSA): Here, the preparation is accomplished spontaneously by mixing intercalating molecules into the solution containing basic component 2D nanosheets of opposite charges.[68,69]

All the physical methods discussed above have been improved tremendously with time, still the demanding conditions, complicated operations, and low yield hinder the large-scale application for industrial purposes. Moreover, the desired strong coupling is compromised in the 2D superlattices synthesized from the above techniques unlike materials coupled by chemical bonding. This weak coupling reduces the strength of property

modulation imposed by moiré superlattices. This could be overcome by replacing the weak coupling with strong chemical bonds.

1.4. Nanoclusters and Its 2D Assembly:

1.4.1 Nanoclusters: Atomically precise noble metal nanoclusters, especially gold, silver and copper nanoclusters, have gained tremendous research interest since discovery due to their unique molecular-like properties, unlike their bulk counterparts. They are the collection of a few atoms with sizes less than 2 nm. The smaller size-induced quantum confinement effect with discrete energy levels makes metal nanoclusters behave like molecules with interesting optical and electronic properties like multi-band optical absorption, ultra-small size low toxicity, enhanced fluorescence, single-electron magnetism, and high catalytic reactivity.

Furthermore, the structural integrity, uniform dispersity, and reactive stabilizing ligands make metal nanoclusters the best choice in comparison to the other nanomaterials for scientists to design functional materials through hierarchical assembly.

1.4.2 2D Assembly of Metal Nanoclusters: Despite the unique properties of atomically precise metal nanoclusters, the long-term stability of small-sized nanoclusters limits their potential applications. This problem has been partly addressed by organizing metal nanoclusters into hierarchical structures, which provide stability to the individual clusters and also enhance their intrinsic properties by synergic effect. In this regard, the 2D assembly of metal nanoclusters holds potential for novel properties, wide applications, and interlayer interaction-induced phenomena.

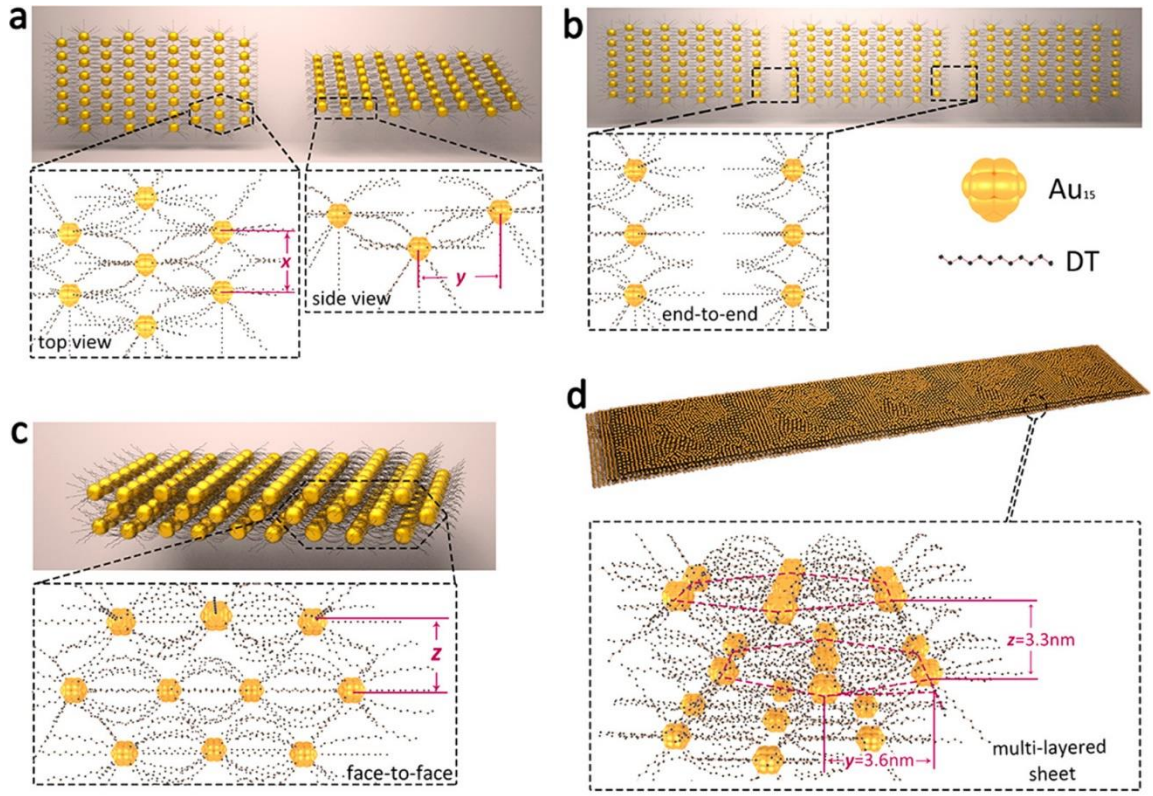

Fig 1.8 . Schematic representation of how the morphology changes when small isolated 2D architectures are heated at 140 °C. (a–d) the secondary assembly of AuNCs into long multilayered architectures- elongated architectures (a), the end-to-end (b) and face-to-face self-assembly (c), and the spatial arrangement of Au_{15} NCs within the multilayered architectures (d). (Reprinted with permission from Reference [70]. Copyright *ACS Nano* 2015 American Chemical Society)

2D layered structures of $Au_{15}(DT)_{15}$ (DT=1-dodecanethiolate) have been reported governed by 1D dipole interactions following asymmetric *van der Waals* (vdW) attractions.[70] Further, recent discoveries in metal ion complexation-based two-dimensional assembly of gold nanoclusters have opened a new route to the hierarchical organization of nanoclusters with potential applications. For example, Zn metal ion mediated complexation-based assemblies of gold nanoclusters not only enhanced the luminescence of the component nanoclusters through structural rigidity but also exhibited room temperature delayed photoluminescence and showed potency in recyclable storage of oxygen.[71,72] Thus the crystalline 2D assembly of other metal nanoclusters also holds the key to expanding the scope of unveiling exciting photophysical properties as well.

However, research on CuNCs has received less attention compared to the research on Au or AgNCs. This is due to their stability in areal conditions and weak photoluminescence properties. However, the extraordinary reactivity of small CuNCs can be harnessed if they are stabilized with small ligands in a crystalline assembly. This could potentially lead to a bright future in nanoscience. In this regard, the 2D assembly may provide unique opportunities.

1.5 Thesis Overview:

Herein, we have introduced a chemical approach to stack two-dimensional nanosheets of red luminescent copper nanoclusters. The basis component nanosheets were prepared through crystalline organizations of small ligand-stabilized CuNCs through a metal ion-mediated complexation reaction, which was followed by twisted stacking in the liquid dispersion based on chemical principles and formed superlattices with superior optical properties.

The present thesis is divided into five chapters-

Chapter 1: describes the introduction comprising of the importance of hierarchical superstructures in nanoscale science and technology, discoveries of novel properties in twisted 2D assembly, and the aim of the current thesis.

Chapter 2: presents the synthesis of small ligand stabilized luminescent copper nanoclusters (CuNCs), and their two-dimensional crystalline assembly with enhanced photoluminescence in comparison to the component CuNCs and delayed photoluminescence property with exceptionally high quantum yield of 83.6 ± 1.3%. Further surface functionalization of the nanosheets with an organic ligand for near white light emission.

Chapter 3: describes achievement in chemically directed stacking of 2D hexagonal crystalline assembly of CuNCs at a specific relative angle of 30° providing regional dodecagonal quasicrystalline lattice diffraction with loss of translational symmetry while maintaining the rotational symmetry.

Chapter 4: reports the successful formation of chemical guided moiré superlattices of two-dimensional crystalline Zn complexed CuNCs (Zn-CuNCs) nanosheets with low relative twist angle in a liquid medium. The resulting super-assembled Zn-CuNCs nanosheets, with additional large-scale periodicities, generated an additional quantum emissive state in the

blue region due to the inter-nanocluster coprophilic interactions of the interactive layers and also generated white light emission with a chromaticity index value of (0.32, 0.39).

Chapter 5: contains the summarization and plausible future prospects of the thesis.

1.6 Bibliography:

1. Dean, C. R.; Young, A. F.; Meric, I.; Lee, C.; Wang, L.; Sorgenfrei, S.; Watanabe, K.; Taniguchi, T.; Kim, P.; Shepard, K. L.; Hone, J., Boron nitride substrates for high-quality graphene electronics. *Nature Nanotechnology* **2010,** *5* (10), 722-726.
2. Ponomarenko, L. A.; Gorbachev, R. V.; Yu, G. L.; Elias, D. C.; Jalil, R.; Patel, A. A.; Mishchenko, A.; Mayorov, A. S.; Woods, C. R.; Wallbank, J. R.; Mucha-Kruczynski, M.; Piot, B. A.; Potemski, M.; Grigorieva, I. V.; Novoselov, K. S.; Guinea, F.; Fal'ko, V. I.; Geim, A. K., Cloning of Dirac fermions in graphene superlattices. *Nature* **2013,** *497* (7451), 594-597.
3. Dean, C. R.; Wang, L.; Maher, P.; Forsythe, C.; Ghahari, F.; Gao, Y.; Katoch, J.; Ishigami, M.; Moon, P.; Koshino, M.; Taniguchi, T.; Watanabe, K.; Shepard, K. L.; Hone, J.; Kim, P., Hofstadter's butterfly and the fractal quantum Hall effect in moiré superlattices. *Nature* **2013,** *497* (7451), 598-602.
4. Gao, S.; Wang, Z.; Wang, H.; Meng, F.; Wang, P.; Chen, S.; Zeng, Y.; Zhao, J.; Hu, H.; Cao, R.; Xu, Z.; Guo, Z.; Zhang, H., Graphene/MoS2/Graphene Vertical Heterostructure-Based Broadband Photodetector with High Performance. *Advanced Materials Interfaces* **2021,** *8* (3), 2001730.
5. Massicotte, M.; Schmidt, P.; Vialla, F.; Schädler, K. G.; Reserbat-Plantey, A.; Watanabe, K.; Taniguchi, T.; Tielrooij, K. J.; Koppens, F. H. L., Picosecond photoresponse in van der Waals heterostructures. *Nature Nanotechnology* **2016,** *11* (1), 42-46.
6. Dall'Agnese, Y.; Lukatskaya, M. R.; Cook, K. M.; Taberna, P.-L.; Gogotsi, Y.; Simon, P., High capacitance of surface-modified 2D titanium carbide in acidic electrolyte. *Electrochemistry Communications* **2014,** *48*, 118-122.

7. Wen, Y.; Rufford, T. E.; Chen, X.; Li, N.; Lyu, M.; Dai, L.; Wang, L., Nitrogen-doped Ti3C2Tx MXene electrodes for high-performance supercapacitors. *Nano Energy* **2017,** *38*, 368-376.
8. VahidMohammadi, A.; Mojtabavi, M.; Caffrey, N. M.; Wanunu, M.; Beidaghi, M., Assembling 2D MXenes into Highly Stable Pseudocapacitive Electrodes with High Power and Energy Densities. *Advanced Materials* **2019,** *31* (8), 1806931.
9. Xu, S.; Wei, G.; Li, J.; Han, W.; Gogotsi, Y., Flexible MXene–graphene electrodes with high volumetric capacitance for integrated co-cathode energy conversion/storage devices. *Journal of Materials Chemistry A* **2017,** *5* (33), 17442-17451.
10. Li, H.; Hou, Y.; Wang, F.; Lohe, M. R.; Zhuang, X.; Niu, L.; Feng, X., Flexible All-Solid-State Supercapacitors with High Volumetric Capacitances Boosted by Solution Processable MXene and Electrochemically Exfoliated Graphene. *Advanced Energy Materials* **2017,** *7* (4), 1601847.
11. Jiang, L.; Duan, J.; Zhu, J.; Chen, S.; Antonietti, M., Iron-Cluster-Directed Synthesis of 2D/2D Fe–N–C/MXene Superlattice-like Heterostructure with Enhanced Oxygen Reduction Electrocatalysis. *ACS Nano* **2020,** *14* (2), 2436-2444.
12. Furukawa, H.; Cordova, K. E.; O'Keeffe, M.; Yaghi, O. M., The Chemistry and Applications of Metal-Organic Frameworks. *Science* **2013,** *341* (6149), 1230444.
13. Li, J.-R.; Sculley, J.; Zhou, H.-C., Metal–Organic Frameworks for Separations. *Chemical Reviews* **2012,** *112* (2), 869-932.
14. Schwotzer, F.; Horak, J.; Senkovska, I.; Schade, E.; Gorelik, T. E.; Wollmann, P.; Anh, M. L.; Ruck, M.; Kaiser, U.; Weidinger, I. M.; Kaskel, S., Cooperative Assembly of 2D-MOF Nanoplatelets into Hierarchical Carpets and Tubular Superstructures for Advanced Air Filtration. *Angewandte Chemie International Edition* **2022,** *61* (22), e202117730.
15. Ang, H.; Hong, L., Polycationic Polymer-Regulated Assembling of 2D MOF Nanosheets for High-Performance Nanofiltration. *ACS Applied Materials & Interfaces* **2017,** *9* (33), 28079-28088.
16. Wang, Y.; Zhao, M.; Ping, J.; Chen, B.; Cao, X.; Huang, Y.; Tan, C.; Ma, Q.; Wu, S.; Yu, Y.; Lu, Q.; Chen, J.; Zhao, W.; Ying, Y.; Zhang, H., Bioinspired Design of Ultrathin 2D Bimetallic Metal–Organic-Framework Nanosheets Used as Biomimetic Enzymes. *Advanced Materials* **2016,** *28* (21), 4149-4155.

17. Hashemi, R.; Shojaei, S.; Rezaei, B.; Liu, Z., Valley-optical absorption in planar transition metal dichalcogenide superlattices. *Scientific Reports* **2023,** *13* (1), 5439.
18. Gong, Y.; Lin, J.; Wang, X.; Shi, G.; Lei, S.; Lin, Z.; Zou, X.; Ye, G.; Vajtai, R.; Yakobson, B. I.; Terrones, H.; Terrones, M.; Tay, Beng K.; Lou, J.; Pantelides, S. T.; Liu, Z.; Zhou, W.; Ajayan, P. M., Vertical and in-plane heterostructures from WS2/MoS2 monolayers. *Nature Materials* **2014,** *13* (12), 1135-1142.
19. Huang, C.; Wu, S.; Sanchez, A. M.; Peters, J. J. P.; Beanland, R.; Ross, J. S.; Rivera, P.; Yao, W.; Cobden, D. H.; Xu, X., Lateral heterojunctions within monolayer MoSe2–WSe2 semiconductors. *Nature Materials* **2014,** *13* (12), 1096-1101.
20. Gong, Y.; Lei, S.; Ye, G.; Li, B.; He, Y.; Keyshar, K.; Zhang, X.; Wang, Q.; Lou, J.; Liu, Z.; Vajtai, R.; Zhou, W.; Ajayan, P. M., Two-Step Growth of Two-Dimensional WSe2/MoSe2 Heterostructures. *Nano Letters* **2015,** *15* (9), 6135-6141.
21. Kang, J.; Sahin, H.; Peeters, F. M., Tuning Carrier Confinement in the MoS2/WS2 Lateral Heterostructure. *The Journal of Physical Chemistry C* **2015,** *119* (17), 9580-9586.
22. Cao, Y.; Fatemi, V.; Fang, S.; Watanabe, K.; Taniguchi, T.; Kaxiras, E.; Jarillo-Herrero, P., Unconventional superconductivity in magic-angle graphene superlattices. *Nature* **2018,** *556* (7699), 43-50.
23. Li, G.; Luican, A.; Lopes dos Santos, J. M. B.; Castro Neto, A. H.; Reina, A.; Kong, J.; Andrei, E. Y., Observation of Van Hove singularities in twisted graphene layers. *Nature Physics* **2010,** *6* (2), 109-113.
24. Yankowitz, M.; Chen, S.; Polshyn, H.; Zhang, Y.; Watanabe, K.; Taniguchi, T.; Graf, D.; Young, A. F.; Dean, C. R., Tuning superconductivity in twisted bilayer graphene. *Science* **2019,** *363* (6431), 1059-1064.
25. Cao, Y.; Fatemi, V.; Demir, A.; Fang, S.; Tomarken, S. L.; Luo, J. Y.; Sanchez-Yamagishi, J. D.; Watanabe, K.; Taniguchi, T.; Kaxiras, E.; Ashoori, R. C.; Jarillo-Herrero, P., Correlated insulator behaviour at half-filling in magic-angle graphene superlattices. *Nature* **2018,** *556* (7699), 80-84.
26. Ju, L.; Shi, Z.; Nair, N.; Lv, Y.; Jin, C.; Velasco, J.; Ojeda-Aristizabal, C.; Bechtel, H. A.; Martin, M. C.; Zettl, A.; Analytis, J.; Wang, F., Topological valley transport at bilayer graphene domain walls. *Nature* **2015,** *520* (7549), 650-655.
27. Talapin, D. V.; Shevchenko, E. V.; Bodnarchuk, M. I.; Ye, X.; Chen, J.; Murray, C. B., Quasicrystalline order in self-assembled binary nanoparticle superlattices. *Nature* **2009,** *461* (7266), 964-967.

28. Nagaoka, Y.; Zhu, H.; Eggert, D.; Chen, O., Single-component quasicrystalline nanocrystal superlattices through flexible polygon tiling rule. *Science* **2018,** *362* (6421), 1396-1400.
29. Sun, Y.; Ma, K.; Kao, T.; Spoth, K. A.; Sai, H.; Zhang, D.; Kourkoutis, L. F.; Elser, V.; Wiesner, U., Formation pathways of mesoporous silica nanoparticles with dodecagonal tiling. *Nature Communications* **2017,** *8* (1), 252.
30. Wang, Y.; Chen, J.; Li, R.; Götz, A.; Drobek, D.; Przybilla, T.; Hübner, S.; Pelz, P.; Yang, L.; Apeleo Zubiri, B.; Spiecker, E.; Engel, M.; Ye, X., Controlled Self-Assembly of Gold Nanotetrahedra into Quasicrystals and Complex Periodic Supracrystals. *Journal of the American Chemical Society* **2023,** *145* (32), 17902-17911.
31. Metere, A.; Oleynikov, P.; Dzugutov, M.; Lidin, S., A smectic dodecagonal quasicrystal. *Soft Matter* **2016,** *12* (43), 8869-8875.
32. Deng, B.; Wang, B.; Li, N.; Li, R.; Wang, Y.; Tang, J.; Fu, Q.; Tian, Z.; Gao, P.; Xue, J.; Peng, H., Interlayer Decoupling in 30° Twisted Bilayer Graphene Quasicrystal. *ACS Nano* **2020,** *14* (2), 1656-1664.
33. Ahn, S. J.; Moon, P.; Kim, T.-H.; Kim, H.-W.; Shin, H.-C.; Kim, E. H.; Cha, H. W.; Kahng, S.-J.; Kim, P.; Koshino, M.; Son, Y.-W.; Yang, C.-W.; Ahn, J. R., Dirac electrons in a dodecagonal graphene quasicrystal. *Science* **2018,** *361* (6404), 782-786.
34. Bocquet, F. C.; Lin, Y. R.; Franke, M.; Samiseresht, N.; Parhizkar, S.; Soubatch, S.; Lee, T. L.; Kumpf, C.; Tautz, F. S., Surfactant-Mediated Epitaxial Growth of Single-Layer Graphene in an Unconventional Orientation on SiC. *Physical Review Letters* **2020,** *125* (10), 106102.
35. Yao, W.; Wang, E.; Bao, C.; Zhang, Y.; Zhang, K.; Bao, K.; Chan, C. K.; Chen, C.; Avila, J.; Asensio, M. C.; Zhu, J.; Zhou, S., Quasicrystalline 30° twisted bilayer graphene as an incommensurate superlattice with strong interlayer coupling. *Proceedings of the National Academy of Sciences* **2018,** *115* (27), 6928-6933.
36. Park, M. J.; Kim, H. S.; Lee, S., Emergent localization in dodecagonal bilayer quasicrystals. *Physical Review B* **2019,** *99* (24), 245401.
37. Spurrier, S.; Cooper, N. R., Theory of quantum oscillations in quasicrystals: Quantizing spiral Fermi surfaces. *Physical Review B* **2019,** *100* (8), 081405.

38. Moon, P.; Koshino, M.; Son, Y.-W., Quasicrystalline electronic states in ${30}^{\ensuremath{\circ}}$ rotated twisted bilayer graphene. *Physical Review B* **2019,** *99* (16), 165430.
39. Wang, L.; Zihlmann, S.; Liu, M.-H.; Makk, P.; Watanabe, K.; Taniguchi, T.; Baumgartner, A.; Schönenberger, C., New Generation of Moiré Superlattices in Doubly Aligned hBN/Graphene/hBN Heterostructures. *Nano Letters* **2019,** *19* (4), 2371-2376.
40. Ponomarenko, L. A.; Gorbachev, R. V.; Yu, G. L.; Elias, D. C.; Jalil, R.; Patel, A. A.; Mishchenko, A.; Mayorov, A. S.; Woods, C. R.; Wallbank, J. R.; Mucha-Kruczynski, M.; Piot, B. A.; Potemski, M.; Grigorieva, I. V.; Novoselov, K. S.; Guinea, F.; Fal'ko, V. I.; Geim, A. K., Cloning of Dirac fermions in graphene superlattices. *Nature* **2013,** *497* (7451), 594-597.
41. Yankowitz, M.; Xue, J.; Cormode, D.; Sanchez-Yamagishi, J. D.; Watanabe, K.; Taniguchi, T.; Jarillo-Herrero, P.; Jacquod, P.; LeRoy, B. J., Emergence of superlattice Dirac points in graphene on hexagonal boron nitride. *Nature Physics* **2012,** *8* (5), 382-386.
42. Dean, C. R.; Wang, L.; Maher, P.; Forsythe, C.; Ghahari, F.; Gao, Y.; Katoch, J.; Ishigami, M.; Moon, P.; Koshino, M.; Taniguchi, T.; Watanabe, K.; Shepard, K. L.; Hone, J.; Kim, P., Hofstadter's butterfly and the fractal quantum Hall effect in moiré superlattices. *Nature* **2013,** *497* (7451), 598-602.
43. Hunt, B.; Sanchez-Yamagishi, J. D.; Young, A. F.; Yankowitz, M.; LeRoy, B. J.; Watanabe, K.; Taniguchi, T.; Moon, P.; Koshino, M.; Jarillo-Herrero, P.; Ashoori, R. C., Massive Dirac Fermions and Hofstadter Butterfly in a van der Waals Heterostructure. *Science* **2013,** *340* (6139), 1427-1430.
44. Krishna Kumar, R.; Chen, X.; Auton, G. H.; Mishchenko, A.; Bandurin, D. A.; Morozov, S. V.; Cao, Y.; Khestanova, E.; Ben Shalom, M.; Kretinin, A. V.; Novoselov, K. S.; Eaves, L.; Grigorieva, I. V.; Ponomarenko, L. A.; Fal'ko, V. I.; Geim, A. K., High-temperature quantum oscillations caused by recurring Bloch states in graphene superlattices. *Science* **2017,** *357* (6347), 181-184.
45. Gorbachev, R. V.; Song, J. C. W.; Yu, G. L.; Kretinin, A. V.; Withers, F.; Cao, Y.; Mishchenko, A.; Grigorieva, I. V.; Novoselov, K. S.; Levitov, L. S.; Geim, A. K., Detecting topological currents in graphene superlattices. *Science* **2014,** *346* (6208), 448-451.

46. Bistritzer, R.; MacDonald, A. H., Moiré bands in twisted double-layer graphene. *Proceedings of the National Academy of Sciences* **2011,** *108* (30), 12233-12237.
47. Lopes dos Santos, J. M. B.; Peres, N. M. R.; Castro Neto, A. H., Graphene Bilayer with a Twist: Electronic Structure. *Physical Review Letters* **2007,** *99* (25), 256802.
48. Cao, Y.; Luo, J. Y.; Fatemi, V.; Fang, S.; Sanchez-Yamagishi, J. D.; Watanabe, K.; Taniguchi, T.; Kaxiras, E.; Jarillo-Herrero, P., Superlattice-Induced Insulating States and Valley-Protected Orbits in Twisted Bilayer Graphene. *Physical Review Letters* **2016,** *117* (11), 116804.
49. Brihuega, I.; Mallet, P.; González-Herrero, H.; Trambly de Laissardière, G.; Ugeda, M. M.; Magaud, L.; Gómez-Rodríguez, J. M.; Ynduráin, F.; Veuillen, J. Y., Unraveling the Intrinsic and Robust Nature of van Hove Singularities in Twisted Bilayer Graphene by Scanning Tunneling Microscopy and Theoretical Analysis. *Physical Review Letters* **2012,** *109* (19), 196802.
50. Luican, A.; Li, G.; Reina, A.; Kong, J.; Nair, R. R.; Novoselov, K. S.; Geim, A. K.; Andrei, E. Y., Single-Layer Behavior and Its Breakdown in Twisted Graphene Layers. *Physical Review Letters* **2011,** *106* (12), 126802.
51. Fischer, A.; Goodwin, Z. A. H.; Mostofi, A. A.; Lischner, J.; Kennes, D. M.; Klebl, L., Unconventional superconductivity in magic-angle twisted trilayer graphene. *npj Quantum Materials* **2022,** *7* (1), 5.
52. Wang, X.; Yasuda, K.; Zhang, Y.; Liu, S.; Watanabe, K.; Taniguchi, T.; Hone, J.; Fu, L.; Jarillo-Herrero, P., Interfacial ferroelectricity in rhombohedral-stacked bilayer transition metal dichalcogenides. *Nature Nanotechnology* **2022,** *17* (4), 367-371.
53. Zheng, Z.; Ma, Q.; Bi, Z.; de la Barrera, S.; Liu, M.-H.; Mao, N.; Zhang, Y.; Kiper, N.; Watanabe, K.; Taniguchi, T.; Kong, J.; Tisdale, W. A.; Ashoori, R.; Gedik, N.; Fu, L.; Xu, S.-Y.; Jarillo-Herrero, P., Unconventional ferroelectricity in moiré heterostructures. *Nature* **2020,** *588* (7836), 71-76.
54. Yoo, H.; Engelke, R.; Carr, S.; Fang, S.; Zhang, K.; Cazeaux, P.; Sung, S. H.; Hovden, R.; Tsen, A. W.; Taniguchi, T.; Watanabe, K.; Yi, G.-C.; Kim, M.; Luskin, M.; Tadmor, E. B.; Kaxiras, E.; Kim, P., Atomic and electronic reconstruction at the van der Waals interface in twisted bilayer graphene. *Nature Materials* **2019,** *18* (5), 448-453.
55. Quan, J.; Linhart, L.; Lin, M.-L.; Lee, D.; Zhu, J.; Wang, C.-Y.; Hsu, W.-T.; Choi, J.; Embley, J.; Young, C.; Taniguchi, T.; Watanabe, K.; Shih, C.-K.; Lai, K.; MacDonald,

A. H.; Tan, P.-H.; Libisch, F.; Li, X., Phonon renormalization in reconstructed MoS2 moiré superlattices. *Nature Materials* **2021,** *20* (8), 1100-1105.

56. Yang, S.-J.; Jung, J.-H.; Lee, E.; Han, E.; Choi, M.-Y.; Jung, D.; Choi, S.; Park, J.-H.; Oh, D.; Noh, S.; Kim, K.-J.; Huang, P. Y.; Hwang, C.-C.; Kim, C.-J., Wafer-Scale Programmed Assembly of One-Atom-Thick Crystals. *Nano Letters* **2022,** *22* (4), 1518-1524.
57. Gao, L.; Ni, G.-X.; Liu, Y.; Liu, B.; Castro Neto, A. H.; Loh, K. P., Face-to-face transfer of wafer-scale graphene films. *Nature* **2014,** *505* (7482), 190-194.
58. Wang, X.; Zhao, Y.; Kong, X.; Zhang, Q.; Ng, H. K.; Lim, S. X.; Zheng, Y.; Wu, X.; Watanabe, K.; Xu, Q.-H.; Taniguchi, T.; Eda, G.; Goh, K. E. J.; Jin, S.; Loh, K. P.; Ding, F.; Sun, W.; Sow, C. H., Dynamic Tuning of Moiré Superlattice Morphology by Laser Modification. *ACS Nano* **2022,** *16* (5), 8172-8180.
59. Zhou, X.; Yu, G., Preparation Engineering of Two-Dimensional Heterostructures via Bottom-Up Growth for Device Applications. *ACS Nano* **2021,** *15* (7), 11040-11065.
60. Li, J.; Liang, J.; Yang, X.; Li, X.; Zhao, B.; Li, B.; Duan, X., Controllable Preparation of 2D Vertical van der Waals Heterostructures and Superlattices for Functional Applications. *Small* **2022,** *18* (22), 2107059.
61. Zhou, J.; Lin, J.; Huang, X.; Zhou, Y.; Chen, Y.; Xia, J.; Wang, H.; Xie, Y.; Yu, H.; Lei, J.; Wu, D.; Liu, F.; Fu, Q.; Zeng, Q.; Hsu, C.-H.; Yang, C.; Lu, L.; Yu, T.; Shen, Z.; Lin, H.; Yakobson, B. I.; Liu, Q.; Suenaga, K.; Liu, G.; Liu, Z., A library of atomically thin metal chalcogenides. *Nature* **2018,** *556* (7701), 355-359.
62. Li, M.-Y.; Shi, Y.; Cheng, C.-C.; Lu, L.-S.; Lin, Y.-C.; Tang, H.-L.; Tsai, M.-L.; Chu, C.-W.; Wei, K.-H.; He, J.-H.; Chang, W.-H.; Suenaga, K.; Li, L.-J., Epitaxial growth of a monolayer WSe2-MoS2 lateral p-n junction with an atomically sharp interface. *Science* **2015,** *349* (6247), 524-528.
63. Berger, C.; Song, Z.; Li, T.; Li, X.; Ogbazghi, A. Y.; Feng, R.; Dai, Z.; Marchenkov, A. N.; Conrad, E. H.; First, P. N.; de Heer, W. A., Ultrathin Epitaxial Graphite: 2D Electron Gas Properties and a Route toward Graphene-based Nanoelectronics. *The Journal of Physical Chemistry B* **2004,** *108* (52), 19912-19916.
64. Emtsev, K. V.; Bostwick, A.; Horn, K.; Jobst, J.; Kellogg, G. L.; Ley, L.; McChesney, J. L.; Ohta, T.; Reshanov, S. A.; Röhrl, J.; Rotenberg, E.; Schmid, A. K.; Waldmann, D.; Weber, H. B.; Seyller, T., Towards wafer-size graphene layers by atmospheric pressure graphitization of silicon carbide. *Nature Materials* **2009,** *8* (3), 203-207.

65. Davies, A.; Albar, J. D.; Summerfield, A.; Thomas, J. C.; Cheng, T. S.; Korolkov, V. V.; Stapleton, E.; Wrigley, J.; Goodey, N. L.; Mellor, C. J.; Khlobystov, A. N.; Watanabe, K.; Taniguchi, T.; Foxon, C. T.; Eaves, L.; Novikov, S. V.; Beton, P. H., Lattice-Matched Epitaxial Graphene Grown on Boron Nitride. *Nano Letters* **2018,** *18* (1), 498-504.
66. Li, L.; Ma, R.; Ebina, Y.; Fukuda, K.; Takada, K.; Sasaki, T., Layer-by-Layer Assembly and Spontaneous Flocculation of Oppositely Charged Oxide and Hydroxide Nanosheets into Inorganic Sandwich Layered Materials. *Journal of the American Chemical Society* **2007,** *129* (25), 8000-8007.
67. Wang, C.; Sakai, N.; Ebina, Y.; Kikuchi, T.; Snowdon, M. R.; Tang, D.; Ma, R.; Sasaki, T., Three-in-one cathode host based on Nb3O8/graphene superlattice heterostructures for high-performance Li–S batteries. *Journal of Materials Chemistry A* **2021,** *9* (15), 9952-9960.
68. Zhang, J.; Yang, Q.; Cao, H.; Ratcliffe, C. I.; Kingston, D.; Chen, Q. Y.; Ouyang, J.; Wu, X.; Leek, D. M.; Riehle, F. S.; Yu, K., Bright Gradient-Alloyed CdSexS1–x Quantum Dots Exhibiting Cyan-Blue Emission. *Chemistry of Materials* **2016,** *28* (2), 618-625.
69. Wang, C.; He, Q.; Halim, U.; Liu, Y.; Zhu, E.; Lin, Z.; Xiao, H.; Duan, X.; Feng, Z.; Cheng, R.; Weiss, N. O.; Ye, G.; Huang, Y.-C.; Wu, H.; Cheng, H.-C.; Shakir, I.; Liao, L.; Chen, X.; Goddard Iii, W. A.; Huang, Y.; Duan, X., Monolayer atomic crystal molecular superlattices. *Nature* **2018,** *555* (7695), 231-236.
70. Wu, Z.; Liu, J.; Li, Y.; Cheng, Z.; Li, T.; Zhang, H.; Lu, Z.; Yang, B., Self-Assembly of Nanoclusters into Mono-, Few-, and Multilayered Sheets via Dipole-Induced Asymmetric van der Waals Attraction. *ACS Nano* **2015,** *9* (6), 6315-6323.
71. Basu, S.; Chattopadhyay, A., Room-Temperature Delayed Fluorescence of Gold Nanoclusters in Zinc-Mediated Two-Dimensional Crystalline Assembly. *Langmuir* **2019,** *35* (15), 5264-5270.
72. Paul, M.; Basu, S.; Chattopadhyay, A., Complexation Reaction-Based Two-Dimensional Luminescent Crystalline Assembly of Atomic Clusters for Recyclable Storage of Oxygen. *Langmuir* **2020,** *36* (3), 754-759.

Chapter 2

Delayed Dual Emission of Two-Dimensional Copper Nanocluster Assembly

2.1 Abstract:

We report the formation of two-dimensional single crystalline nanosheets of Cu nanoclusters by complexation with Zn metal ion. The so-formed crystals, with augmented prompt photoluminescence and lifetime, exhibited delayed photoluminescence at room temperature with a quantum yield of 83.6 ± 1.3% and a lifetime of 26.4 ± 0.7 μs. The delayed photoluminescence lifetime was further increased to 145.0 ± 7.7 μs by surface functionalization of the nanosheets with 8-hydroxyquinoline. The surface complexation led to the generation of a new emitting channel in the crystal, which thus formed a single nanocomponent with dual channel emitting prompt and delayed near-white light.

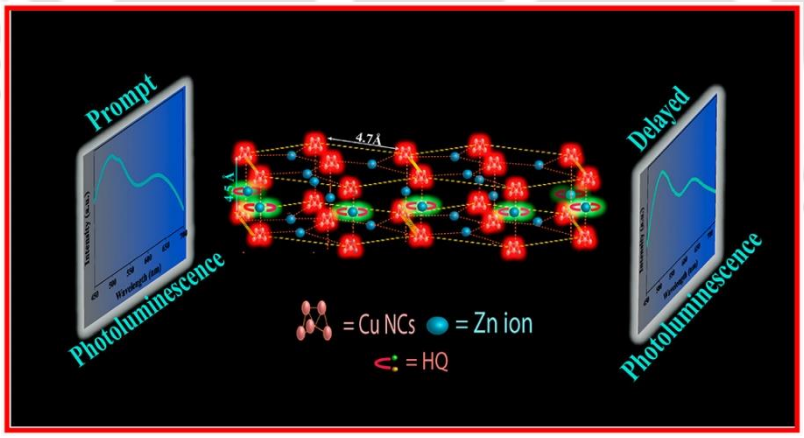

* [Das et al. *The Journal of Physical Chemistry C* **2022,** *126* (2), 997-1005] - Reproduced by permission from the American Chemical Society.

2.2 Introduction:

Nanoclusters (NCs) of coinage metal represent important options for pursuing fundamental studies of nanoscale materials and for realizing their potential practical applications. [1] The precision and reproducibility with which the NCs could be synthesized in liquid media and the established knowledge about their structure and electronic states being correlated to their properties offer advantages that are unique and atomically tunable.[2,3] In that respect, the NCs of Au and Ag have been explored rather extensively especially through the utilization of their photoluminescence and catalytic properties.[4-7] Furthermore, the organic ligands that stabilize the NCs add to the versatility of their properties.[8] In that respect, the NCs of Cu have received scant attention. A reason for this could stem from the instability of Cu(0) due to favorable reduction potential for aerial oxidation (E_0 = −0.34 V). Typical ligands used for stabilizing Ag and Au also do not help in stabilizing the NCs for longer duration under ambient conditions. Thus, the challenge for CuNCs is not only in the synthesis method but also their stabilization under ambient conditions. A way out could be in building well-defined higher order structure out of the ligand-stabilized clusters that would not only bring superior structural specificity but also chemical stability and more importantly selectivity in interactions with small molecules.

Decades-old research have revealed that the physical method of organizing nanoscale materials into higher-dimensional structures requires less stringent consideration about the details of bonding associated with the constituent units. For example, evaporation-induced assembly of AgNCs results in polymorphism with cubic structure, whereas vapor-diffusion-induced assembly resulted in trigonal superstructure.[9] Thus, one could focus more on the nature of the constituent NCs with wide choice of the stabilizing ligands for chemical synthesis in the liquid media. On the other hand, assembly formation through chemical interactions of the outer-shell ligands would require finer understanding of the role of groups and their interactions especially for directed assembly. Importantly, the chemical nature of the atoms constituting the NCs determines the choice of ligands for stabilization (in addition to solvent and other parameters). These have been reflected in the limited growth of the field of assembled atomic clusters. Important examples include aurophilic interaction directed supramolecular assembly of thiolate protected AuNCs into well-defined nanoribbons,[10] hydrophobic interaction mediated supramolecular self-assembly of CuNCs,[11] self-assembly of AgNCs through hydrogen bonding by addition of antisolvent,[12] host–guest interaction assisted assembly of AuNCs,[13] and weak C–H···π and π···π

interactions and strong electrostatic interactions mediated stacking of double nanocluster ionic compounds of Ag and Au.[14] The primary emphasis, however, has been on assembling the NCs based on noncovalent interactions.

Although long-chain organic ligands have been demonstrated to be useful in assembling NCs,[15] however, they may not necessarily be ideal candidates for programmed crystal engineering. An ideal assembly may use smaller ligands where the interactions involving constituent clusters and the functional groups of the ligands would be revealing their potential for practical applications. For example, amino acid stabilized AuNCs when coordinated with zinc ions produced well-defined two and three-dimensional higher order crystalline structures that could be used for chiral recognition, oxygen sensing and hydrogen gas storage and sensing.[16-19] Importantly, the novel photoluminescence properties of the NCs altered by the presence of small molecule analytes, which were due exclusively to the assembled crystals and their structures, with key roles played by both the clusters and the ligands. The early results provide motivation for further pursuit of such metal-ion coordinated crystalline assembly where the correlated properties of the NCs, ligands and the metal ion could be used for chemical sensing, catalysis, biomedical and optoelectronic applications.

The challenging nature of synthesis and stabilization of CuNCs may also hold the potential for dividends in favor of their assembled structures especially crystalline ones. The extraordinary reactivity of small CuNCs when combined with specific small molecule based stabilizing ligands being present in a crystalline assembly formed by using an additional metal ion may be useful for specific and selective chemical reactions of small molecules inside the pores of the assembly. In that respect, in addition to the advantages of three-dimensional (3D) assemblies, two-dimensional (2D) ones may provide unique opportunities. Thus, there is still enough room for pursuing such assemblies of CuNCs.

Herein, we report a new strategy to get augmented physiochemical properties as well as stability from small ligand-stabilized CuNCs, by building ordered crystalline structure of them via an inorganic complexation reaction with Zn metal ion. The so-formed single crystalline 2D nanosheets exhibited room temperature delayed photoluminescence with exceptionally high quantum yield of about 83.6 ± 1.3%. By utilizing the surface unsaturated Zn metal ion of the 2D nanosheets, we were able to synthesize a dual emitting single component nanocompound containing double emission in prompt photoluminescence by surface complexation reaction with HQ. This is probably the first reported single emitting

nanocompound with dual channel emission of any metal nanoclusters holding potential application in LED materials. The dual channel emission in delayed photoluminescence was also attained on changing the concentration of surface complexing agent (i.e., HQ), which may provide future possibilities of making white phosphorescent material from metal nanoclusters.

2.3 Experimental Section:

2.3.1. Materials. Copper(II) nitrate trihydrate (Sigma-Aldrich), 3-mecaptopropanoic acid (MPA, Sigma-Aldrich), 4-mercaptobenzoic acid (MBA, Sigma-Aldrich), zinc acetate dihydrate (Merck), 8-hydroxyquinoline (HQ, Merck), *N*,*N*-dimethylformamide (DMF, Merck), and methanol (Merck) were purchased and used without further purification. Elix-grade water from a Milli-Q purification system was used for the experiments.

2.3.2. Synthesis of CuNCs. CuNCs were synthesized at 0 °C temperature by stirring for 30 min 2.4 mL of 10 mM copper nitrate trihydrate aqueous solution with 0.8 mL of 0.11 M MPA, followed by addition of ~6 mg of MBA in 20 mL of DMF solvent. Then the obtained pale-yellow colored solution was kept in refrigerator at 4 °C and used for further experiment. Here both the ligands were used as reducing as well as stabilizing agents.

2.3.3 Synthesis of Zn–CuNCs. First, 1.5 mL H_2O was added to the 1.5 mL of the above prepared solution and then 350 μL of 100 mM of zinc acetate solution was added dropwise, which generated a white dispersion. The dispersion was then centrifuged at 10000 rpm for 10 min and the obtained pellet was redispersed in 1 mL of water for further experiment.

2.3.4. Complexation Reaction of Zn–CuNCs with HQ. Several samples containing 2 mL of H_2O with 500 μL of the dispersed 1 mL solution of Zn–CuNCs was prepared separately. That was followed by the addition of different concentrations of 10 mM HQ solution (in MeOH) followed by centrifugation at 20000 rpm for 15 min. Each of the so-obtained pellets was redispersed in 1 mL of water separately.

2.3.5. Optical Measurements. UV–visible spectra and photoluminescence spectra for all the samples were recorded using the Agilent Cary 100 UV–vis spectrophotometer and the HORIBA FluoroMax-4 spectrofluorimeter, respectively. Fourier-transform infrared spectroscopy (FTIR) analyses were performed using the PerkinElmer (Spectrum Two) FTIR

spectrometer. The pellets used for FTIR spectral recording were prepared by adding the evaporated dry sample to the heat dried KBr.

2.3.6. Transmission Electron Microscopic (TEM) Analysis and Selected Area Electron Diffraction (SAED) Analysis. TEM and SAED of CuNCs and Zn–CuNCs nanosheets were performed in JEOL JEM 2100 and JEOL JEM 2100F at a maximum accelerating voltage of 200 kV. For preparation of TEM samples, appropriately ten times diluted samples of the as-prepared CuNCs and Zn–CuNC nanosheets were drop-cast on carbon-coated copper grids and left overnight for drying. The same TEM experiments involving Zn–CuNCs were also performed on Ni grid.

2.3.7. Atomic Force Microscopic (AFM) Analysis. AFM analysis was performed using Bruker Innova SPM. The samples were prepared by appropriate dilution of the dispersion of Zn–CuNCs nanosheets followed by spin coating on a silicon wafer, which was dried and used for further analysis.

2.3.8. Delayed Photoluminescence Spectra Acquisition. Delayed photoluminescence emission spectra and time-resolved delayed photoluminescence decay spectra were acquired in Horiba Jobin Yvon Fluoromax 4P. Parameters for acquisition of delayed photoluminescence emission spectra were set as follows: time per flash= 61 ms; sample window = 500 s; delay after flash = 50 μs; flash count = 100.

2.3.9. Time-Resolved Photoluminescence Study. Time resolved PL analysis of all the samples were performed in the Life-Spec-II spectrofluorometer (Edinburgh Instrument).Excitation laser of 405 nm and 375 nm were used for CuNCs and Zn-CuNCs respectively.

2.4. Results and Discussion:

2.4.1. Characterization of CuNCs.

Reaction of MPA and MBA with copper nitrate solution in ice cold condition led to the formation of a pale-yellow colored solution in about 30 min. The medium showed photoluminescence with a maximum at 615 nm upon excitation with UV light (λ_{ex} at 405 nm), which indicated the possible formation of luminescent CuNCs (Fig. A.2.1A, Appendix). TEM image of the sample prepared from the medium indicated the presence of particles with size typically less than 2 nm (Fig. A.2.1C, Appendix). The selected area electron diffraction (SAED) pattern exhibited that the particles were devoid of any crystallinity (Fig. A.2.1D,

Appendix). Furthermore, the absence of the characteristic peak of Cu nanoparticles at 560 nm in the UV–vis spectrum discarded the possible formation of larger sized plasmonic nanoparticles (Fig. A.2.1B, Appendix). Electrospray ionization mass spectrometric analysis (ESI) confirmed the presence of Cu_5 species with its matching proper isotopic distributions at *m*/*z* value of 1236.65 (Fig. A.2.2, Appendix). The species was formulated as $[(Cu_5(MPA)_3(MBA)_3 + 2 \text{ solvent}) - H]^-$. The obtained formula matched well with the simulation pattern obtained using m-mass software (Fig. A.2.3, Appendix). FTIR spectrum of the ligand-stabilized NCs revealed the absence of peaks at 2568 and 2556 cm^{-1}, generally attributed to the S–H stretching frequency of MPA and MBA molecules, respectively, thus indicating the Cu–S bond formation (Fig. A.2.4A, Appendix). Time resolved photoluminescence decay study revealed the excited state lifetime of the CuNCs to be 10.8 ± 0.1 ns (Fig. A.2.4B, Appendix). The as-prepared two small ligand-stabilized CuNCs were observed to be luminescent for several days when stored at 4 °C.

2.4.2. Complexation Reaction between CuNCs and Zn^{2+}

Previous works in the laboratory have shown the hierarchical programming of assembled AuNCs through inorganic complexation reaction with Zn metal ion.[20] The interaction of stabilizing ligands with Zn metal ion provided the additional stability by forming crystalline structure. In the present work, the programming of the assembly was successfully pursued with CuNCs to form single crystalline assembly of CuNCs. The complexation reaction was carried out at room temperature, which resulted in white dispersion. The obtained white dispersion showed augmented luminescence intensity (around 14 times higher) with emission maximum at 600 nm when excited at 365 nm (Fig. 2.1A) and increased lifetime (τ = 18.2 ± 0.3 ns) as compared to the NCs (τ = 10.8 ± 0.1 ns) (Fig. A.2.14; Table A.2.1 Appendix). The excitation maximum was shifted to 365 nm (from 405 nm) upon complexation (Fig. 2.1B), which might be related to the delocalization of the π electrons of the ligand MBA when bonded with Zn metal ion. The UV–vis spectrum showed no change following complexation (Fig. 2.1C). Even after purification by centrifugation with several washing, the property of the white dispersion remained the same, which confirmed the successful complexation between Zn^{2+} and CuNCs. The six ligands attached to the NC were possibly bonded through the sulfur moiety of the thiol group (as revealed through the changes in the FTIR spectrum upon cluster synthesis). The carboxylate groups of the ligands were thus free to bond to Zn^{2+} ions through complexation reaction. The FTIR spectral analysis showed blue shift of the peaks─due to carboxylate stretching frequency of the ligands (MPA

and MBA)─occurring at 1696 and 1624 cm^{-1} to 1656 and 1587 cm^{-1} upon binding with the metal ions (Fig. 2.1D). Thus, the complexation might have occurred through bonding between the carboxylate groups of MPA and MBA with Zn^{2+} ion. The complexation reaction was carried out at pH (3.3) of the as-synthesized CuNCs. On the other hand, when the same reaction was carried out at several pH values in the range of 2.0–12.0, the photoluminescence intensity of the product was higher in the pH range of 5–9 (Fig. A.2.11, Appendix). At above pH 5, MPA and MBA might have been bonded to the metal ion through carboxylate anions,[21,22] thus facilitating metal to ligand charge transfer leading to increased emission intensity. On the other hand, at above pH 9, strongly alkaline medium might not have been favorable for complexation reaction. The complexation reaction might have led to assembly formation that also resulted in significant increase in the photoluminescence intensity of the clusters.[16-19,23] The so-formed assembly would lead to restriction in the motion of the ligands bound to the NCs thus reducing nonradiative energy transfer, thereby increasing the luminescence intensity and lifetime. The selected area electron diffraction pattern of Zn–CuNCs (Fig. A.2.16, Appendix) produced a diffraction pattern of distance 2.5 Å, which matches well with the reported bond distance of Cu(0)–Cu(0) in Cu_5 that lies between 2.3 and 2.5 Å.[24] The results confirmed the presence of Cu(0) in Zn–CuNCs. Additional photophysical parameters of Zn-CuNCs have been calculated and presented in Table A.2.4 in the Appendix.

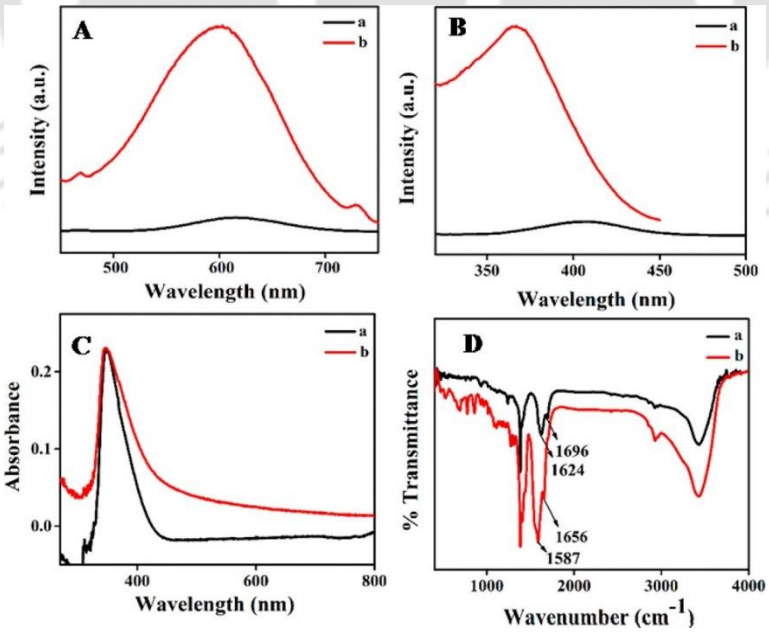

Fig 2.1. (**A**) Emission spectra of (**a**) as synthesized CuNCs and (**b**) Zn–CuNCs (the excitation wavelength was set to 365 nm). (**B**) Excitation spectra of (**a**) as synthesized CuNCs and (**b**) Zn–CuNCs (the emission wavelength was set to 600 nm). (**C**) UV–vis spectra of (**a**) as-synthesized CuNCs and (**b**) Zn–CuNCs. (**D**) FTIR spectra of (**a**) as-synthesized CuNCs and (**b**) Zn–CuNCs.

2.4.3. Single Crystalline Two-Dimensional Nanosheets of Zn–CuNCs

Transmission electron microscopy (TEM) images of the centrifuged white dispersion of Zn complexed CuNCs revealed the formation of 2D nanosheet like structures. Those nanosheets were found to be forming multilayer structures of dimensions ranging from 350 to 700 nm (edge lengths in 2D) (Fig. 2.2(A,B)). Single crystalline nature of the nanosheets was observed in the selected area electron diffraction (SAED) measurements (Fig. 2.2(C,D)). The edge length of each hexagon was calculated to be 4.7 ± 0.2 Å. The growth in the direction of *z* axis generated the diffraction of rectangular pattern with nearly same dimension of 4.5 ± 0.2 Å (as found from another diffraction pattern). From TEM analysis, the probable structure of the nanosheets was predicted as the diffraction pattern showed the hexagonal arrangement of the constituent CuNCs with one cluster positioned at the center of the hexagon. Further TEM measurement was also performed using a Ni grid. Scanning transmission electron microscopy with elemental mapping of the sample indicated the presence of copper, in addition to zinc, oxygen, and sulfur (Fig. A.2.10, Appendix) alike the results obtained using Cu grid (Fig. A.2.9, Appendix). Hence, it can be assumed that these hexagons were connected with each other through bonding with Zn metal ion forming the sheet like structure. Importantly, the aromatic ring of MBA might have helped in forming 2D network through π–π interactions.[25] Further, AFM analysis was pursued to confirm the 2D nature of the crystal. The obtained AFM image showed the presence of 2D sheet like structures with wide size distributions (typically 300–700 nm of edge lengths) (Fig. 2.2E). The minimum height distribution of the nanosheets was found to be 4–8 nm of the nanosheets of around 200 nm (Fig. A.2.6, Appendix), while the maximum height distribution was found to be 40–80 nm of the nanosheets of size around 700 nm (Fig 2.2F), which matched well with the TEM images featuring multilayer stacking.

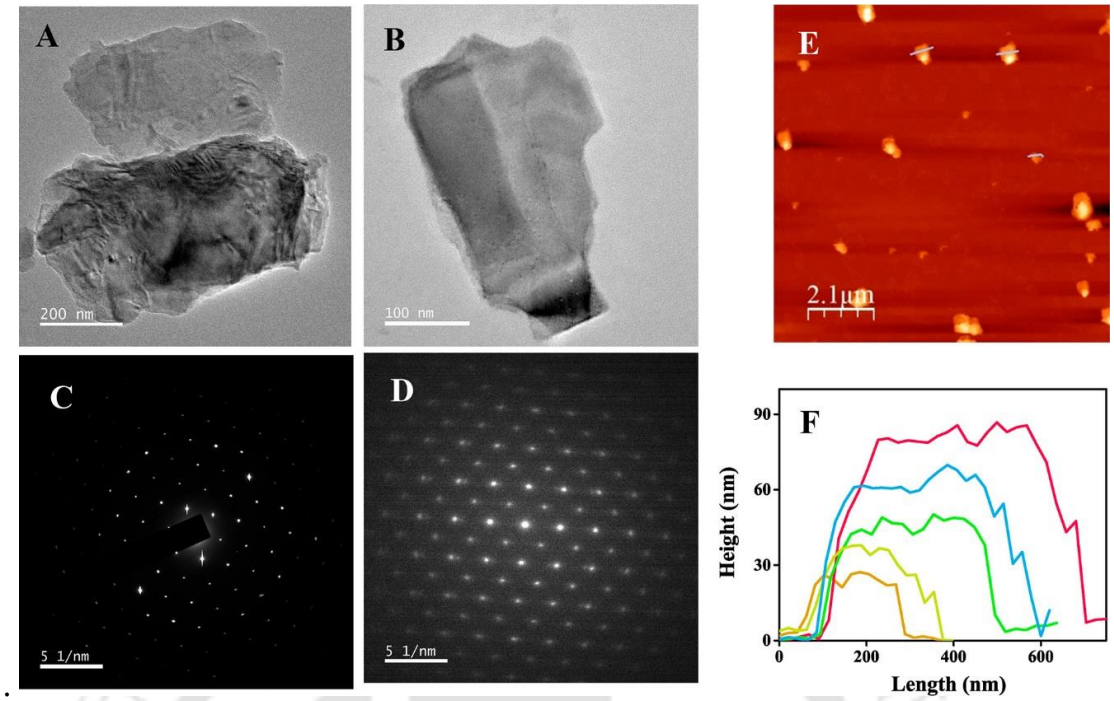

Fig 2.2. (**A, B**) Transmission electron microscopy images of the multilayer stacked sheets of Zn–CuNCs. (**C**, **D**) Selected area electron diffraction patterns of the crystalline 2D assembly of Zn–CuNCs. (**E**) Atomic force microscopy image of Zn–CuNCs featuring the presence of 2D nanosheets. (**F**) Corresponding height profiles of Zn–CuNCs as obtained from part E.

Computational simulation was also done with Avogadro software (Fig. A.2.8, Appendix) to establish a tentative structure of the nanosheets (Fig. 2.3) correlated with SAED analysis. According to the proposed structure, the nanosheets comprised of regular hexagonal arrangement of CuNCs with one additional CuNC positioned at the center in the *XY* plane. The two CuNCs at the apex were connected with the center one through bonding of three MPA ligands (one from each CuNC) with one Zn metal ion. The distance of the side length of the hexagon thus was calculated to be 5.0 ± 0.4 Å, which matched well with the experimentally obtained value in SAED pattern of 4.7 ± 0.2 Å. In the other dimension, each CuNC of the hexagon of one layer was connected with the CuNC positioned below in the lower layered hexagon─through bonding with four MBA ligands (two from each CuNC) with one Zn metal ion, where additional stability was attained by π–π stacking of the aromatic rings in MBA. The so-calculated length of the other dimension was 5.2 ± 0.2 Å, which closely matched with the experimentally obtained value of 4.5 ± 0.2 Å.

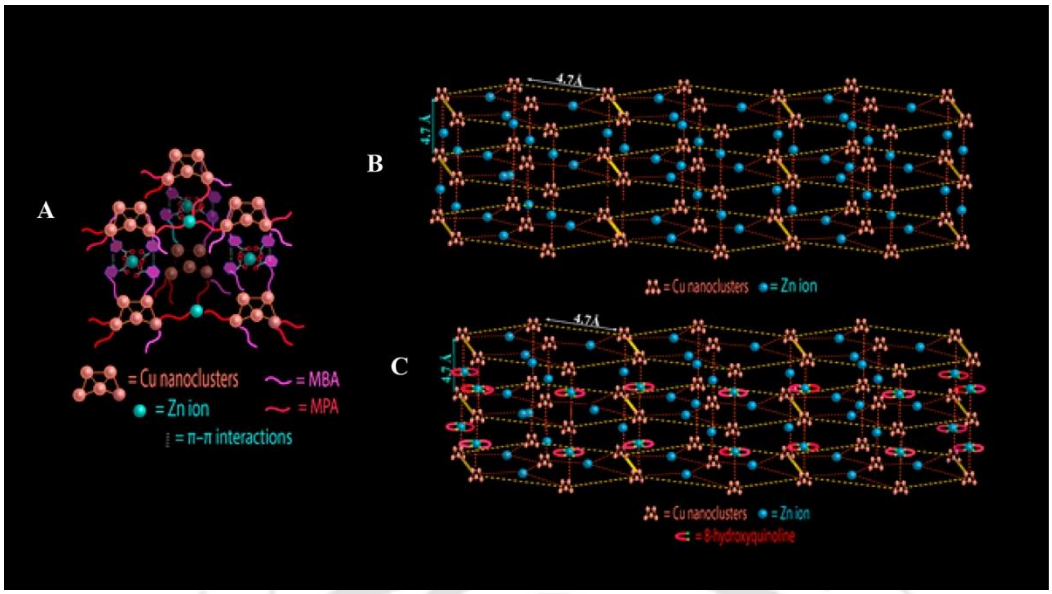

Fig 2.3. (**A**) Schematic representation of the possible bonding modes between MPA and MBA ligand stabilized CuNCs and Zn metal ion. (**B**) Schematic representation of two-dimensional assembly of as synthesized CuNCs following complexation with Zn metal ion. (**C**) Schematic representation of two-dimensional assembly of as synthesized CuNCs following subsequent complexation of Zn metal ion and HQ.

2.4.4. Delayed Photoluminescence with High Quantum Yield

It has been established that 2D or 3D assembly formation of ligand stabilized NCs leads to the augmentation of the photophysical properties as compared to the constituents.[23] However, achievement of novel properties that are not present in the constituent NCs would make the assembly formation more appealing. In the current work, we observed the appearance of room temperature delayed photoluminescence at 615 nm (λ_{ex} at 365 nm) that was absent in the as-synthesized NCs (Fig. A.2.5, Appendix). Delayed photoluminescence is the emission from the same singlet state as in the case of prompt photoluminescence but with much longer lifetime. Emitters with delayed photoluminescence are potential new generation materials for light emitting diodes (LEDs) due to their ability to accommodate electrons in both singlet and triplet states at room temperature,[26,27] and thus are able to provide high luminescent quantum yield up to a reported value of 100%.[28] Quantum dots and rare earth metal complexes are mostly used in LEDs; however, noble metal NCs could potentially replace them especially owing to their environmental friendliness. Very few NCs have been reported to have delayed photoluminescence property.[19,29-30] In this respect,

our discovery of having delayed photoluminescence property in the assembled NCs adds one more important information in designing NC-based LEDs. The synthesized Zn complexed 2D single crystalline CuNCs showed exceptionally high delayed photoluminescence quantum yield of 83.6 ± 1.3% (Table A.2.3, Appendix) and lifetime 26.4 ± 0.7 μs in time-resolved delayed photoluminescence decay measurement with an initial delay of 50 μs. The results are also consistent with measurements in the range of ns to 50 μs (Fig. A.2.15 and Table A.2.5, Appendix). Literature reports suggest that most of the delayed photoluminescent materials contained aromatic groups having delocalized π electrons.[19,31-32] In a recent work, it has been shown that intermolecular π–π interactions could generate a new excited state with lower energy involving interactions of HOMOs and LUMOs of the π systems, which decrease the energy gap between singlet and triplet energy states and stabilize the triplet state.[33] In our system, we have already discussed about the role of π–π interactions in stabilizing the crystal structure. Here, the intermolecular π–π interactions upon complexation─in addition to the restricted intramolecular motions attained upon crystallization─might be attributed to the origin of the delayed photoluminescence in Zn–CuNCs with stabilization of the excited state electrons.

2.4.5. Dual Channel Emission from Single Component Nanocrystal

The approach of multichannel emission from a single component nanoparticle holds an important place in the development of light emitting materials with high quantum yield and better control over the chromaticity index. Several successful complexation reactions of metal NCs with Zn metal ion, leading to a crystalline structure, have already given rise to photophysical and chemical properties that are superior to the component NCs. Further study on modifying that crystal to obtain new property may provide us with better options for applications. One way of achieving such an additional property could be to further functionalize the available unsaturated surface Zn metal ions in the Zn–CuNCs nanosheets with an organic ligand. We have used 8-hydroxy quinoline (HQ) as the organic ligand for functionalization with nanosheet surface Zn metal ion.

Zn^{2+} binds strongly with HQ leading to the formation of ZnQ_2, which is an important inorganic compound for LED material.[34-37] HQ addition to the white dispersion of Zn–CuNCs led to the emergence of a new emission peak at 500 nm (λ_{ex} at 365 nm) and the peak due to Zn–CuNCs appeared at 615 nm. Gradual addition of 0.025 mM, 0.075 mM and 0.125 mM of HQ to the as-prepared Zn–CuNCs enhanced the emission intensity at 500 nm with

simultaneous quenching of the peak at 615 nm (λ_{ex} at 365 nm) (Fig. A.2.7, Appendix). The emission of free ZnQ_2 is reported to be at 550 nm,[38] and that appears at 500 nm when bonded with quantum dot surface upon excitation with 364 nm.[39] Therefore, it can be concluded that ZnQ_2 complex might have been formed on the surface of the nanocrystal creating two independent emitting channels from a single component nanocrystal. To further confirm the formation of ZnQ_2, the HQ added Zn–CuNCs pellet was dispersed in DMSO solvent (ZnQ_2 is reported to be highly soluble in DMSO solvent) and the collected supernatant after centrifugation of the same was analyzed by ^{1}H NMR which showed an upfield shift in the characteristic peak of HQ which is same as obtained in NMR spectrum of free ZnQ_2 (Fig. A.2.13, Appendix). Further the complexation of HQ molecule on the nanosheets was substantiated by IR spectroscopy. The peaks appearing at 642 cm^{-1} (in plane ring deformation), 742 and 822 cm^{-1} (C–H out plane wagging), 1502 and 1471 cm^{-1} (corresponding to both the pyridyl and phenyl groups of ZnQ_2), 1577 cm^{-1} (C–N stretching) supported the complexation of HQ on the surface of the Zn–CuNCs. (Fig. A.2.12, Appendix).[40,41]

The lifetime of the red luminescent CuNCs increased after each of the aforementioned complexation reactions. The prompt photoluminescence lifetime (τ) of the CuNCs changed to 18.2 ± 0.3 ns (Fig. 2.4A) and then to 30.8 ± 0.4 ns (Fig. 2.4B; Table A.2.1,Appendix) from initial lifetime of 10.8 ± 0.1 ns after complexation with Zn metal ion followed by surface complexation with HQ. The delayed photoluminescence lifetime (τ) that originated after reaction with Zn metal ion also increased noticeably from 26.4 ± 0.7 μs to 145.0 ± 7.7 μs (Fig. 2.4(C, D) ; Table A.2.2, Appendix) following surface complexation. This increment can be explained through the reduction of nonradiative transitions due to the restriction of ligands' internal motions through bonding upon complexation, which led to the enhancement of the lifetime of the photoexcited electron.

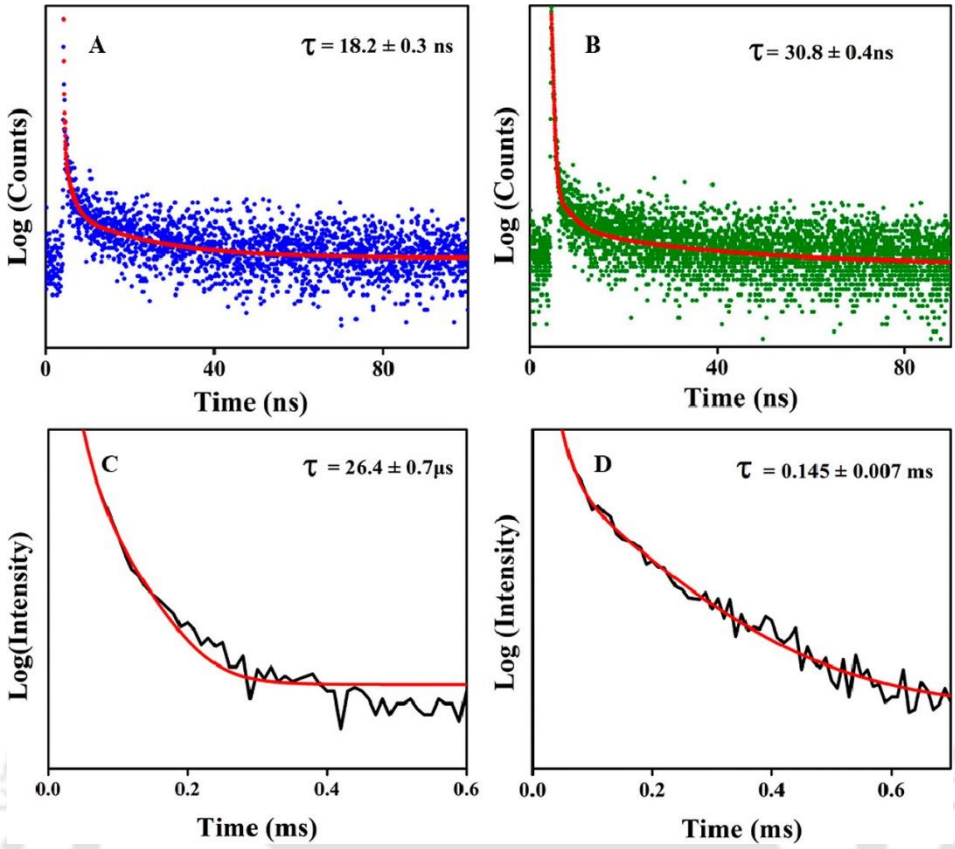

Fig 2.4. Typical time-resolved photoluminescence decay profiles of (**A**) Zn–CuNCs nanosheets and (**B**) 0.1 mM HQ added Zn–CuNCs. Typical time-resolved delayed photoluminescence decay profiles of (**C**) Zn–CuNCs nanosheets and (**D**) 0.1 mM HQ added Zn–CuNCs.

This is probably the first reported strategy of making dual emitting single component crystalline material of assembled metal NCs. The decreased intensity at 615 nm upon addition of HQ, may be attributed to the competitive absorption of the light at the excitation wavelength by both the luminophores. The emission spectra of 0.1 mM HQ added Zn–CuNCs at different excitation wavelength of 360, 370, 380, 390, and 400 nm were obtained (Fig. 2.5A), which gave the chromaticity index values of (0.41, 0.42), (0.39, 0.43), (0.38, 0.43), (0.35, 0.41), and (0.33, 0.40), respectively, thus providing a near white light chromaticity index value at 400 nm excitation wavelength (Fig. 2.5B).

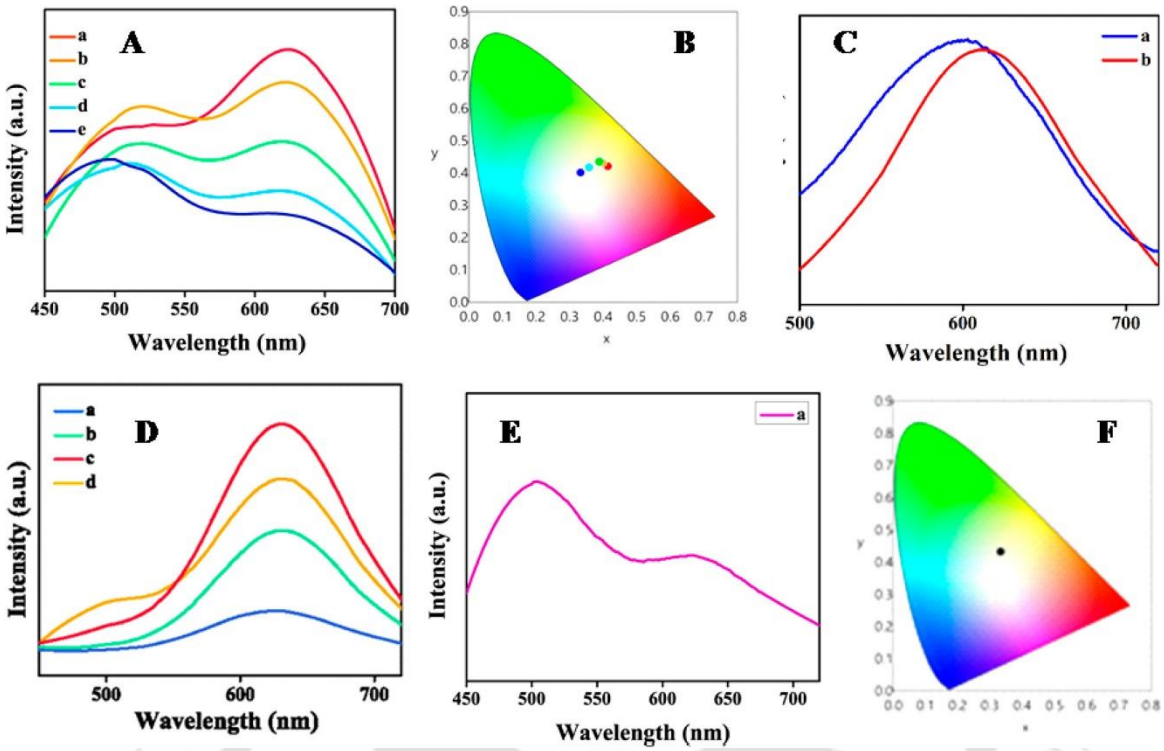

Fig 2.5. (**A**) Prompt photoluminescence spectra and (**B**) corresponding chromaticity color coordinates in CIE diagram of 0.1 mM HQ added Zn–CuNCs at (a) 360, (b) 370, (c) 380, (d) 390, and (e) 400 nm excitation wavelengths. (**C**) (a) Prompt and (b) delayed photoluminescence spectra of Zn–CuNCs (the excitation wavelength was set to 365 nm). (**D**) Delayed photoluminescence spectra of Zn–CuNCs recorded upon addition of (a) 0.05, (b) 0.1, (c) 0.15, and (d) 0.2 mM of HQ. (**E**) Delayed photoluminescence spectrum and (**F**) corresponding chromaticity index in CIE diagram of 0.25 mM HQ added Zn–CuNCs. For parts D and E, the excitation wavelength was set at 365 nm.

The surface attached ZnQ_2 not only have been observed to create an additional emitting channel in the prompt photoluminescence and enhance the luminescence lifetime but also have significant effect on the delayed emission of Zn–CuNCs as well. While the obtained delayed photoluminescence emission spectrum of Zn–CuNCs matched closely with prompt photoluminescence emission spectrum of the same (Fig. 2.5C), the addition of HQ increased the lifetime of the delayed emission of the Zn–CuNCs nanosheets exceptionally (145.0 ± 7.7 μs) with red shift of the peak from 615 to 630 nm. Considering the origin of the emission of CuNCs from the ligand to metal charge transfer, the addition of HQ, which bonded with the surface Zn metal ion attached with the ligands stabilizing the CuNCs

affected the bonding involving metal ion and the ligands, which resulted in a red shift of the emission spectrum.

Delayed photoluminescence materials are considered as the third generation OLED material due to their both singlet-triplet exciton participation efficiency and low toxicity.[42,43] Many white light emitting delayed photoluminescent materials have been reported until date, but most of them are results of mixing of more than one component. Hence synthesis of single white light emitting delayed photoluminescence material is still a major challenge. In our system, the emergence of delayed photoluminescence property in the nanosheet of Zn–CuNCs and then dual emission through surface functionalization had provided us with an opportunity to probe dual channel emission in delayed photoluminescence. It was observed that after a certain concentration of HQ (0.1 mM), further addition of it led to the origin of the emission peak at 500 nm in delayed photoluminescence measurement also, which was proposed as the emission from surface complexed ZnQ_2 (Fig. 2.5D). Initially when lower concentration of ZnQ_2 was used, on the surface of the nanosheets, intermolecular π–π interactions among the aromatic groups of the quinoline parts might not have been favourable. Thus, the additional luminophore on the surface showed its emission in the prompt photoluminescence measurement only. As with increasing amount of ZnQ_2 on the surface with increasing concentration of HQ addition, intermolecular π–π interactions might have become attainable. Thus, the luminophore started showing emission in delayed photoluminescence measurement as well. Hence, the intermolecular π–π interactions along with the restricted intramolecular motions might have played major roles in the origin of the delayed photoluminescence herein. The chromaticity coordinates calculated from the delayed emission spectrum of 0.25 mM HQ added Zn–CuNCs were (0.33, 0.43), which are close to the perfect white light chromaticity coordinate values (0.33, 0.33). Thus, we were able to synthesize a dual channel emitting delayed photoluminescent material, which gave rise to near white light emission (Fig. 2.5 (E,F)).

2.5. Conclusions:

In summary, we have synthesized double ligand stabilized red luminescent CuNCs and assembled them into a single crystalline nanosheets via complexation reaction with Zn metal ion. The so-formed 2D sheets not only gave enhanced photoluminescence properties but also exhibited delayed photoluminescence at room temperature with exceptionally high quantum yield of 83.6 ± 1.3%. Then through surface functionalization of the nanosheets with HQ, we developed a new dual emitting single component nanomaterial

with enhancement of lifetime to millisecond. The so formed nanomaterial gave near white light emission in both prompt and delayed photoluminescence measurements in combination of the emissions from both the channels. Thus, the strategy opened a new path for future possibilities of modeling white phosphorescent or delayed emitting nanomaterials from photoluminescent metal NCs. This not only may be beneficial in replacing heavy toxic materials in light emitting diodes but also may extend the ambit of application potential of metal NCs.

2.6. Bibliography:

1. Li, D.; Kumari, B.; Makabenta, J. M.; Tao, B.; Qian, K.; Mei, X.; Rotello, V. M., Development of coinage metal nanoclusters as antimicrobials to combat bacterial infections. *J. Mater. Chem. B* **2020,** *8* (41), 9466-9480.

2. Jin, R.; Zeng, C.; Zhou, M.; Chen, Y., Atomically Precise Colloidal Metal Nanoclusters and Nanoparticles: Fundamentals and Opportunities. *Chem. Rev.* **2016,***116* (18), 10346-10413.

3. Du, Y.; Sheng, H.; Astruc, D.; Zhu, M., Atomically Precise Noble Metal Nanoclusters as Efficient Catalysts: A Bridge between Structure and Properties. *Chem. Rev.***2020,** *120* (2), 526-622.

4. Kauffman, D. R.; Alfonso, D.; Matranga, C.; Ohodnicki, P.; Deng, X.; Siva, R. C.; Zeng, C.; Jin, R., Probing active site chemistry with differently charged Au25q nanoclusters (q = −1, 0, +1 *Chem. Sci.* **2014,***5* (8), 3151-3157.

5. Chakraborty, S.; Babanova, S.; Rocha, R. C.; Desireddy, A.; Artyushkova, K.; Boncella, A. E.; Atanassov, P.; Martinez, J. S., A Hybrid DNA-Templated Gold Nanocluster For Enhanced Enzymatic Reduction of Oxygen. *J. Am. Chem. Soc.* **2015,***137* (36), 11678-11687.

6. Yang, X.; Gan, L.; Zhu, C.; Lou, B.; Han, L.; Wang, J.; Wang, E., A dramatic platform for oxygen reduction reaction based on silver nanoclusters. *Chem. Commun.***2014,***50* (2), 234-236.

7. Du, X. L.; Wang, X. L.; Li, Y. H.; Wang, Y. L.; Zhao, J. J.; Fang, L. J.; Zheng, L. R.; Tong, H.; Yang, H. G., Isolation of single Pt atoms in a silver cluster: forming highly efficient silver-based cocatalysts for photocatalytic hydrogen evolution. *Chem. Commun.* **2017,***53* (68), 9402-9405.

8. Chen, D.; Li, J., Ultrasmall Au nanoclusters for bioanalytical and biomedical applications: the undisclosed and neglected roles of ligands in determining the nanoclusters' catalytic activities. *Nanoscale Horiz.* **2020,***5* (10), 1355-1367.

9. Nag, A.; Chakraborty, P.; Bodiuzzaman, M.; Ahuja, T.; Antharjanam, S.; Pradeep, T., Polymorphism of Ag29(BDT)12(TPP)43− cluster: interactions of secondary ligands and their effect on solid state luminescence. *Nanoscale* **2018,***10* (21), 9851-9855.

10. u, Z.; Du, Y.; Liu, J.; Yao, Q.; Chen, T.; Cao, Y.; Zhang, H.; Xie, J., Aurophilic Interactions in the Self-Assembly of Gold Nanoclusters into Nanoribbons with Enhanced Luminescence. *Angew. Chem. Int. Ed.***2019,***58* (24), 8139-8144.

11. Yuan, J.; Liu, Z.; Dong, M.; Wang, L.; Dong, S.; Hao, J., Self-Assembly of Amphiphilic Copper Nanoclusters Driven by Cationic Surfactants. *Langmuir* **2021,***37* (22), 6613-6622.

12. Xie, Z.; Sun, P.; Wang, Z.; Li, H.; Yu, L.; Sun, D.; Chen, M.; Bi, Y.; Xin, X.; Hao, J., Metal–Organic Gels from Silver Nanoclusters with Aggregation-Induced Emission and Fluorescence-to-Phosphorescence Switching. *Angew. Chem. Int. Ed.***2020,***59* (25), 9922-9927.

13. Jiang, T.; Qu, G.; Wang, J.; Ma, X.; Tian, H., Cucurbiturils brighten Au nanoclusters in water. *Chem. Sci.***2020,***11* (13), 3531-3537.

14. He, L.; Gan, Z.; Xia, N.; Liao, L.; Wu, Z., Alternating Array Stacking of Ag26Au and Ag24Au Nanoclusters. *Angew. Chem. Int. Ed.***2019,***58* (29), 9897-9901.

15. Wu, Z.; Liu, J.; Li, Y.; Cheng, Z.; Li, T.; Zhang, H.; Lu, Z.; Yang, B., Self-Assembly of Nanoclusters into Mono-, Few-, and Multilayered Sheets via Dipole-Induced Asymmetric van der Waals Attraction. *ACS Nano* **2015,***9* (6), 6315-6323.

16. Basu, S.; Paul, A.; Chattopadhyay, A., Zinc mediated crystalline assembly of gold nanoclusters for expedient hydrogen storage and sensing. *J. Mater. Chem. A* **2016,***4* (4), 1218-1223.

17. Basu, S.; Paul, A.; Chattopadhyay, A., Zinc-Coordinated Hierarchical Organization of Ligand-Stabilized Gold Nanoclusters for Chiral Recognition and Separation. *Chem. Eur. J* **2017,***23* (38), 9137-9143.

18. Paul, M.; Basu, S.; Chattopadhyay, A., Complexation Reaction-Based Two-Dimensional Luminescent Crystalline Assembly of Atomic Clusters for Recyclable Storage of Oxygen. *Langmuir* **2020,***36* (3), 754-759.

19. Basu, S.; Chattopadhyay, A., Room-Temperature Delayed Fluorescence of Gold Nanoclusters in Zinc-Mediated Two-Dimensional Crystalline Assembly. *Langmuir* **2019,***35* (15), 5264-5270.

20. Basu, S.; Bhandari, S.; Pan, U. N.; Paul, A.; Chattopadhyay, A., Crystalline nanoscale assembly of gold clusters for reversible storage and sensing of CO2via modulation of photoluminescence intermittency. *J. Mater. Chem. C* **2018,***6* (30), 8205-8211.

21. Shambetova, N.; Chen, Y.; Xu, H.; Li, L.; Solandt, J.; Zhou, Y.; Wang, J.; Su, H.; Brismar, H.; Fu, Y., Acid Dissociation of 3-Mercaptopropionic Acid Coated CdSe–CdS/Cd0.5Zn0.5S/ZnS Core–Multishell Quantum Dot and Strong Ionic Interaction with Ca2+ Ion. *J. Phys. Chem. C* **2016,** *120* (6), 3519-3529.

22. Hiramatsu, H.; Osterloh, F. E., pH-Controlled Assembly and Disassembly of Electrostatically Linked CdSe−SiO2 and Au−SiO2 Nanoparticle Clusters. *Langmuir* **2003,** *19* (17), 7003-7011.

23. Huang, H.-Y.; Cai, K.-B.; Talite, M. J.; Chou, W.-C.; Chen, P.-W.; Yuan, C.-T., Coordination-induced emission enhancement in gold-nanoclusters with solid-state quantum yields up to 40% for eco-friendly, low-reabsorption nano-phosphors. *Sci. Rep.* **2019,***9* (1), 4053.

24. Jaque, P.; Toro–Labbé, A., Polarizability of neutral copper clusters. *J. Mol. Model.* **2014,** *20* (9), 2410.

25. Han, L.; Wang, M.; Jia, X.; Chen, W.; Qian, H.; He, F., Uniform two-dimensional square assemblies from conjugated block copolymers driven by π–π interactions with controllable sizes. *Nat. Commun.***2018,** *9* (1), 865.

26. Kim, J. U.; Park, I. S.; Chan, C.-Y.; Tanaka, M.; Tsuchiya, Y.; Nakanotani, H.; Adachi, C., Nanosecond-time-scale delayed fluorescence molecule for deep-blue OLEDs with small efficiency rolloff. *Nat. Commun.***2020,***11* (1), 1765.

27. Tanaka, H.; Shizu, K.; Miyazaki, H.; Adachi, C., Efficient green thermally activated delayed fluorescence (TADF) from a phenoxazine–triphenyltriazine (PXZ–TRZ) derivative. *Chem. Commun.***2012,***48* (93), 11392-11394.

28. Zhang, Q.; Tsang, D.; Kuwabara, H.; Hatae, Y.; Li, B.; Takahashi, T.; Lee, S. Y.; Yasuda, T.; Adachi, C., Nearly 100% Internal Quantum Efficiency in Undoped Electroluminescent Devices Employing Pure Organic Emitters. *Adv. Mater.***2015,***27* (12), 2096-2100.

29. Krause, S.; Cerretani, C.; Vosch, T., Disentangling optically activated delayed fluorescence and upconversion fluorescence in DNA stabilized silver nanoclusters. *Chem. Sci.***2019,***10* (20), 5326-5331.

30. Lin, H. T.; Cai, K. B.; Huang, H. Y.; Lin, T. N.; Shen, J. L.; Lin, C. A. J.; Yuan, C. T., Thermally-activated delayed fluorescence from biocompatible, solid-state gold nanoclusters embedded into ionic-crystal matrices. *J. Lumin.***2017,***187*, 269-273.

31. Salazar, F. A.; Fedorov, A.; Berberan-Santos, M. N., A study of thermally activated delayed fluorescence in C60. *Chem. Phys. Lett.* **1997,***271* (4), 361-366.

32. Li, M.; Liu, Y.; Duan, R.; Wei, X.; Yi, Y.; Wang, Y.; Chen, C.-F., Aromatic-Imide-Based Thermally Activated Delayed Fluorescence Materials for Highly Efficient Organic Light-Emitting Diodes. *Angew.Chem.Int. Ed.***2017,***56* (30), 8818-8822.

33. Yang, J.; Zhen, X.; Wang, B.; Gao, X.; Ren, Z.; Wang, J.; Xie, Y.; Li, J.; Peng, Q.; Pu, K.; Li, Z., The influence of the molecular packing on the room temperature phosphorescence of purely organic luminogens. *Nat. Commun.***2018,***9* (1), 840.

34. Sapochak, L. S.; Benincasa, F. E.; Schofield, R. S.; Baker, J. L.; Riccio, K. K. C.; Fogarty, D.; Kohlmann, H.; Ferris, K. F.; Burrows, P. E., Electroluminescent Zinc(II) Bis(8-hydroxyquinoline): Structural Effects on Electronic States and Device Performance. *J. Am. Chem. Soc.***2002,***124* (21), 6119-6125.

35. Hopkins, T. A.; Meerholz, K.; Shaheen, S.; Anderson, M. L.; Schmidt, A.; Kippelen, B.; Padias, A. B.; Hall, H. K.; Peyghambarian, N.; Armstrong, N. R., Substituted Aluminum and Zinc Quinolates with Blue-Shifted

Absorbance/Luminescence Bands: Synthesis and Spectroscopic, Photoluminescence, and Electroluminescence Characterization. *Chem. Mater.***1996,***8* (2), 344-351.

36. Hamada, Y.; Sano, T.; Fujita, M.; Fujii, T.; Nishio, Y.; Shibata, K., Organic Electroluminescent Devices with 8-Hydroxyquinoline Derivative-Metal Complexes as an Emitter. *Jpn. J. Appl. Phys.***1993,***32* (Part 2, No. 4A), L514-L515.

37. Donzé, N.; Péchy, P.; Grätzel, M.; Schaer, M.; Zuppiroli, L., Quinolinate zinc complexes as electron transporting layers in organic light-emitting diodes. *Chem. Phys. Lett.***1999,***315* (5), 405-410.

38. Khaorapapong, N.; Ogawa, M., Solid-state intercalation of 8-Hydroxyquinoline into Li(I)-, Zn(II)- and Mn(II)-montmorillonites. *Appl. Clay Sci.* **2007,***35* (1), 31-38.

39. Bhandari, S.; Roy, S.; Pramanik, S.; Chattopadhyay, A., Double Channel Emission from a Redox Active Single Component Quantum Dot Complex. *Langmuir* **2015,***31* (1), 551-561.

40. Roy, S.; Bhandari, S.; Chattopadhyay, A., Quantum Dot Surface Mediated Unprecedented Reaction of Zn2+ and Copper Quinolate Complex. *J. Phys. Chem. C* **2015,** *119* (36), 21191-21197.

41. Bhandari, S.; Roy, S.; Chattopadhyay, A., Enhanced photoluminescence and thermal stability of zinc quinolate following complexation on the surface of quantum dots. *RSC Adv.* **2014,** *4* (46), 24217-24221.

42. Wong, M. Y.; Zysman-Colman, E., Purely Organic Thermally Activated Delayed Fluorescence Materials for Organic Light-Emitting Diodes. *Adv. Mater.* **2017,***29* (22), 1605444.

43. Liu, Y.; Li, C.; Ren, Z.; Yan, S.; Bryce, M. R., All-organic thermally activated delayed fluorescence materials for organic light-emitting diodes. *Nat. Rev. Mater.***2018,***3* (4), 18020.

Appendix

A.2 Chapter 2

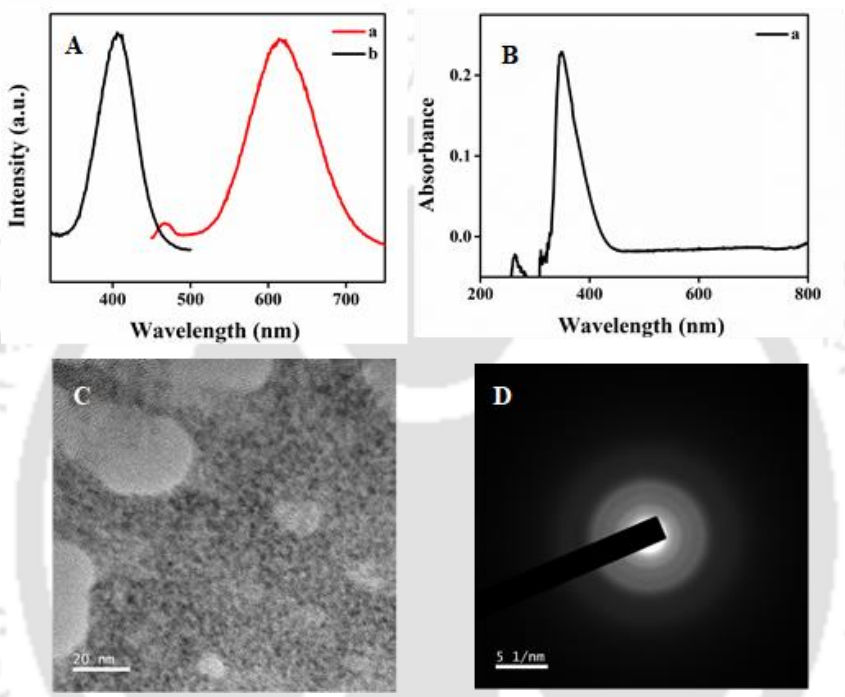

Fig. A.2.1. (A) (a) Emission (excitation wavelength was set at 405 nm) and (b) excitation spectra (emission wavelength was set at 615 nm) of the as-synthesized Cu nanoclusters (CuNCs). (B) UV-Vis spectrum of the CuNCs. (C) Transmission electron microscopy (TEM) image of the CuNCs. (D) Selected area electron diffraction (SAED) pattern acquired on a typical area shown in image C.

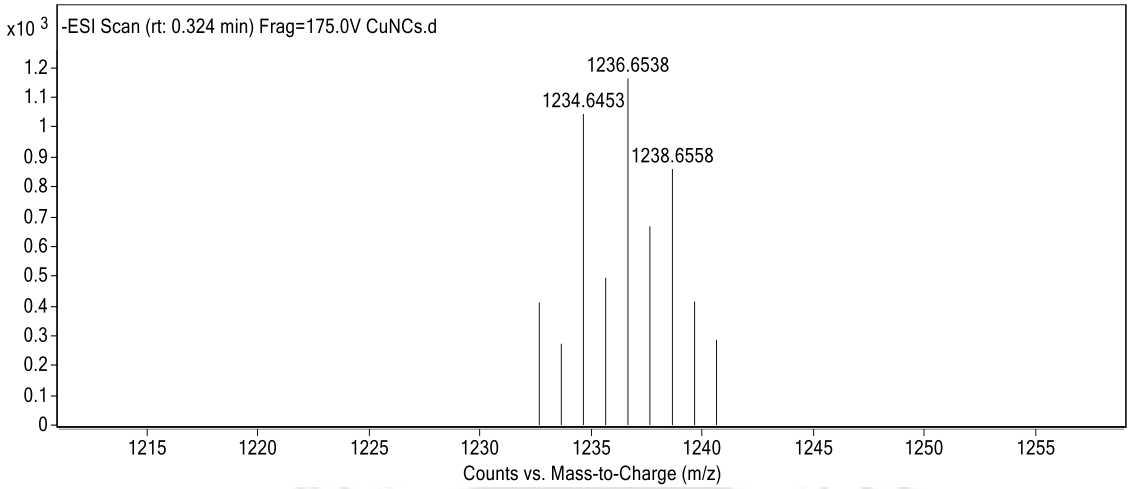

Fig. A.2.2 Isotopic distribution pattern of experimentally obtained mass spectrum of CuNCs at m/z value of 1236.65..

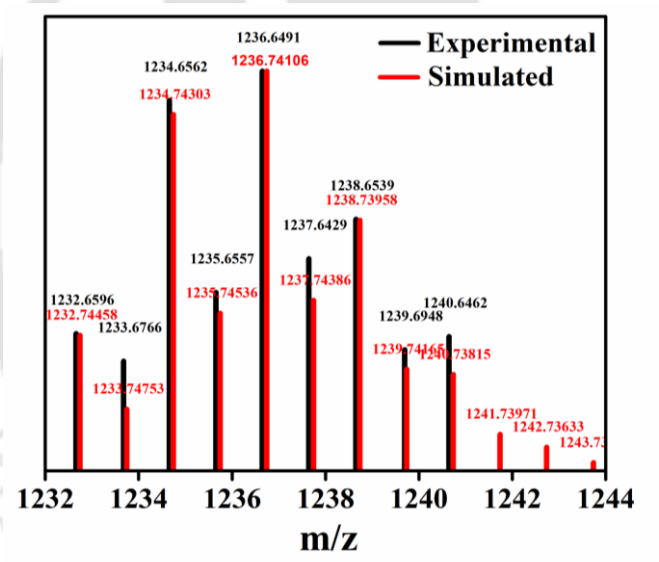

Fig. A.2.3. Overlapping of simulated and experimental isotopic mass distribution spectra of as-synthesized CuNCs at m/z value of 1236.65.

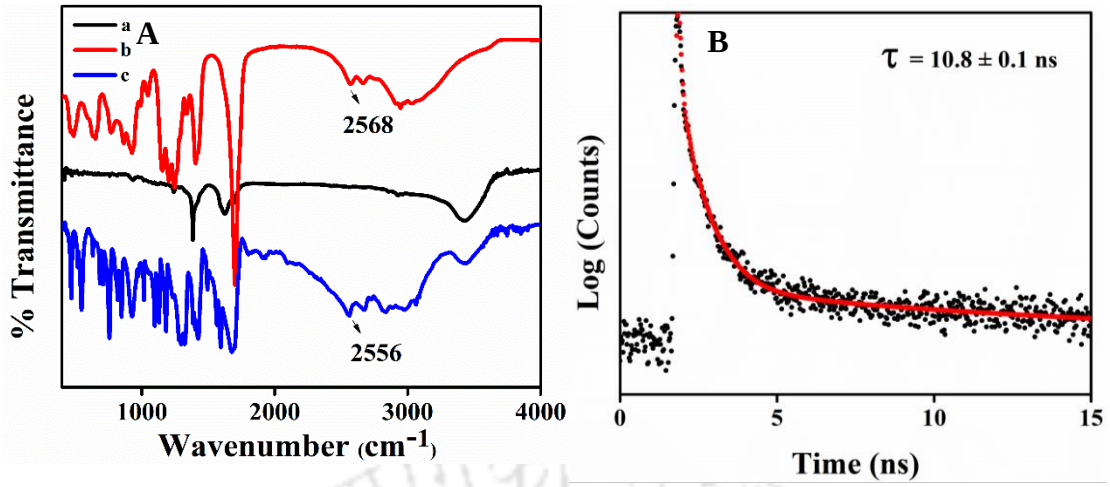

Fig A.2.4. (A) FTIR spectra of (a) MPA, (b) as synthesized CuNCs and (c) MBA. (B) Typical time-resolved photoluminescence decay profile of the as-synthesized CuNCs.

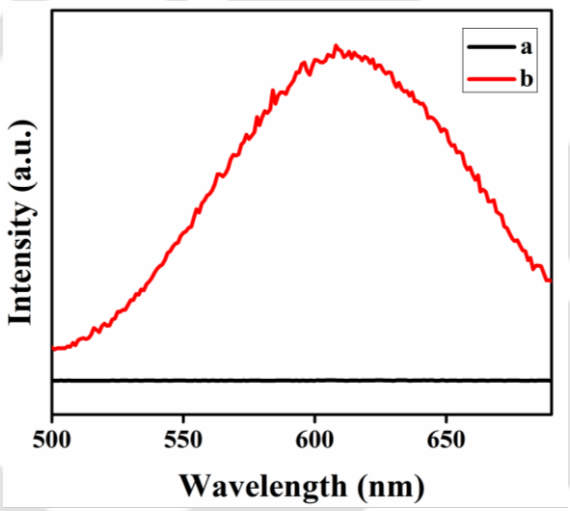

Fig A.2.5. Delayed photoluminescence spectra of (a) CuNCs and (b) that of Zn-CuNCs. The excitation wavelength was set at 365 nm.

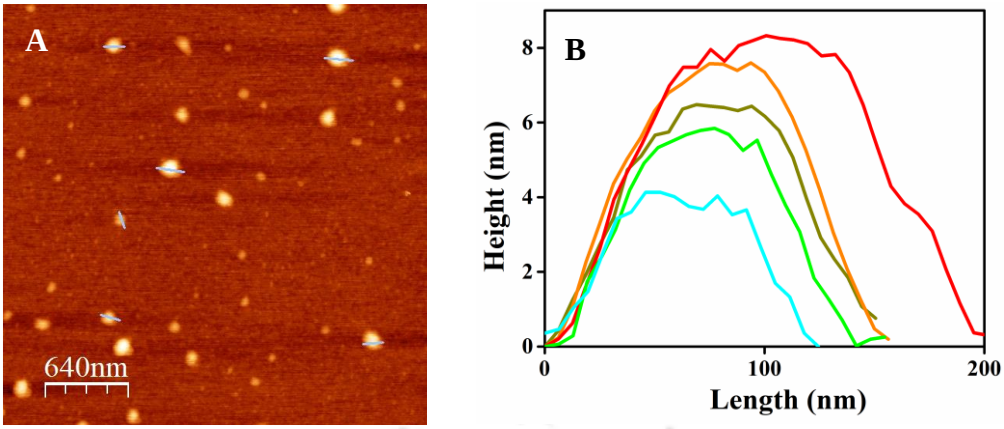

Fig A.2.6. (A) AFM image of Zn-CuNCs featuring the presence of 2D nanosheets. (B) Corresponding height profiles of Zn-CuNCs as obtained from A.

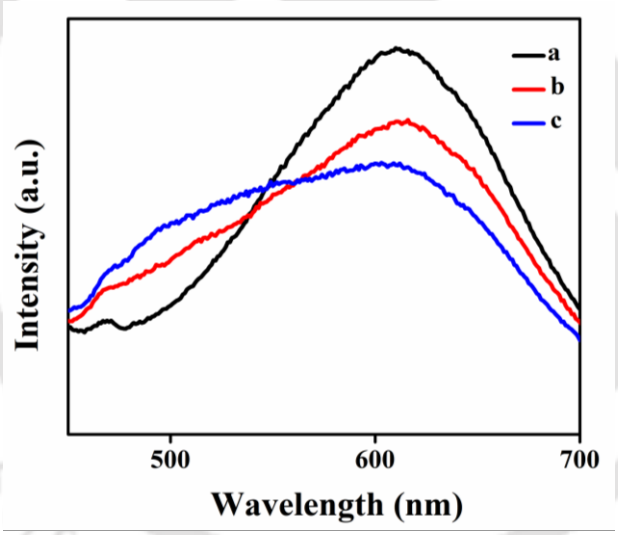

Fig. A.2.7. Prompt photoluminescence spectra of Zn-CuNCs upon addition of (a) 0.025 mM, (b) 0.075 mM and (c) 0.125 mM of HQ.

Table A.2.1. Calculated parameters as-obtained from time-resolved photoluminescence study of CuNCs and Zn-CuNCs .

Sample	CuNCs			Zn-CuNCs			HQ-Zn-CuNCs		
Experiment No	1	2	3	1	2	3	1	2	3
χ^2	1.03	1.02	1.10	1.03	1.03	0.98	1.00	1.04	1.06
First component α_1 (%)	31.48	60.73	16.84	17.96	12.78	11.31	23.42	32.14	20.86
First component lifetime τ_1 (ns)	0.060 (fixed)	0.060 (fixed)	0.110 (fixed)	0.060 (fixed)	0.060 (fixed)	0.060	0.398	0.646	0.445
Second component α_2 (%)	27.77	14.93	15.21	12.96	5.42	6.76	12.53	26.22	10.08
Second component lifetime τ_2 (ns)	0.72	0.74	0.68	1.58	0.58	0.63	3.42	12.97	3.32
Third component α_3 (%)	40.75	24.34	67.95	69.08	81.80	81.92	64.05	41.64	69.06
Third component lifetime τ_3 (ns)	11.15	11.39	11.11	18.25	18.74	18.17	31.96	35.34	31.16
Average lifetime τ_{av} (ns)	10.66	10.84	10.93	17.97	18.69	18.11	31.24	30.79	30.42
Average lifetime with standard error bar τ_{av} (ns)	10.8±0.1			18.2±0.3			30.8±0.4		

Table A.2.2. Calculated parameters as-obtained from time resolved delayed photoluminescence decay study ofZn-CuNCs and HQ-Zn-CuNCs in submillisecondrange.

Sample	Zn-CuNCs			HQ-Zn-CuNCs		
Experiment No	1	2	3	1	2	3
χ^2	0.99	0.99	0.99	0.99	0.99	0.99
First component α_1 (%)	1.86×10^7	1.96×10^7	1.08×10^7	7.36×10^5	2.33×10^6	1.82×10^6
First component lifetime τ_1 (ms)	0.012	0.015	0.015	0.019	0.175	0.027
Second component α_2 (%)	6.97×10^6	2.72×10^6	1.20×10^6	8.78×10^5	2.65×10^6	1.93×10^6
Second component lifetime τ_2 (ms)	0.037	0.051	0.056	0.161	0.026	0.155
Average lifetime τ_{av} (µs)	25.6	26.7	27.0	148.0	152.0	137.0
Average lifetime from three experimental results with standard error bar τ_{av} (µs)	26.4±0.7			145.0 ±7.7		

Quantum Yield Measurement

Delayed photoluminescence quantum yield was measured with respect to bis[2-(4,6-difluorophenyl)pyridinato-C2 ,N]- (picolinato)iridium(III), commonly known as FIRPIC, in acetonitrile solution as a standard phosphor with reported quantum yield (QY) of 60% and prompt photoluminescence quantum yield was measured with respect to quinine sulphate in 0.1 M H_2SO_4 with reported quantum yield of 54% using the following equation-

$$\varphi_S = \varphi_R \times \frac{I_s}{I_R} \times \frac{A_R}{A_S} \times \frac{\eta_S^2}{\eta_R^2} \quad \text{.....Equation S1}$$

Here, φ_S = quantum yield of the sample; φ_R = quantum yield of the reference; I_S = area under the emission spectrum of the sample; I_R = area under the emission spectrum of reference; A_R = absorbance of reference; A_S = absorbance of the sample; η_S = refractive index of the sample solution; η_R = refractive index of reference. Refractive index of water = 1.33 , Refractive index of acetonitrile= 1.34, QY of FIRPIC = 0.6 and QY of quinine sulphate=0.54

Table A.2.3. Parameters obtained from quantum yield measurements.

Type of photoluminescence		Prompt Photoluminescence			Delayed Photoluminescence			
Reference	Area under the PL curve at 365 nm excitation (I_R) (a.u.)	1.80×10^9			4.28×10^7			
	Absorbance at 365 nm (A_R)	0.104			0.105			
Experiment No		1	2	3	1	2	3	4
Sample (Zn-CuNCs)	Area under the PL curve at 365 nm excitation (I_S) (a.u.)	5.79×10^6	3.22×10^6	5.75×10^6	6.18×10^7	6.01×10^7	6.10×10^7	6.81×10^7
	Absorbance at 365 nm (A_S)	0.102	0.110	0.100	0.106	0.102	0.107	0.102
Quantum yield of the sample (φ_S) (%)		0.18	0.09	0.18	84.4	85.0	82.0	83.0
Average quantum yield with standard error bar (%)		0.18±0.05			83.6±1.3			

Table A.2.4. Photophysical parameters of as synthesized Zn-CuNC nanosheets.

Sample (Zn-CuNCs)	**Photo physical parameters**			
Measurements	1	2	3	Average value with standard error bar
Average φ_{PF} (%)	0.18	0.18	0.18	0.18±0.05
τ_{PF} (ns)	18.69	17.97	18.11	18.2±0.3
K_{PF} (s^{-1})	9.6×10^4	10.0×10^4	9.9×10^4	$(9.7 \pm 0.2) \times 10^4$
Average φ_{DF} (%)	83.6	83.6	83.6	83.6±1.3
τ_{DF} (µs)	25.6	26.7	27.0	26.4±0.7
K_{DF} (s^{-1})	3.3×10^4	3.1×10^4	3.1×10^4	$(3.2 \pm 0.1) \times 10^4$

$$\tau_{av} = \frac{\sum_i \alpha_i \tau_i^2}{\sum_i \alpha_i \tau_i} \quad \text{..... Equation S2}$$

$$K_{PF} = \frac{\varphi_{PF}}{\tau_{PF}} \quad \text{..... Equation S3}$$

$$K_{DF} = \frac{\varphi_{DF}}{\tau_{DF}} \quad \text{..... Equation S4}$$

φ_{PF} = Prompt photoluminescence quantum yield

τ_{PF} = Lifetime of prompt photoluminescence

K_{PF} = Radiative rate constant of prompt photoluminescence

φ_{DF} = Delayed photoluminescence quantum yield

τ_{DF} = Lifetime of delayed photoluminescence

K_{DF} = Radiative rate constant of delayed photoluminescence

Average lifetime of prompt and delayed photoluminescence were calculated using equation S2 .Radiative rate constant of prompt and delayed photoluminescence were measured using equation S3 and equation S4.

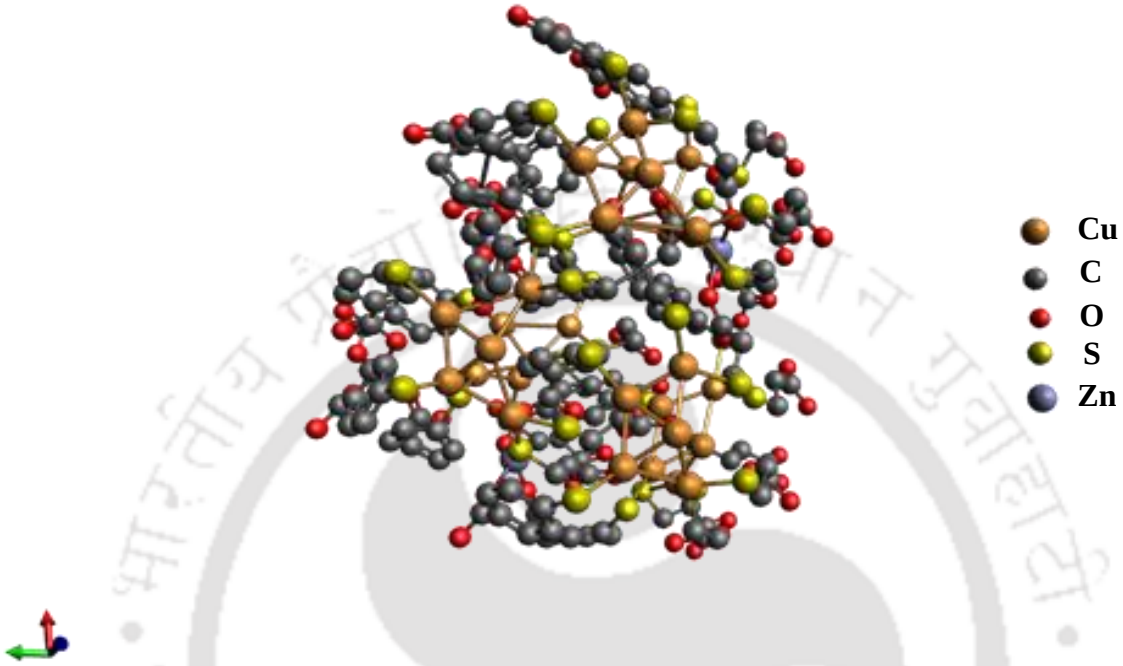

Fig A.2.8. Computationally optimized structure of a unit of Zn-CuNCs calculated using Avogadro.

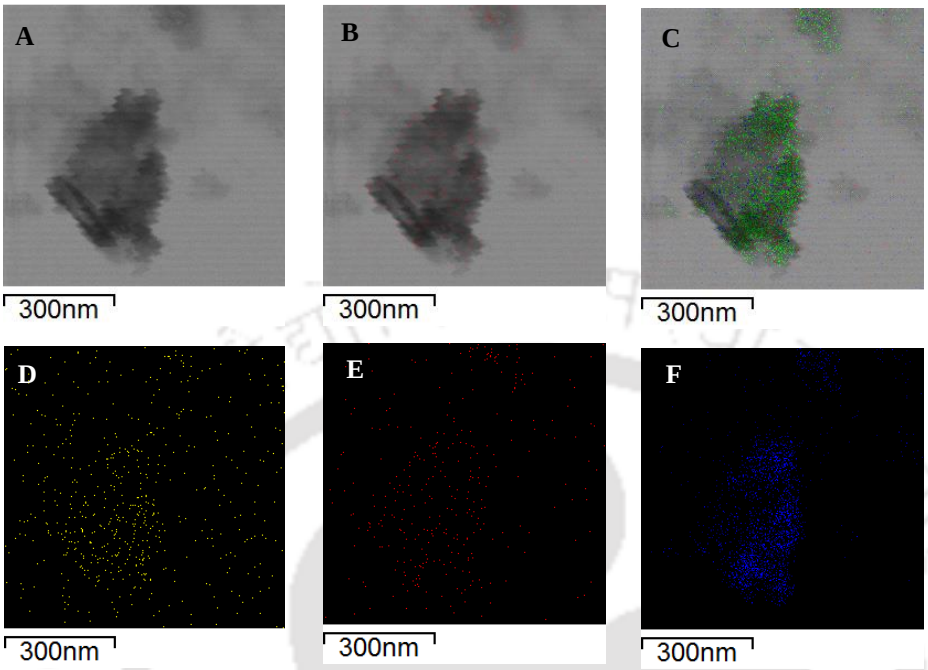

Fig A.2.9. (A-C) STEM images of the product of reaction between MPA and MBA stabilized CuNCs and Zn ions and elemental mapping analysis of (D) Cu, (E) Zn and (F) O performed on Cu grid.

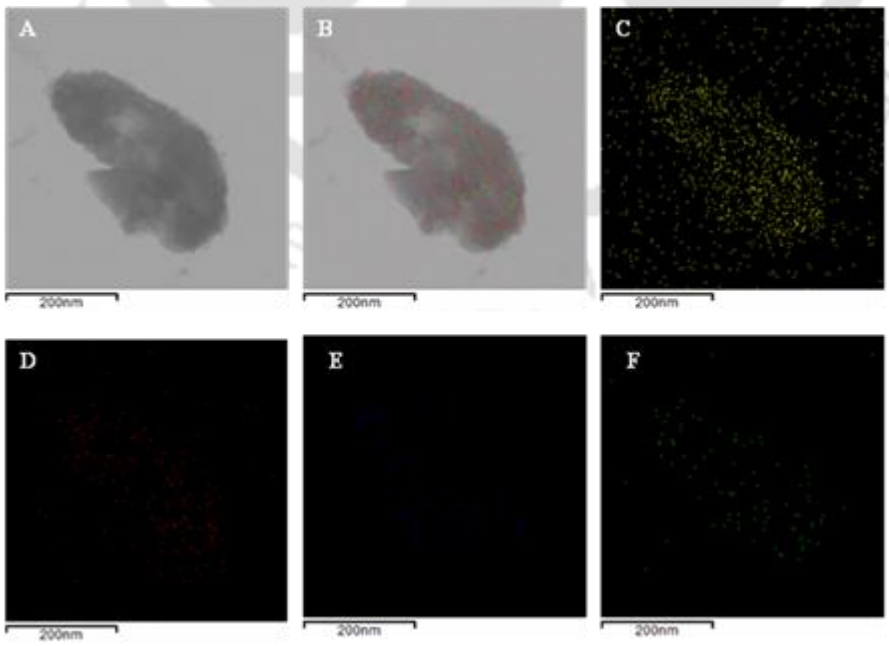

Fig A.2.10: (A-B) STEM images of the product of reaction between MPA and MBA stabilized CuNCs and Zn ions and elemental mapping analysis of (C) Cu, (D) Zn and (E) O (F) S performed on Ni grid.

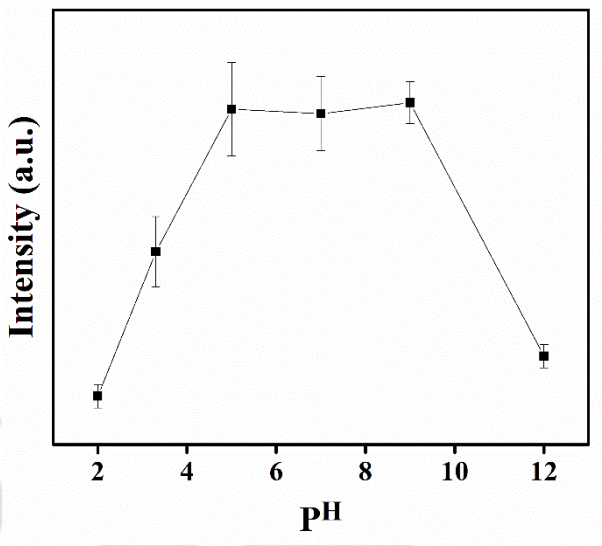

Fig. A.2.11: Photoluminescence intensity of Zn-CuNCs at 600 nm wavelength Vs P^H plot. The excitation wavelength was set at 365 nm.

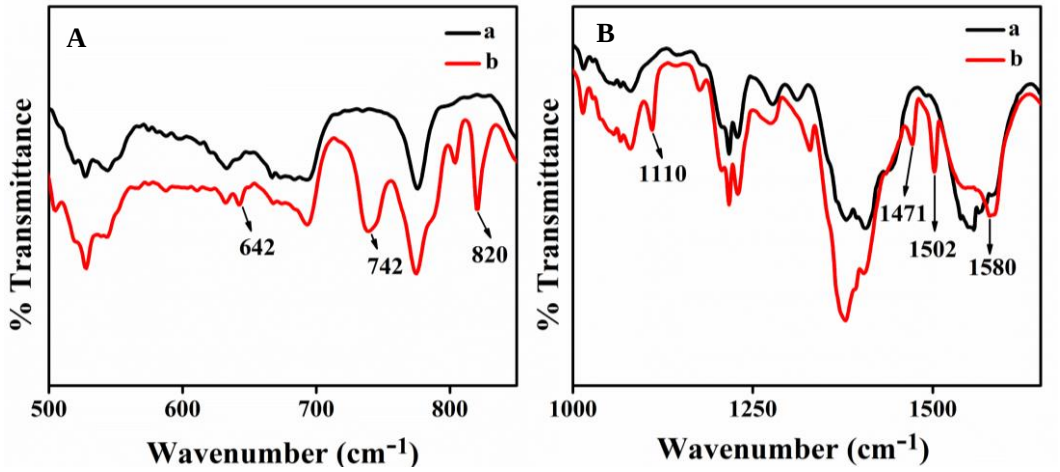

Fig A.2.12: (A) Attenuated total reflectance (ATR) FTIR spectra in the range of 500-800 cm^{-1} and (B) the same spectra in the range of 1000 – 1650 cm^{-1} of (a) Zn-CuNCs and (b) HQ-Zn-CuNCs.

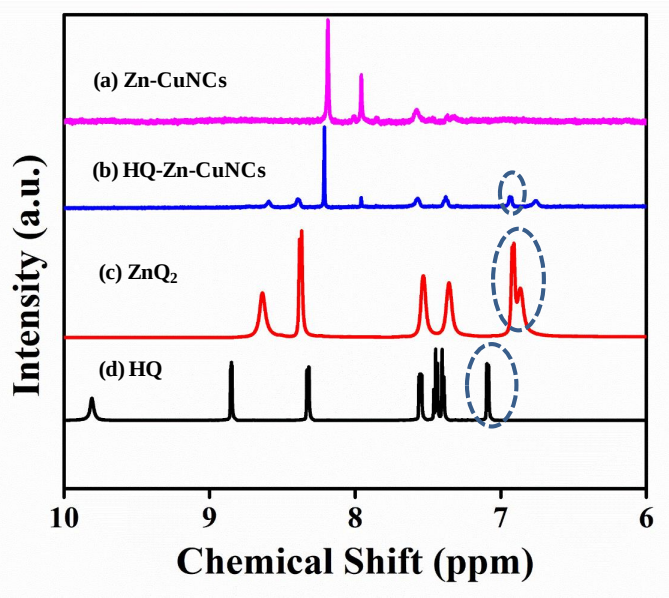

Fig. A.2.13. ^{1}H nuclear magnetic resonance (NMR) spectra of (a) Zn-CuNCs, (b) HQ-Zn-CuNCs, (c) ZnQ_2, and (d) only HQ.

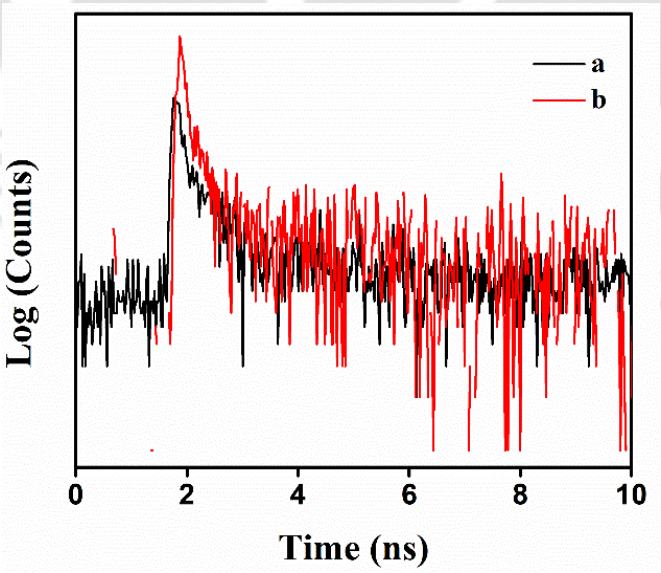

Fig. A.2.14: Time resolved photoluminescence (TRPL) decay profile of (a) as-synthesized CuNCs and (b) Zn-CuNCs in nanoscale range.

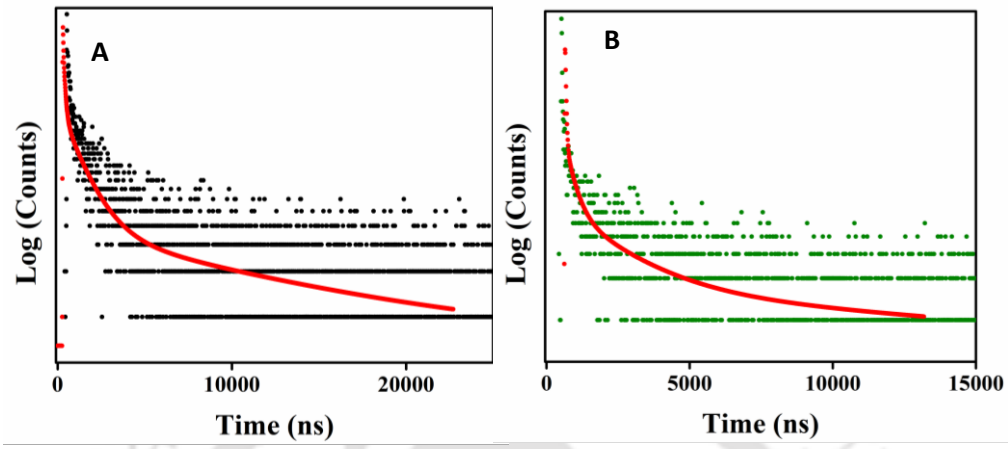

Fig. A.2.15: Time resolved photoluminescence (TRPL) decay profile of (A) Zn-CuNCs and (B) 0.1 mM HQ added Zn-CuNCs in microsecond range (upto 50 µs).

From the fitted parameters (Table S5) of the decay spectrum of Zn-CuNCs in Fig.A.2.15A, one component of 20.33 ns was obtained, which was nearly same as measured before (18.2 ns; Fig. 2.4A), while the microsecond range component of 11.8 µs also matched well with one of the components in decay fitting obtained from decay by delay measurement in the Horiba Jobin Yvon Fluoromax 4P (12 µs; Table A.2.2). For HQ added Zn-CuNCs also, the nanosecond range component was reproduced (30.93 ns; Table A.2.5) and the microsecond range component of 26.5 µs matched with one of the components in decay fitting obtained from decay by delay measurement in the Horiba Jobin Yvon Fluoromax 4P (26 µs; Table A.2.2).

Table A.2.5. Calculated parameters as-obtained from time-resolved photoluminescence study of Zn-CuNCs and HQ-Zn-CuNCs in microsecond region.

Sample	χ^2	First component α_1(%)	First component lifetime τ_1(ns)	Second component α_2(%)	Second component lifetime τ_2(ns)	Third component α_3(%)	Third component lifetime τ_3(ns)	Fourth component α_4(%)	Third component lifetime τ_4(ns)
Zn-CuNCs	0.97	1.63	20.33	8.65	107.12	32.96	1203.46	56.75	11875.47
HQ-Zn-CuNCs	0.99	7.02	307.93	7.60	30.93	15.61	2017.68	69.74	26584.42

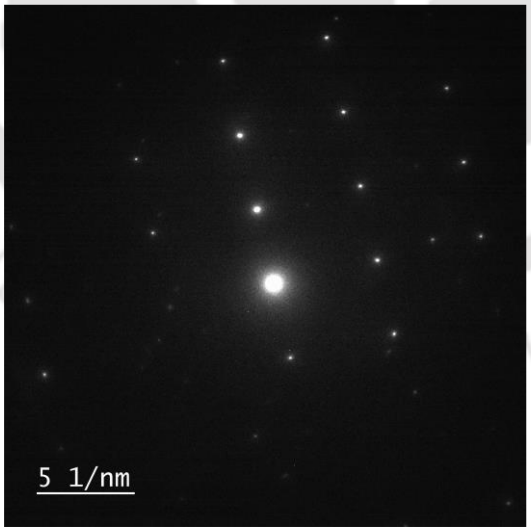

Fig. A.2.16: Surface area electron diffraction (SAED) pattern of as-synthesized Zn-CuNC nanosheets.

Chapter 3

Enhanced Chemical Stability in the Twisted Dodecagonal Stacking of Two-Dimensional Copper Nanocluster Assemblies

3.1 Abstract:

Deterministic chemical stacking of two-dimensional materials with controlled symmetry is a synthetic chemistry challenge that deserves attention. It is plausible that depending on the angle of stacking the material properties of the assembly could be tuned. Herein, we report 30° twisted stacking of two-dimensional nanosheets of a hexagonal assembly of organic ligand-stabilized Cu nanoclusters formed through a Zn^{2+}-mediated complexation reaction. Electron diffraction in transmission electron microscopy revealed the presence of regions of dodecagonal symmetry with the apparent loss of translation symmetry. Photoluminescence measurements indicated the formation of the stacked assembly in the liquid medium. The as-synthesized twisted stacking structure exhibited superior delayed photoluminescence and chemical stability─in the presence of molecular iodine─as compared to the hexagonal crystal. The discovery can lead to a bright future in exploring new chemical and physical properties through the design of stacked assemblies of luminescent or other materials.

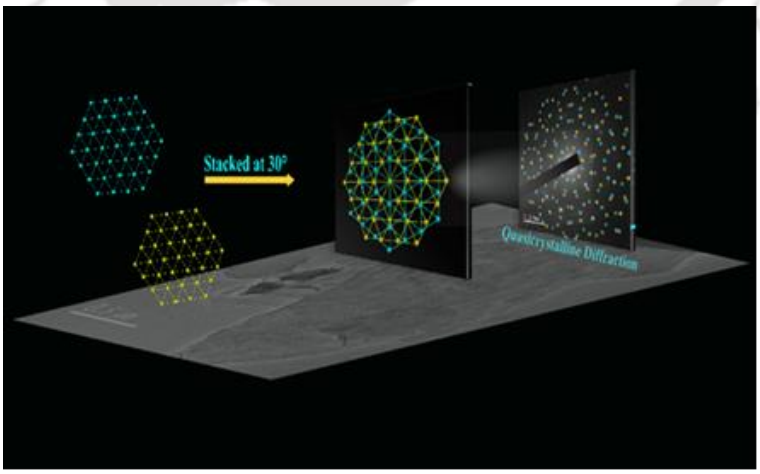

* [Das et al. *The Journal of Physical Chemistry Letters* **2022,** *13* (37), 8793-8800.] - Reproduced by permission from the American Chemical Society.

3.2 Introduction:

The discovery of quasicrystallinity in the Al–Mn alloy brought extraordinary interest in finding new materials that are devoid of translation symmetry but that possess forbidden rotational symmetry.[1] Interestingly, even after nearly four decades, reports on the development of such materials with quasiperiodic symmetry are few and far between. A reason for the impediment could be that such crystals are still very challenging to synthesize using the established principles of chemistry. However, recent results suggest that angular/twisted stacking of two-dimensional crystals with hexagonal symmetry could provide an option in which knowledge of synthetic chemistry may bring new avenues for organizing crystalline quasiperiodicity. For example, twisted bilayer graphene has been reported to generate quasicrystalline symmetry when stacked at a specific angle of 30°.[2] Further, the discovery of superconductivity in magic-angle twisted bilayer and multilayer graphene brings the hope of finding novel properties in materials with similar organization.[3-5] Additionally, twisted multilayered structures in silicene and kagomé sheets in layered intermetallics have revealed their novel electronic and magnetic properties obtained through such stacking.[6-7] Further, ferroelectric properties in twisted $AgBiP_2Se_6$ bilayer, Raman spectra in twisted multilayer graphene, and optical rotation in twisted two-dimensional black phosphorus emphasize the arising of novel physical properties out of twisted two-dimensional materials.[8-10] In this regard, nanoscale particles may be ideal candidates for organization into higher-order structures with well-defined aperiodicity. Thus, there is a strong case in favour of pursuing chemical reaction-based organization of nanoscale structures into quasicrystallinity.

Beyond the metal alloys, a variety of materials such as colloids, polymers, micelles, and nanoparticles were found to exhibit quasiperiodicity when self-assembled into super structures, driven primarily by entropy. For example, slow evaporation of a mixture of binary nanocrystals (Fe_2O_3–Au or PbS–Pd) of controlled size ratios led to aperiodic dodecagonal superlattices as a consequence of general sphere packing.[11] On the other hand, single-component truncated tetrahedral quantum dots with anisotropic patchiness were also observed to have formed a 10-fold symmetric quasicrystalline assembly.[12] Interestingly, mesoporous silica nanoparticles were reported to self-assemble into dodecagonal tiling.[13] It is important to note that the aforementioned aperiodic assemblies leading to the superlattice structures are the result of random tiling of two different components or a single component

capable of adopting different shapes because of its flexibility. What is needed is to develop means of quasicrystalline arrangement of a single component such as those of uniform-sized nanomaterials. As mentioned above, oriented stacking of two-dimensional nanosheets such as graphene could generate quasiperiodic arrangements with important applications.[14-1] For example, twisted stacking of metal organic framework (MOF) nanosheets was observed to form highly ordered mesopores of subnanometer size useful for separation of isomers.[17] Further, a recent simulation study showed the possibility of twisting two hexagonal sheets of single-component colloidal particles at 30° that could generate quasicrystalliniy.[18]

An important example of hierarchical organizations of nanoscale particles into super structures involves atomic nanoclusters, especially those of coinage metal. In this regard, it has been established that ligand-stabilized metal nanoclusters could be crystallized into larger particles based on interactions of the ligand-stabilized nanoclusters. In addition, it has also been reported that ligand-stabilized nanoclusters of Au and Ag could be turned into single-crystalline two-dimensional nanosheets of hexagonal symmetry via complexation reaction with Zn^{2+} ions in liquid media. These nanosheets exhibited novel properties such as storage and sensing of H_2 and CO_2 gases,[19-20] cell-targeted cancer theranostics,[21] recyclable storage of oxygen,[22] chiral recognition and separation, and delayed photoluminescence.[23,24] The above-mentioned observations bring an important question regarding the possibility of organization of the metal nanoclusters into higher-order structures with quasiperiodic arrangements of the constituent clusters and metal ions. In other words, would it be possible to change the reaction conditions such that stacked two-dimensional nanosheets be formed with loss of translation symmetry but with forbidden rotational symmetry?

We report here that indeed it is possible to organize ligand-stabilized atomic nanoclusters into hierarchical two-dimensional nanosheets of quasiperiodic symmetry. In that respect, by suitably changing the reaction conditions, which involves lowering of metal ion concentration added to the reaction medium, the complexation reaction involving the metal ions and ligand-stabilized Cu_5 atomic clusters could be suitably controlled to produce significant population of twisted two-dimensional nanosheets with dodecagonal quasiperiodic lattice having novel optical properties, including enhanced delayed emission lifetime and chemical stability against molecular iodine in the dispersion medium. The results indicated stacking of two-dimensional nanosheets mutually aligned at an angle of 30°/90° in order to

produce nanosheets with translational quasi periodicity having dodecagonal rotational symmetry.

3.3 Experimental Section:

3.3.1 Materials. Copper(II) nitrate trihydrate (SigmaAldrich), 3-mecaptopropanoic acid (MPA, Sigma-Aldrich), 4- mercaptobenzoic acid (MBA, Sigma-Aldrich), zinc acetate dihydrate (Merck), N, N dimethylformamide (DMF, Merck), molecular iodine crystal (Merck) and methanol (Merck) were purchased and used without further purification. Elixgrade water from a Milli-Q purification system was used for the experiments.

3.3.2 Synthesis of CuNCs. Copper nanoclusters were synthesized at 0°C in a round bottom flask containing 20 mL of DMF as solvent, in which 2.4 mL of 10 mM copper nitrate solution and 0.8 mL of 0.11M MPA solution were added and stirred for 5 min, followed by addition of 6 mg of MBA and the mixture solution were kept stirring for another 30 min. The obtained pale yellow coloured CuNCs solution was stored at 4°C for further experiments.

3.3.3 Synthesis of hexagonal Zn-CuNCs. 1.5 mL of as prepared CuNCs solution was added to 1.5 mL of H_2O followed by addition of 350 µL of 100 mM zinc acetate solution resulting in white dispersion. The white pellet was then collected by centrifugation of the dispersion at 10,000 rpm for 10 min and then dispersed in water for further experiments.

3.3.4 Synthesis of quasicrystalline Zn-CuNCs. 200 µL of 100 mM zinc acetate solution was added to 3 mL of the as prepared CuNCs solution and the resulted white dispersion was centrifuged at 10,000 rpm for 10 min. The collected pellet was redispersed in water for further experiments.

3.3.5 Optical measurements. UV-visible spectra and photoluminescence spectra for all the samples were recorded using the Agilent Cary 100 UV−vis spectrophotometer and the HORIBA FluoroMax-4 spectrofluorimeter, respectively. Fourier-transform infrared spectroscopy (FTIR) analyses were performed using the PerkinElmer (Spectrum Two) FTIR spectrometer. The pellets used for FTIR spectral recording were prepared by adding the evaporated dry sample to the heat dried KBr.

3.3.6 Transmission electron microscopic (TEM) analysis and selected area electron diffraction (SAED) analysis. TEM and SAED of CuNCs, hexagonal Zn- CuNCs and quasicrystalline Zn-CuNCs were performed in JEOL JEM 2100 and JEOL JEM 2100F at a maximum accelerating voltage of 200 kV. TEM samples were prepared by diluting the above-

mentioned samples to appropriately ten times and thereafter drop-casting the same on carbon-coated copper grids. The same TEM experiments involving quasicrystalline Zn−CuNCs were also performed on Ni grid.

3.3.7 Delayed photoluminescence spectra acquisition. Delayed photoluminescence emission spectra and time resolved delayed photoluminescence decay spectra were acquired in Horiba Jobin Yvon Fluoromax 4P. Parameters for acquisition of delayed photoluminescence emission spectra were set as follows: time per flash= 61 ms; sample window = 500 μs; delay after flash = 50 μs; flash count = 100.

3.3.8 Time-resolved photoluminescence study. Time resolved PL analysis of all the samples were performed in the Life-Spec-II spectrofluorometer (Edinburgh Instrument). Excitation laser of 405 nm was used for CuNCs and that of 375 nm for both hexagonal nanosheets and twisted quasiperiodic nanosheets of Zn-CuNCs.

3.4 Results and Discussion:

Copper nanoclusters (CuNCs) stabilized by mercaptopropanoic acid (MPA) and mercaptobenzoic acid (MBA) were synthesized according to a reported procedure.[25] The red luminescent CuNCs with emission maximum at 615 nm did not exhibit any characteristic absorption peak of larger sized nanoparticles at 560 nm in the UV–vis spectrum (Fig. A.3.1, Appendix). The particle sizes of the as-synthesized NCs were also found to be less than 2 nm and were devoid of any crystallinity (Fig. A.3.1, Appendix). Thus, the obtained luminescent CuNCs were attributed to $Cu_5(MPA)_3(MBA)_3$ from typical electrospray ionization (ESI) mass spectrometry results given in the Supporting Information (Fig. A.3.2, Appendix). Fourier transform infrared spectroscopy (FTIR) spectrum of the CuNCs also supported the Cu–S bond formation (Fig. A.3.3, Appendix).

The as-synthesized CuNCs were then assembled into two-dimensional structure of hexagonal symmetry via complexation reaction with Zn metal ion (~21 mM) at the molar ratio of Cu:Zn of 1:21.[25] The Zn complexed CuNCs showed significant increment in photoluminescence intensity supporting the crystalline organization of the NCs (Fig. A.3.4A, Appendix). The successful formation of the two-dimensional nanosheet (Fig. A.3.4B, Appendix) exhibited a hexagonal diffraction pattern with lattice constant 4.7 ± 0.2 Å in the selected area electron diffraction pattern (SAED) analysis (Fig. A.3.4C, Appendix). This was

consistent with the proposed hexagonal structure of the Zn-CuNC nanosheets where CuNCs were proposed to be arranged in a continuous hexagonal pattern with one additional CuNC at the center of each hexagon.[25] Further details of structural bonding are presented later. The FTIR spectrum with significant shifts in carboxylate stretching frequencies also supported the probable bond formation between Zn and carboxylate groups of the ligands attached to the NCs (Fig. A.3.5, Appendix).

Interestingly, when we pursued the same complexation reaction with a lower concentration of Zn (~6 mM) with molar ratio of Cu:Zn of 1:6, we obtained a broad emission spectrum (giving near white light) with longer photoluminescence lifetime and higher quantum yield (τ = 42.70 ± 1.34 ns and Φ = (0.18 ± 0.02) %) in comparison with the hexagonal Zn- CuNC nanosheets (τ = 18.35 ± 0.18 ns and Φ = (0.11 ± 0.02) %) (Table. A.3.1 and Table 4.3.2 Appendix). Deconvolution of the spectrum resulted in two components: the minor one with emission maximum at 600 nm similar to the spectrum of the hexagonal Zn-CuNCs given in Fig. A.3.4A, Appendix and the major one with emission maximum at 540 nm (Fig. 3.1A). The new peak at 540 nm suggested the formation of an additional CuNC-based emitting species that might contain closely spaced emitting NCs in the assembly.[26-28] Transmission electron microscopy (TEM) analysis of the product manifested twisted layers without any Moiré pattern generated from only 30° twisted stacking of the nanosheets (Fig. 3.1B). On the other hand, two-dimensional nanosheets with Moiré pattern were also present occasionally, originating from smaller angular twisting of the stacked structures, which were present in sections of the same stacked structures that had angular twisting of 30° (Fig. A.3.6, Appendix). SAED analysis on the overlapping area of two nanosheets of the typical nanosheet in Fig. 3.1B exhibited a complex diffraction pattern that was different from the regular hexagonal diffraction pattern (Fig. 3.1C), while that on the area representing single nanosheet (outside) in Fig. 3.1B exhibited hexagonal diffraction pattern (Fig. A.3.7, Appendix).

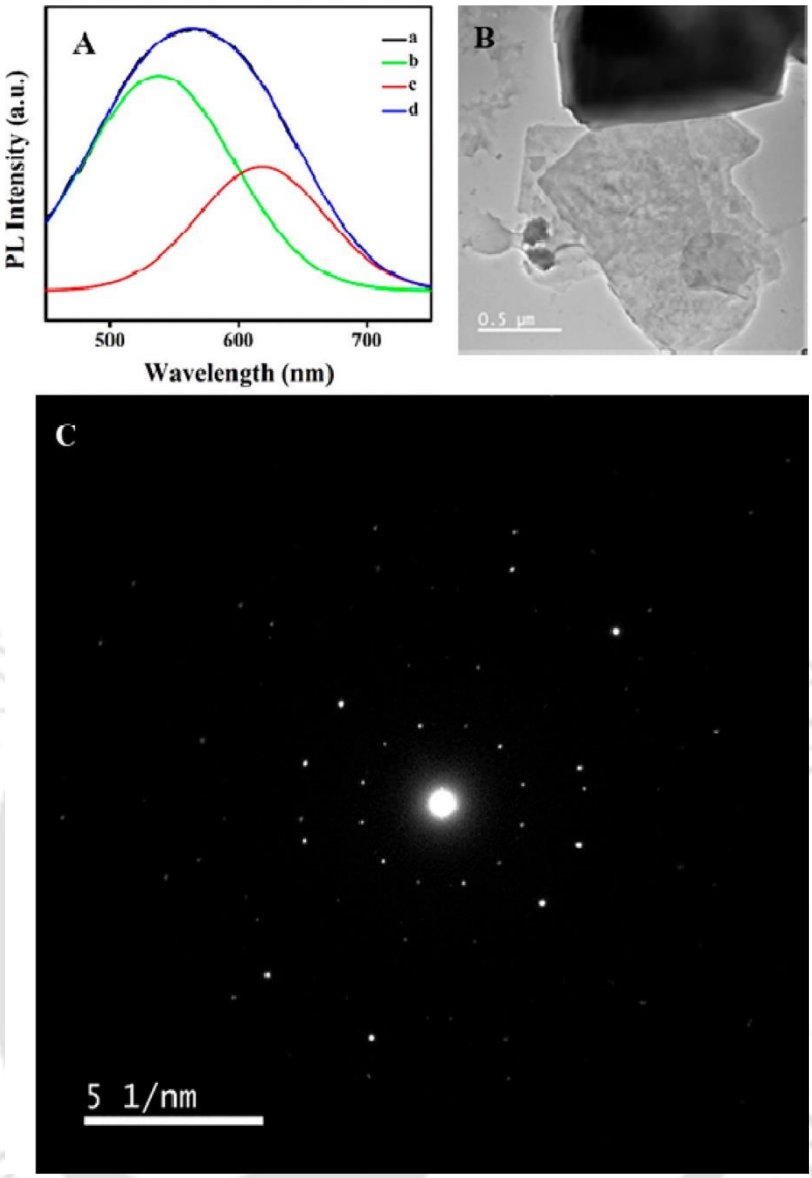

Fig 3.1. (**A**) Photoluminescence emission spectrum of (**a**) twisted quasiperiodic nanosheets of Zn-CuNCs, (**b** and **c**) two Gaussian components obtained on deconvolution of the broad spectrum in trace a and (**d**) cumulative fitted curve. (**B**) Transmission electron microscopy (TEM) image of twisted quasiperiodic nanosheets of Zn-CuNCs and (**C**) a typical selected area electron diffraction (SAED) pattern of the image in panel B.

It is worth noting here that the diffraction with a hexagonal pattern similar to the previous one causing the red emission also was found on separate nanosheets of the same sample, as shown in Fig. A.3.8, Appendix. Analysis of the complex diffraction pattern revealed the presence of 12 diffraction spots separated with equal distance from the center, resulting in 12-fold rotational symmetry (Fig. 3.2A). Additional product images and

corresponding dodecagonal SAED patterns are included in the Supporting Information as Fig.A.3.9, Appendix. This kind of unique diffraction pattern might have resulted from the twisted stacking of nanosheets as observed from the images. Scanning transmission electron microscopy (STEM) with elemental mapping analysis using a sample evaporated on a Ni grid also revealed the presence of Cu with simultaneous existence of Zn, S, and O in the nanosheet (Fig. A.3.10(a,b), Appendix). Atomic force microscopy (AFM) analysis confirmed the presence of two-dimensional nanosheet-like structures with height ranging from 50 to 100 nm and the length varying from 0.8 to 1.2 μm (Fig. A.3.11, Appendix). Further, the twisted nanosheets with quasiperiodic symmetry gave rise to delayed photoluminescence at 540 nm (the same as prompt luminescence; Fig. A.3.12, Appendix) with longer decay lifetime of 87.3 ± 2.5 μs in comparison with that at 600 nm by hexagonal nanosheets (26.0 ± 3.6 μs) (Table A.3.3 and Fig. A.3.12, Appendix).

Attempts to correlate the diffraction lattice with the twisted superposition of nanosheets elucidated that the diffraction pattern of 12-fold rotational symmetry could be accounted for by placing two hexagonal lattices of the same lattice constant (4.7 ± 0.2 Å), one on top of the other and rotated at an angle of 30°/90° against each other (Fig. 3.2B). This type of lattice pattern possessing forbidden 12-fold rotational symmetry without any translational symmetry is termed a dodecagonal quasicrystal. Although the atoms in the quasicrystal are aperiodic, they follow a Fibonacci sequence, in which atoms are radially inflated by a multiplication of a common value, i.e., golden mean ($\tau = 1.618$). In the current diffraction pattern as shown in Fig. 3.2C , the spots in the radial direction followed the Fibonacci sequence with the ratio of two consecutive distances (larger/smaller = ob/oa) calculated to be 1.71 ± 0.05, which is close to the golden mean (τ) (Fig. A.3.13 and Table A.3.4, Appendix). Two-dimensional dodecagonal quasicrystals are comparatively less explored aperiodic system than the three-dimensional one (e.g., icosahedral). Although several works on twisted graphene sheets report the formation of dodecagonal quasicrystal, the lack of a physical method for deterministic production limited the growth of the field of quasicrystal of other materials,[2,14,29] and the quasicrystalline arrangement of soft matter are reported so far is a consequence of self-assembly.

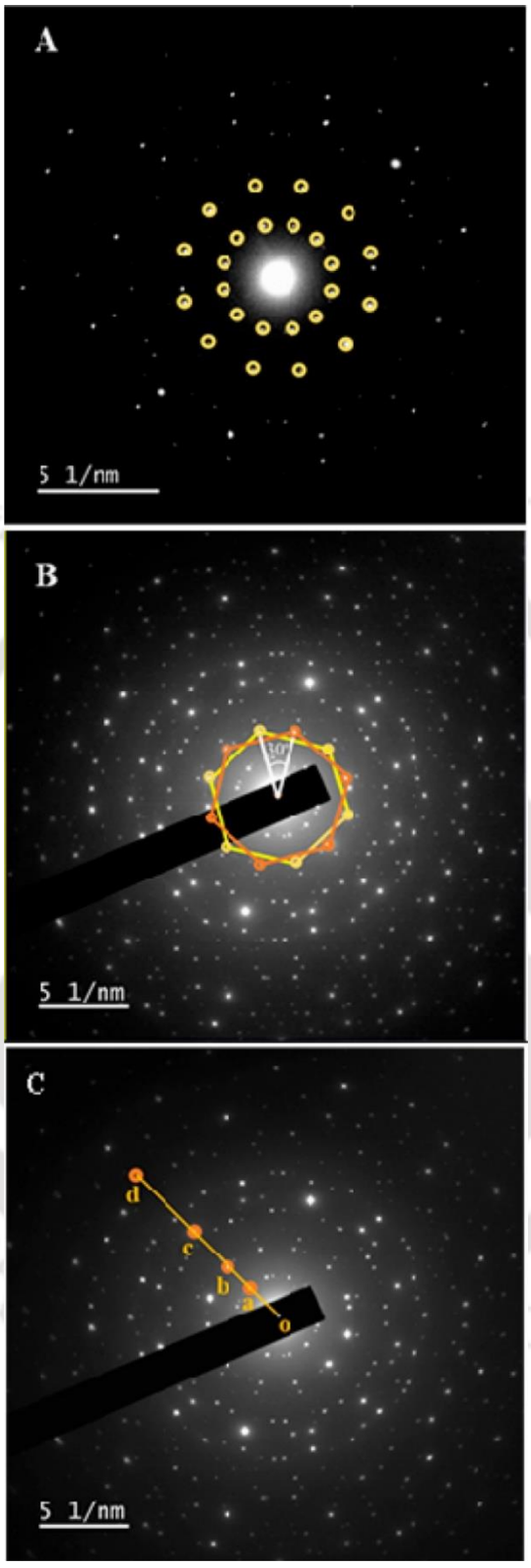

Fig 3.2. Selected area electron diffraction (SAED) pattern images of twisted quasiperiodic nanosheets of Zn-CuNCs depicting (**A**) 12-fold rotational symmetry, (**B**) twisted superimposition of two hexagonal lattices at an angle of 30°, and (**C**) spots following a

Fibonacci sequence of separation distance. The figures along with Fig. 3.1C were recorded under different contrasts/resolutions for the same spot as in Fig. 3.1B.

It has been found that organization of metal nanoclusters stabilized by small ligands through complexation reactions with metal ions mostly leads to the formation of two-dimensional structures, which have been shown to adsorb and desorb gas molecules through surface unsaturated atoms.[22] Interestingly, in a recent work on the complexation of CuNCs with Zn^{2+} ions that resulted in two-dimensional nanosheets, it was shown that the structures could further be functionalized with 8-hydroxyquinoline, thereby suggesting the presence of Zn with unsaturated coordination on the surface.[25]

However, it is also known that there were ligands bound to the NCs but not coordinated to the Zn in the hexagonal nanosheets. This would mean that it is plausible that two hexagonal nanosheets could again react with each other involving Zn^{2+} ions on the surface of one nanosheet and the free ligands dangling from the surface nanoclusters of the other.

Also, the internanosheets reaction could possibly be carried out by varying the concentration of Zn^{2+} ions in the medium. We thus pursued the complexation reaction of the as-synthesized CuNCs with varying concentration of Zn metal ions. It was observed that with the lower concentration of Zn^{2+} ions in the medium (~6 mM), the emission spectrum was broad (Fig. 3.1A), representing two peaks at 600 and 540 nm. On the other hand, at a higher concentration (typically ~21 mM) of Zn^{2+} ions, a sharper emission peak with a maximum at 600 nm appeared (Fig. A.3.4A, Appendix). Further, TEM studies of the evaporated media revealed that when the metal ion concentration was high the complexation reaction produced a nearly exclusive population of hexagonal nanosheets. However, reaction in the presence of a lower concentration of Zn^{2+} ions resulted in the complex diffraction pattern as mentioned above (Fig. 3.1C). It may also be mentioned here that the results of Zn^{2+} ion concentration-dependent complexation reaction revealed that the structures observed in the TEM images most likely were not induced by the evaporation of the solvent. On the other hand, the structures were formed in the media as a result of reactions of Zn^{2+} ions with the ligand-stabilized CuNCs. The photoluminescence results mentioned above also supported the formation of the aforementioned structures in the reaction media.

The regular hexagonal structure of the Zn-CuNC nanosheets was predicted as that following repeating units of six CuNCs with one additional CuNC at the center of the hexagon forming the *xy* plane. Two CuNCs at the apex of each hexagon were connected with the CuNC at the center through bonding with a Zn^{2+} ion with three MPA ligands from each of the three CuNCs in agreement with the lattice constant of 4.7 ± 0.2 Å. Such bonding led to the hexagonal arrangement of both CuNCs and Zn individually at two parallel planes. In the plane perpendicular to the nanosheets (*z* direction), two CuNCs of two consecutive hexagonal layers (*xy* plane) were bonded with additional Zn metal ion─located between the layers─through two MBA ligands, and the corresponding dimension was matched with 4.5 ± 0.2 Å. The bonding in the *z* direction led to the formation of a multilayered nanosheet of hexagonal lattice. However, it has been observed that the further stacking of two such hexagonal nanosheets could be made possible by controlling the concentration of the metal ion used for the complexation reaction. With a lower concentration of Zn metal ion, stacking of two hexagonal nanosheets occurred, thus generating a twisted structure. Complexation of the NCs with several concentrations of Zn metal ion was also examined (Fig. A.3.14, Appendix); however, the twisted stacking with particular rotational angle was observed reproducibly with molar ratio of Cu:Zn of 1:6 and thus was pursued. The obtained dodecagonal diffraction pattern of the two superimposed nanosheets revealed the rotation angle of 30° against each other. The adaption of this typical rotational angle can be elucidated from the bonding of the hexagonal packing of the NCs. Lowering of the metal ion concentration reduced the availability of free Zn^{2+} ions in the medium for further growth of the nanosheets as such. The electron diffraction pattern from the stacking of the nanosheets matched well with the simulated structure of two hexagonal lattices rotated at an angle of 30° that resulted in electron diffraction pattern with 12-fold rotational symmetry (Fig. 3.3(A–C)). As can be observed from the hexagonal arrangement forming nanosheets, the Zn metal ions were positioned at the middle of the two NCs forming an arm of the hexagon but at a plane lower than the NCs (Fig. 3.3D). When the nanosheets were formed under higher metal ion concentrations, the metal ions bonded to the ligands would be the moieties exposed to the medium. The excess Zn^{2+} ions in the medium can easily connect two such nanosheets through vertical coordination as mentioned before. On the other hand, when nanosheets were formed at low Zn^{2+} medium concentration, the organic ligands bound to the CuNCs were exposed to the medium. In order for the stacking of the nanosheets to take place through chemical bonding in the dispersion medium, the Zn^{2+} ions placed immediately below the surface planes of each of the nanosheets can bind to the carboxylate groups of the other sheet. This would be

possible only when the nanosheets are stacked at 30° to each other and the metal ions form tetrahedral coordination with the fourth coordination linking metal ion of one nanosheet with the ligand of the other (Fig. 3.3D). The chemical connectivity among Zn^{2+} and CuNCs (stabilized by the ligands) in both the cases of regular and twisted stacking of hexagonal nanosheets are clearly shown through the schematic representation in Fig. 3.3D. Additionally, the loss of long-range translational symmetry and the appearance of dodecagonal rotational symmetry is depicted in Fig. 3.3E where two nanosheets of hexagonal symmetry were stacked at 30° against each other. Furthermore, analysis of FTIR spectra of both products obtained using high and low concentrations of Zn^{2+} clarified the absence of any new bond formation (Fig. A.3.15, Appendix). Thus, the diffraction pattern (dodecagonal) different from the regular hexagonal one did not arise from a different structure produced in the solution but from the twisted stacking of the nanosheets. Moreover, the proposed connectivity in the twisted structure brought the CuNCs of the two adjacent layers close enough for interatomic interaction in comparison to what it was in the hexagonal stacking, which made the inter-nanocluster distances less than 4.5 ± 0.2 Å. The shorter distance of CuNCs activated the intercluster cuprophilic interaction, which was not initially there in the hexagonal Zn-CuNCs nanosheets because of the larger distances among CuNCs (4.7 and 4.5 Å). Interatomic distances between adjacent clusters have been reported to have an impact on the emission property, and thus, shorter Cu–Cu distances in the assembly would contribute to blue shifting of the emission wavelength. Our observation of the blue shifts in the product with twisted stacking of nanosheets is in consonance with literature reports.[26-28] Moreover, since the fluorescence measurement was performed in the liquid state, it can be also stated firmly that the dodecagonal structure formation here is the chemically driven phenomenon only and not an evaporation-induced one. This aperiodic arrangement of single NCs has opened a path for future modelling of quasiperiodic nanomaterials with novel physical and chemical properties.

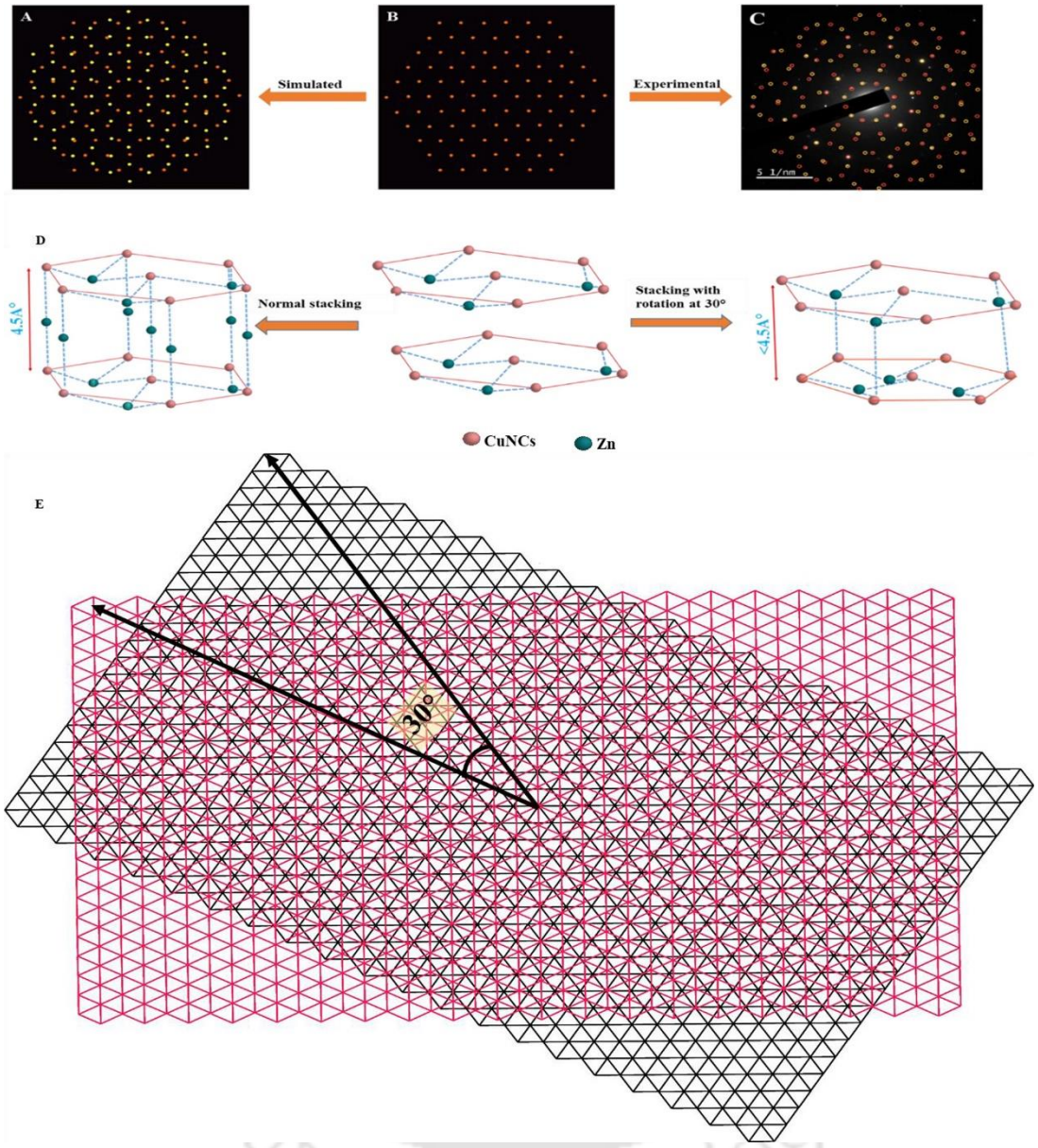

Fig 3.3. Schematic diagram (**A**) representing rotated structure of two hexagonal lattices at an angle of 30°, (**B**) a hexagonal lattice, and (**C**) experimental selected area electron diffraction (SAED) pattern image of the twisted quasiperiodic nanosheets of Zn-CuNCs in Fig. 3.1B with markings on the diffraction spots. Schematic representations of (**D**) regular and twisted (at 30°) stacking of two hexagonal lattices, depicting the proposed bonding in both the hexagonal and twisted quasiperiodic nanosheets and (**E**) two hexagonal nanosheets mutually aligned at 30° against each other, indicating loss of translational symmetry and arising of dodecagonal rotational symmetry.

Interestingly, gradual addition of 0.42 mM aqueous iodine into the dispersion of hexagonal crystals led to lowering of the photoluminescence intensity with a minimal red shift to the peak of the original NCs (Fig. 3.4A). On the other hand, the same treatment to the twisted quasiperiodic nanostructure gave rise to shifting of the emission maximum to longer wavelength without significant change of the luminescence intensity (Fig. 3.4B). The plot of relative photoluminescence intensity (I/I_0) with different iodine concentrations in Fig. 3.4C also indicated considerable chemical stability of the quasiperiodic structures in comparison to the hexagonal counterparts. TEM analysis of the final product obtained after reaction of hexagonal crystals with molecular iodine showed the presence of small sized NCs that were devoid of any crystallinity (Fig. 3.4D and Fig. A.3.16A, Appendix). On the other hand, TEM analysis of the twisted quasiperiodic nanosheets─obtained after iodine treatment─indicated retention of the two-dimensional nanosheets (Fig. 3.4E and Fig. A.3.16B, Appendix). It is plausible that the hexagonal two-dimensional arrangements of the nanoclusters following complexation with zinc consists of sufficient space (with a typical vertical distance of 4.5 Å) for molecular iodine (diameter of iodine atom being 2.6 Å) to percolate into the structure and interact preferably with the aromatic π-groups and thus reduce the photoluminescence quantum yield and chemical stability. On the other hand, the more compact twisted quasiperiodic (with a typical vertical distance of much less than 4.5 Å) structure may not provide sufficient space for accommodation of molecular iodine, thus providing chemical stability. The change in the luminescence peak position could be due to interactions of the NCs with molecular iodine in the dispersion medium. Further, it is also plausible that quasiperiodic arrangements in the stacking provided additional chemical stability to the hexagonal structures just above and below these twisted layers.

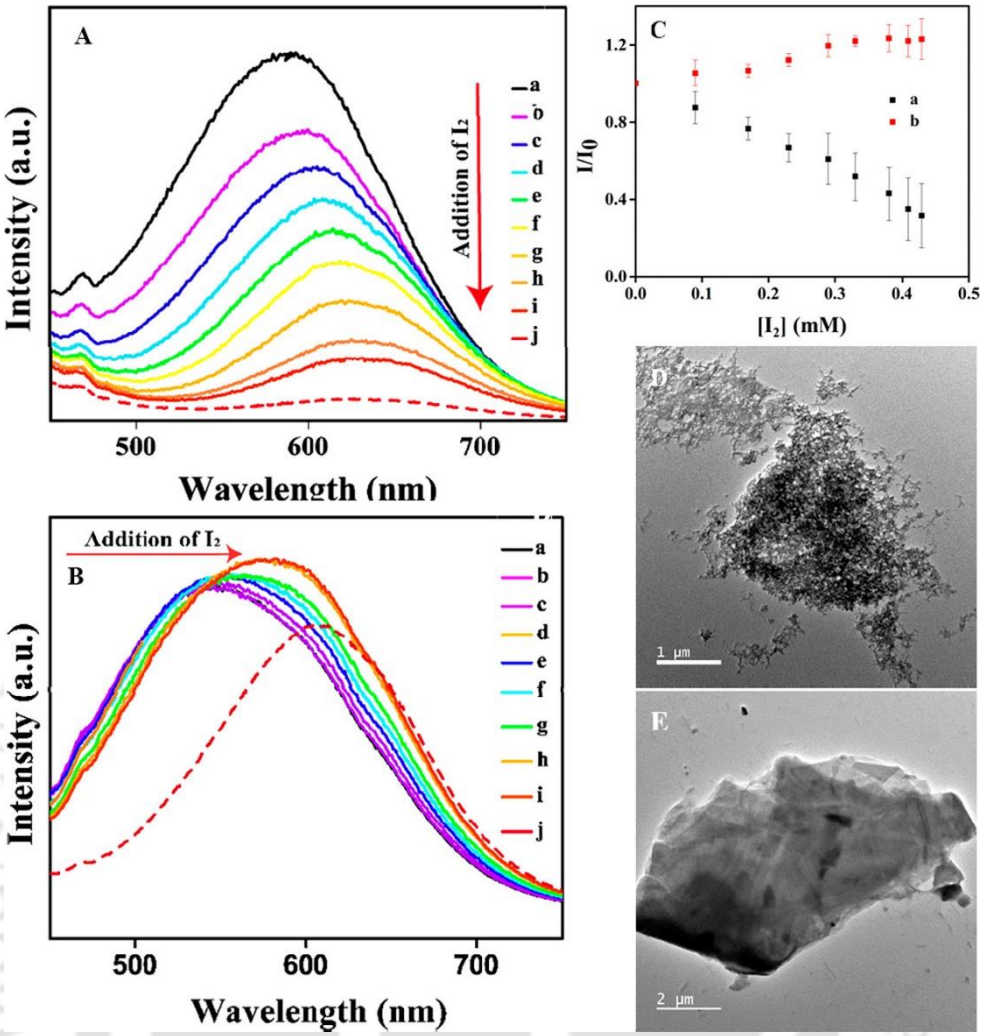

Fig 3.4. Photoluminescence of (**A**) hexagonal and (**B**) twisted quasiperiodic nanosheets of Zn-CuNCs on gradual addition of (**a**) 0 mM, (**b**) 0.09 mM, (**c**) 0.17 mM, (**d**) 0.23 mM, (**e**) 0.29 mM, (**f**) 0.33 mM, (**g**) 0.38 mM, (**h**) 0.41 mM, and (**i**) 0.42 mM iodine solution and (**j**) that after purification. (**C**) Plot of photoluminescencee intensity ratio (I/I_0) at 600 nm versus iodine concentration for (**a**) hexagonal and (**b**) twisted quasiperiodic nanosheets. Transmission electron microscopy images of (**D**) hexagonal and (**E**) twisted quasiperiodic nanosheets of Zn-CuNCs after addition of 0.42 mM I_2.

Table 3.1: Comparison of physical parameters between hexagonal and twisted quasiperiodic nanosheets of Zn-CuNCs.

Physical Parameters	Hexagonal Zn-CuNCs	Twisted Quasiperiodic Zn-CuNCs
Quantum Yield of Prompt Photoluminescence φ_{PF} (%)	0.12±0.03	0.19±0.02
Average Lifetime of Prompt Photoluminescence τ_{PF} (ns)	18.35 ± 0.18	42.70 ± 1.34
Rate Constant of Prompt Photoluminescence K_{PF} (s^{-1})	$(6.5 \pm 2)\times10^{4}$	$(4.5 \pm 0.6)\times10^{4}$
Average Lifetime of Delayed Photoluminescence τ_{PF} (μs)	26.0 ± 3.6	87.3 ± 2.5
Reactivity with I_2 (mM^{-1}) (Slope of change in prompt photoluminescence intensity with respect to concentration)	-(1.6 ± 0.4)	0.6 ± 0.3

3.5 Conclusion:

In summary, we have reported a strategy to chemically synthesize twisted stacking of two dimensional nanosheets of single component luminescent CuNCs exhibiting dodecagonal quasiperiodic lattice. This was pursued by assembling two-dimensional nanosheets -followed by stacking at 30° - through complexation reaction by suitable tuning of the metal ion concentration. The photophysical properties of the twisted quasiperiodic nanosheets as compared to the hexagonal ones are briefly presented in Table 1. The results essentially indicated that the chemical stability against molecular iodine and the photophysical properties of the twisted stacking induced dodecagonal quasiperiodic assembly in Zn-CuNCs were superior as compared to the hexagonal crystalline nanosheets. The results reported herein bring hope of extending the idea of deterministic chemical twisting of two-dimensional crystalline assemblies in generating materials with anisotropic structure-based novel chemical, optical, electronic and magnetic properties.

3.6 Bibliography:

1. Shechtman, D.; Blech, I.; Gratias, D.; Cahn, J. W., Metallic Phase with Long-Range Orientational Order and No Translational Symmetry. *Physical Review Letters* **1984,** *53* (20), 1951-1953.

2. Deng, B.; Wang, B.; Li, N.; Li, R.; Wang, Y.; Tang, J.; Fu, Q.; Tian, Z.; Gao, P.; Xue, J.; Peng, H., Interlayer Decoupling in 30° Twisted Bilayer Graphene Quasicrystal. *ACS Nano* **2020,** *14* (2), 1656-1664

3. Oh, M.; Nuckolls, K. P.; Wong, D.; Lee, R. L.; Liu, X.; Watanabe, K.; Taniguchi, T.; Yazdani, A., Evidence for unconventional superconductivity in twisted bilayer graphene. *Nature* **2021,** *600* (7888), 240-245.

4. Cao, Y.; Fatemi, V.; Fang, S.; Watanabe, K.; Taniguchi, T.; Kaxiras, E.; Jarillo-Herrero, P., Unconventional superconductivity in magic-angle graphene superlattices. *Nature* **2018,** *556* (7699), 43-50.

5. Park, J. M.; Cao, Y.; Xia, L.-Q.; Sun, S.; Watanabe, K.; Taniguchi, T.; Jarillo-Herrero, P., Robust superconductivity in magic-angle multilayer graphene family. *Nature Materials* **2022**.

6. Li, Z.; Zhuang, J.; Chen, L.; Ni, Z.; Liu, C.; Wang, L.; Xu, X.; Wang, J.; Pi, X.; Wang, X.; Du, Y.; Wu, K.; Dou, S. X., Observation of van Hove Singularities in Twisted Silicene Multilayers. *ACS Central Science* **2016,** *2* (8), 517-521.

7. Sinha, M.; Vivanco, H. K.; Wan, C.; Siegler, M. A.; Stewart, V. J.; Pogue, E. A.; Pressley, L. A.; Berry, T.; Wang, Z.; Johnson, I.; Chen, M.; Tran, T. T.; Phelan, W. A.; McQueen, T. M., Twisting of 2D Kagomé Sheets in Layered Intermetallics. *ACS Central Science* **2021,** *7* (8), 1381-1390.

8. Shang, J.; Shen, S.; Wang, L.; Ma, Y.; Liao, T.; Gu, Y.; Kou, L., Stacking-Dependent Interlayer Ferroelectric Coupling and Moiré Domains in a Twisted AgBiP2Se6 Bilayer. *The Journal of Physical Chemistry Letters* **2022**, 13 (8), 2027-2032.

9. Gupta, N.; Walia, S.; Mogera, U.; Kulkarni, G. U., Twist-Dependent Raman and Electron Diffraction Correlations in Twisted Multilayer Graphene. *The Journal of Physical Chemistry Letters* **2020**, 11 (8), 2797-2803.

10. Wang, S.-Y.; Huang, K.-X.; Guo, Q.-Q.; Guo, H.-W.; Tian, J.-G.; Liu, Z.-B., Tunable Optical Rotation in Twisted Black Phosphorus. *The Journal of Physical Chemistry Letters* **2021**, 12 (19), 4755-4761.

11. Talapin, D. V.; Shevchenko, E. V.; Bodnarchuk, M. I.; Ye, X.; Chen, J.; Murray, C. Quasicrystalline order in self-assembled binary nanoparticle superlattices. *Nature* **2009,** *461* (7266), 964-967.

12. Lee, S.; Leighton, C.; Bates Frank, S., Sphericity and symmetry breaking in the formation of Frank–Kasper phases from one component materials. *Proceedings of the National Academy of Sciences* **2014,** *111* (50), 17723-17731.

13. Sun, Y.; Ma, K.; Kao, T.; Spoth, K. A.; Sai, H.; Zhang, D.; Kourkoutis, L. F.; Elser, V.; Wiesner, U., Formation pathways of mesoporous silica nanoparticles with dodecagonal tiling. *Nature Communications* **2017,** *8* (1), 252.

14. Pezzini, S.; Mišeikis, V.; Piccinini, G.; Forti, S.; Pace, S.; Engelke, R.; Rossella, F.; Watanabe, K.; Taniguchi, T.; Kim, P.; Coletti, C., 30°-Twisted Bilayer Graphene Quasicrystals from Chemical Vapor Deposition. *Nano Letters* **2020,** *20* (5), 3313-3319.

15. Yu, G.; Wu, Z.; Zhan, Z.; Katsnelson, M. I.; Yuan, S., Dodecagonal bilayer graphene quasicrystal and its approximants. *npj Computational Materials* **2019,** *5* (1), 122.

16. Ahn Sung, J.; Moon, P.; Kim, T.-H.; Kim, H.-W.; Shin, H.-C.; Kim Eun, H.; Cha Hyun, W.; Kahng, S.-J.; Kim, P.; Koshino, M.; Son, Y.-W.; Yang, C.-W.; Ahn Joung, R., Dirac electrons in a dodecagonal graphene quasicrystal. *Science* **2018,** *361* (6404), 782-786.

17. Tao, Z.-R.; Wu, J.-X.; Zhao, Y.-J.; Xu, M.; Tang, W.-Q.; Zhang, Q.-H.; Gu, L.; Liu, D.-H.; Gu, Z.-Y., Untwisted restacking of two-dimensional metal-organic framework nanosheets for highly selective isomer separations. *Nature Communications* **2019,** *10* (1), 2911.

18. Metere, A.; Oleynikov, P.; Dzugutov, M.; Lidin, S., A smectic dodecagonal quasicrystal. *Soft Matter* **2016,** *12* (43), 8869-8875.

19. Basu, S.; Paul, A.; Chattopadhyay, A., Zinc mediated crystalline assembly of gold nanoclusters for expedient hydrogen storage and sensing. *Journal of Materials Chemistry A* **2016,** *4* (4), 1218-1223.

20. Basu, S.; Bhandari, S.; Pan, U. N.; Paul, A.; Chattopadhyay, A., Crystalline nanoscale assembly of gold clusters for reversible storage and sensing of CO2via modulation of photoluminescence intermittency. *Journal of Materials Chemistry C* **2018,** *6* (30), 8205-8211.

21. Basu, S.; Goswami, U.; Paul, A.; Chattopadhyay, A., Crystalline assembly of gold nanoclusters for mitochondria targeted cancer theranostics. *Journal of Materials Chemistry B* **2018,** *6* (11), 1650-1657.

22. Paul, M.; Basu, S.; Chattopadhyay, A., Complexation Reaction-Based Two-Dimensional Luminescent Crystalline Assembly of Atomic Clusters for Recyclable Storage of Oxygen. *Langmuir* **2020,** *36* (3), 754-759.

23. Basu, S.; Paul, A.; Chattopadhyay, A., Zinc-Coordinated Hierarchical Organization of Ligand-Stabilized Gold Nanoclusters for Chiral Recognition and Separation. *Chemistry – A European Journal* **2017,** *23* (38), 9137-9143.

24. Basu, S.; Chattopadhyay, A., Room-Temperature Delayed Fluorescence of Gold Nanoclusters in Zinc-Mediated Two-Dimensional Crystalline Assembly. *Langmuir* **2019,** *35* (15), 5264-5270.

25. Das, P.; Chattopadhyay, A., Delayed Dual Emission of Two-Dimensional Copper Nanocluster Assembly. *The Journal of Physical Chemistry C* **2022,** *126* (2), 997-1005.

26. Wu, Z.; Liu, J.; Gao, Y.; Liu, H.; Li, T.; Zou, H.; Wang, Z.; Zhang, K.; Wang, Y.; Zhang, H.; Yang, B., Assembly-Induced Enhancement of Cu Nanoclusters Luminescence with Mechanochromic Property. *Journal of the American Chemical Society* **2015,** *137* (40), 12906-12913.

27. Wu, Z.; Liu, J.; Li, Y.; Cheng, Z.; Li, T.; Zhang, H.; Lu, Z.; Yang, B., Self-Assembly of Nanoclusters into Mono-, Few-, and Multilayered Sheets via Dipole-Induced Asymmetric van der Waals Attraction. *ACS Nano* **2015,** *9* (6), 6315-6323.

28. Liu, Y.; Yao, D.; Zhang, H., Self-Assembly Driven Aggregation-Induced Emission of Copper Nanoclusters: A Novel Technology for Lighting. *ACS Applied Materials & Interfaces* **2018,** *10* (15), 12071-12080.

29. Yao, W.; Wang, E.; Bao, C.; Zhang, Y.; Zhang, K.; Bao, K.; Chan Chun, K.; Chen, C.; Avila, J.; Asensio Maria, C.; Zhu, J.; Zhou, S., Quasicrystalline 30° twisted bilayer graphene as an incommensurate superlattice with strong interlayer coupling. *Proceedings of the National Academy of Sciences* **2018,** *115* (27), 6928-6933.

Appendix

A3. Chapter 3

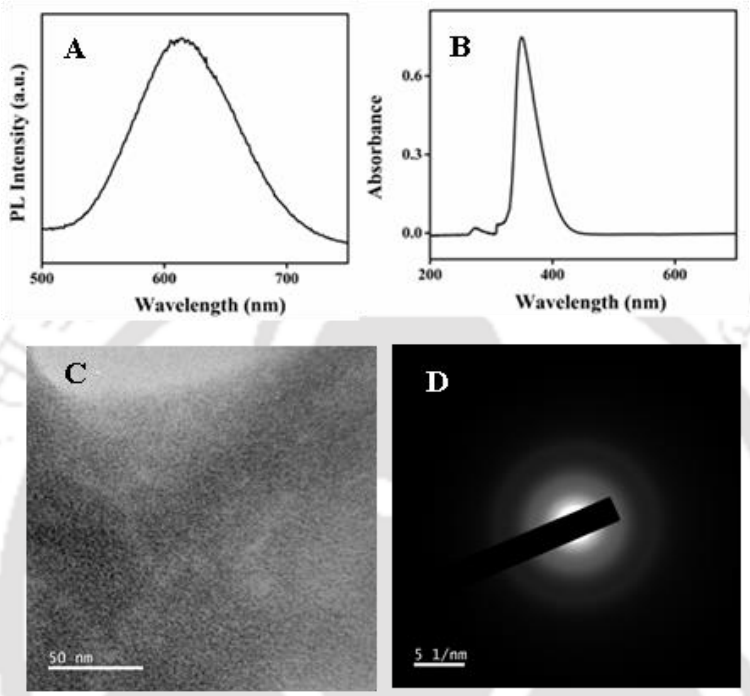

Fig. A.3.1: (**A**) Photoluminescence emission spectrum and (**B**) UV-Vis spectrum of as synthesized copper nanoclusters (CuNCs). (**C**) Transmission electron microscopy (TEM) image and (**D**) selected area electron diffraction (SAED) pattern image of as synthesized CuNCs.[1]

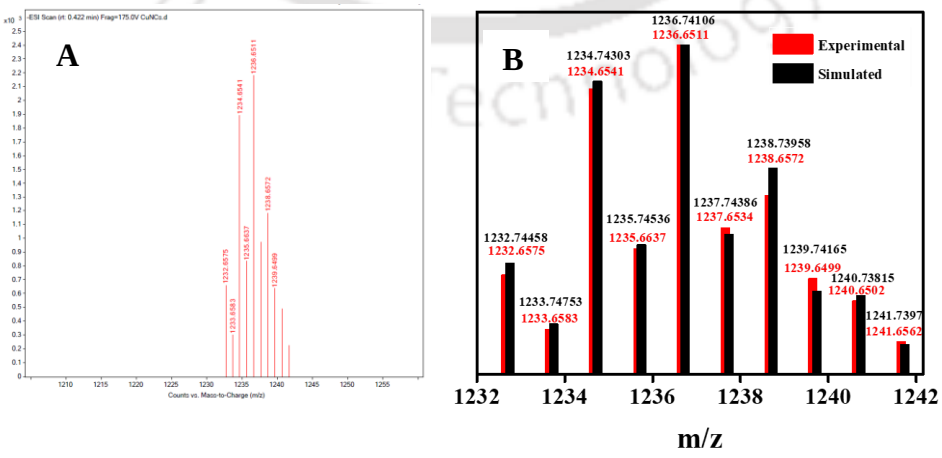

Fig A.3.2: (**A**) Isotopic distribution pattern of experimentally obtained mass spectrum of typical copper nanoclusters at m/z value of 1236.65.[1] (**B**) superimposition of simulated and

experimental isotopic mass distribution spectra of as synthesized copper nanoclusters at m/z value of 1236.65.

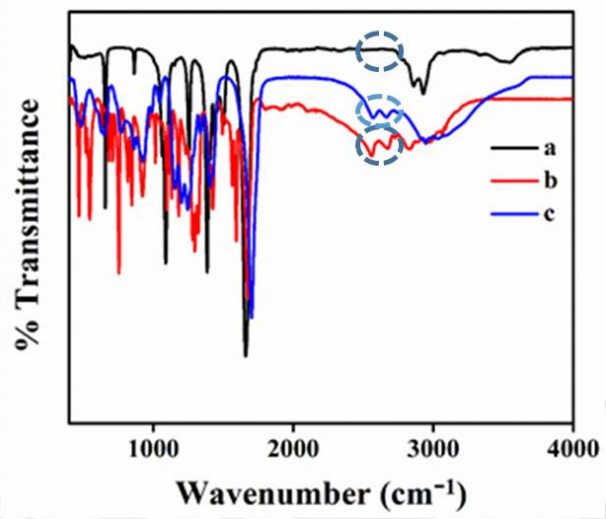

Fig. A.3.3: Attenuated total reflectance (ATR)-Fourier-transform infrared (FTIR) spectra of (**a**) as synthesized copper nanoclusters, (**b**) mercaptobenzoic acid, and (**c**) mercaptopropanoic acid.

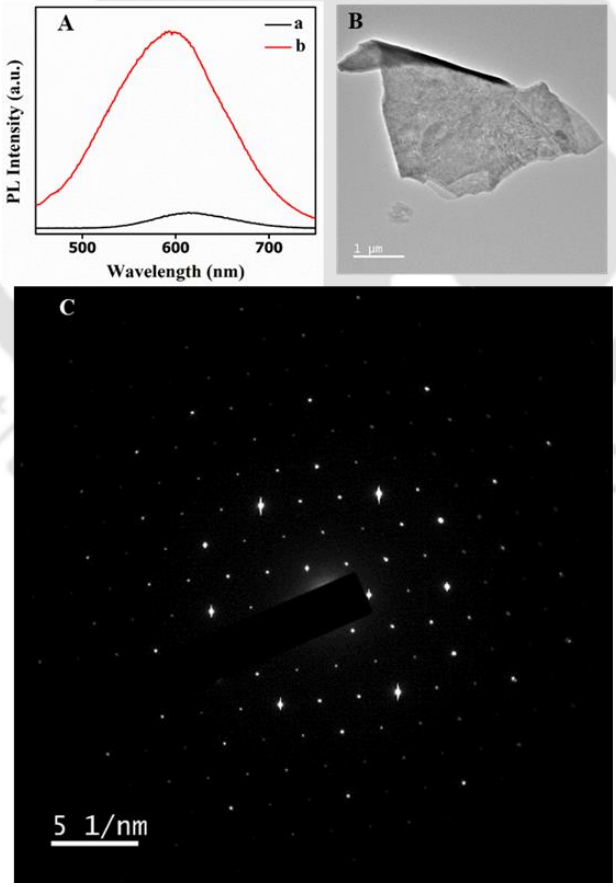

Fig A.3.4. (**A**) Photoluminescence emission spectra of (**a**) as-synthesized CuNCs and (**b**) hexagonal Zn-CuNCs. (**B**) Transmission electron microscopy (TEM) image of hexagonal Zn-

CuNC nanosheet, and (**C**) a typical selected area electron diffraction (SAED) pattern of the image in **B**.

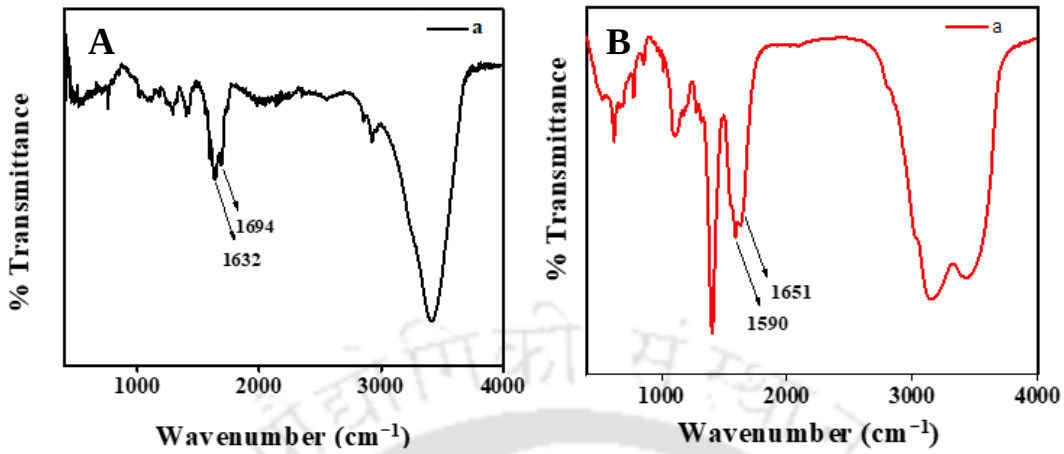

Fig A.3.5: Fourier-transform infrared (FTIR) spectra of (**A**) as synthesized CuNCs and (**B**) hexagonal Zn-CuNC nanosheets.

Quantum Yield Measurement

Photoluminescence quantum yield (Q.Y.) was measured with respect to quinine sulphate (QS) in 0.1 M H_2SO_4 with reported quantum yield of 54% using the following equation-

$$\Phi_S = \Phi_R \times \frac{I_S}{I_R} \times \frac{A_R}{A_S} \times \frac{\eta_S^2}{\eta_R^2} \quad \text{..... Equation S1}$$

Here, Φ_S = quantum yield of the sample, Φ_R = quantum yield of the reference; I_S = area under the emission spectrum of the sample; I_R = area under the emission spectrum of reference; A_R = absorbance of reference. A_S = absorbance of the sample; η_S = refractive index of the sample solution; η_R = refractive index of reference. Refractive index of water = 1.33, Q.Y. of quinine sulphate=0.54.

Table A.3.1: Parameters obtained from quantum yield measurements of hexagonal and twisted quasiperiodic nanosheets of Zn-CuNCs.

Sample	Experi-ment No	Area under the PL curve of QS excited at 365 nm (a.u.) (I_R)	Area under the PL curve of sample excited at 365 nm (a.u.) (I_S)	Absorbance of QS at 365 nm (A_R)	Absorbance of the sample at 365 nm (A_S)	Quantum yield (Q.Y.) (%)	Average quantum yield with error bar (%)
Hexagonal Zn-CuNCs	1	4.7×10^8	7.7×10^5	0.0974	0.1140	0.08	0.11±0.02
	2	4.2×10^8	8.5×10^5	0.1209	0.0998	0.13	
	3	4.2×10^8	8.5×10^5	0.1210	0.1086	0.12	
Twisted Quasiperiodic Zn-CuNCs	1	4.7×10^8	1.78×10^6	0.0974	0.1060	0.19	0.18±0.02
	2	4.2×10^8	1.13×10^6	0.1210	0.1177	0.15	
	3	4.2×10^8	1.47×10^6	0.1209	0.1190	0.19	

Table A.3.2: Calculated parameters as-obtained from time-resolved photoluminescence study of hexagonal and twisted quasiperiodic nanosheets of Zn-CuNCs.

Sample	Hexagonal Zn-CuNCs			Twisted Quasiperiodic Zn-CuNCs		
Experiment no	1	2	3	1	2	3
χ^2	1.0	1.02	1.02	1.00	1.01	1.02
First component α_1 (%)	8.88	9.25	7.59	16.79	29.53	18.05
First component lifetime τ_1 (ns)	0.06	0.06	0.06	0.06	0.13	0.10
Second component α_2 (%)	4.61	4.17	6.23	8.47	2.08	3.36
Second component lifetime τ_2 (ns)	0.49	0.45	0.35	0.44	1.14	0.89
Third component α_3 (%)	86.51	86.58	86.18	74.75	68.38	78.58
Third component lifetime τ_3 (ns)	18.64	18.29	18.28	43.07	43.96	41.29
Average lifetime τ_{av} (ns)	18.55	18.29	18.21	43.01	43.87	41.23
Average Lifetime with error bar τ_{av} (ns)	18.35 ± 0.18			42.70 ± 1.34		

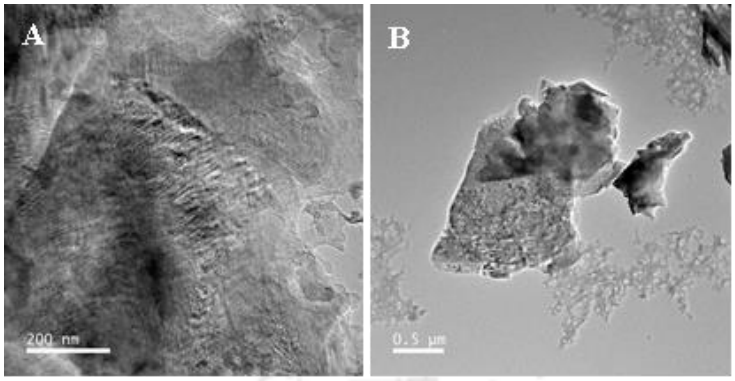

Fig A.3.6. (**A-B**) Transmission electron microscopy (TEM) images of additional twisted quasiperiodic nanosheets of Zn-CuNCs with Moiré pattern originating from smaller angular twisting of the stacked structures, present in sections of the same stacked structures that had angular twisting of 30°.

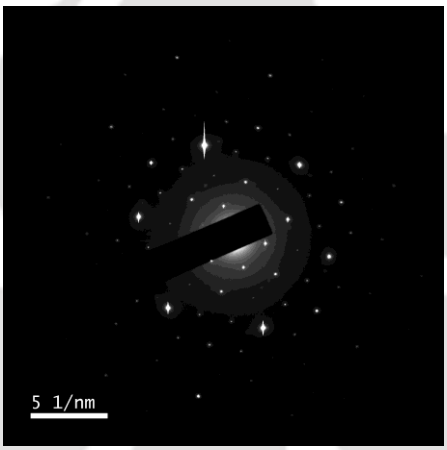

Fig A.3.7. Selected area electron diffraction (SAED) image on the non-overlapped area of the image (Fig. 3.1B) given in the Chapter 3.

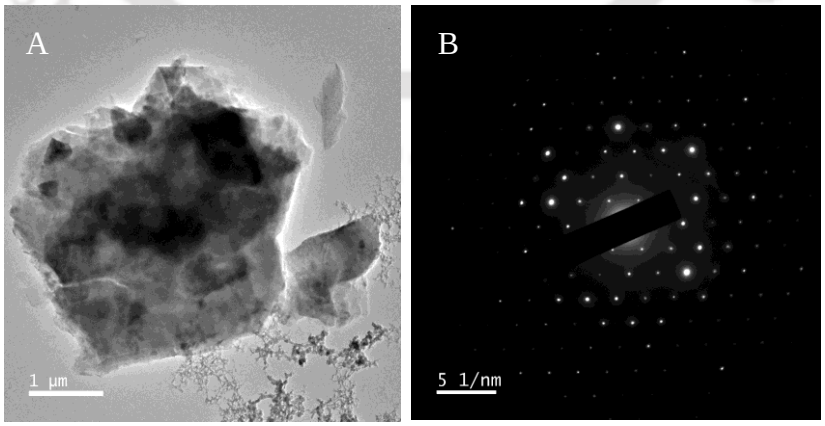

Fig. A.3.8: (**A**) Transmission electron microscopy image of additional hexagonal Zn-CuNC nanosheet and (**B**) the corresponding selected area electron diffraction pattern image.

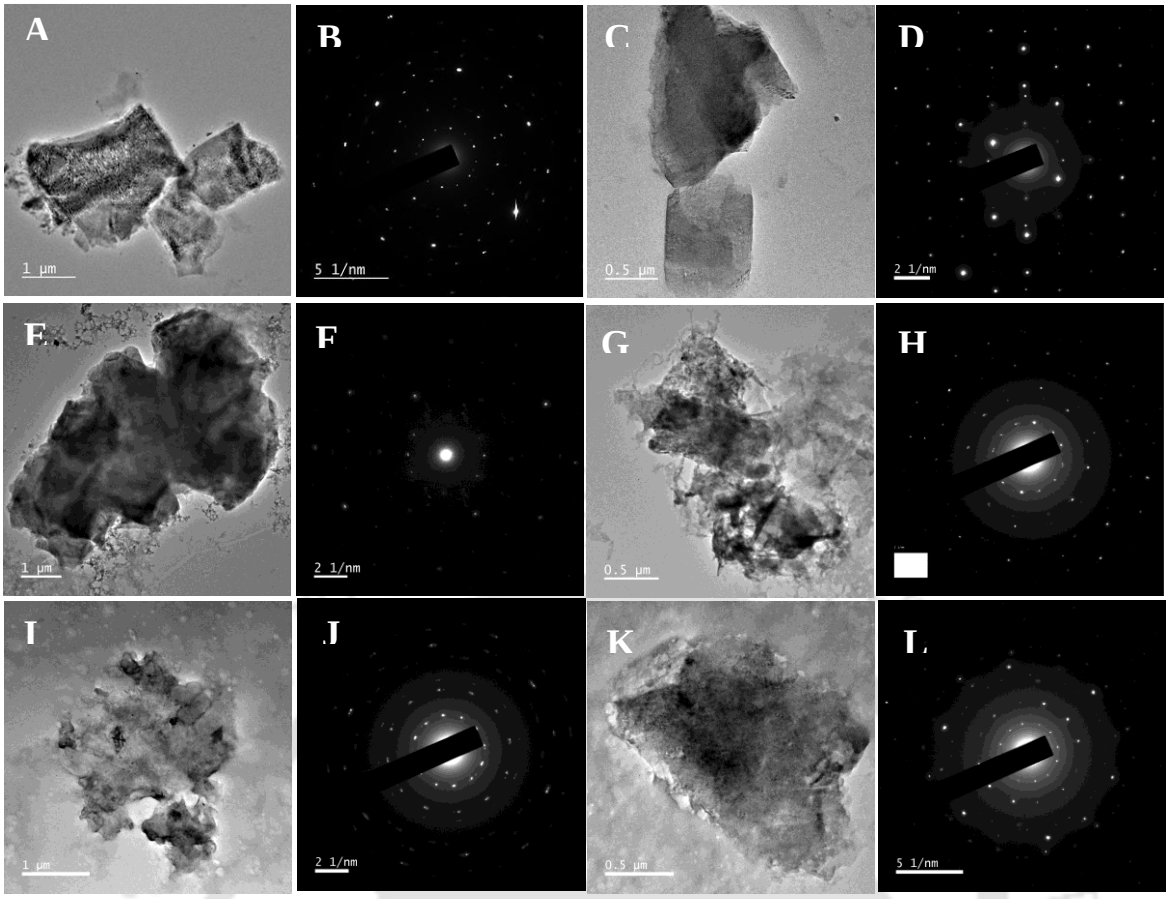

Fig. A.3.9. A collection of transmission electron microscopy (TEM) images and corresponding selected area electron diffraction (SAED) pattern images of the twisted quasiperiodic nanosheets of Zn-CuNCs (A,**B**), (C,**D**), (E,**F**), (G,**H**), (I,**J**), (**K,L**), respectively.

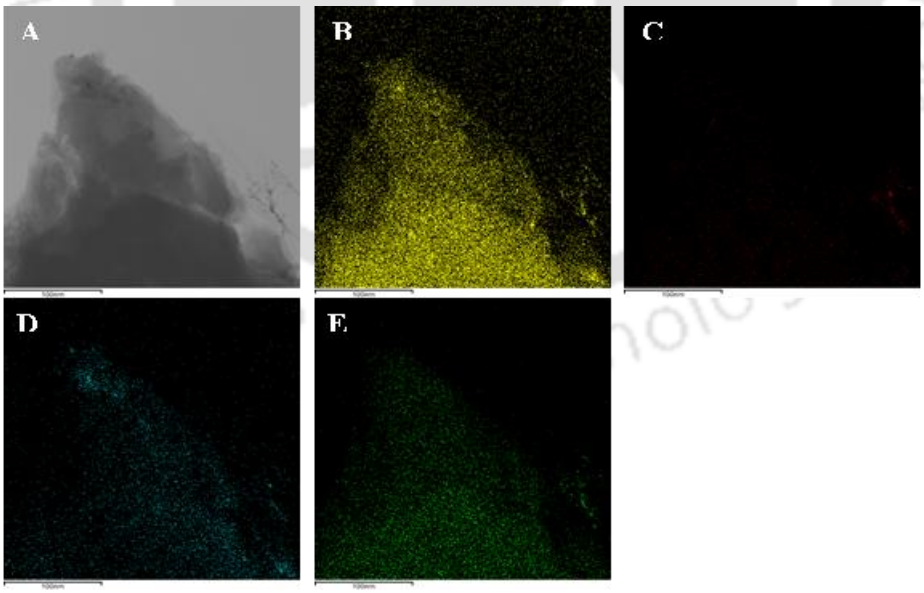

Fig A.3.10a. (**A**) Scanning transmission electron microscopy (STEM) image of the twisted nanosheets of Zn-CuNCs and elemental mapping of (**B**) Cu, (**C**) Zn, (**D**) O and (**E**) S on that nanosheet performed using Ni grid.

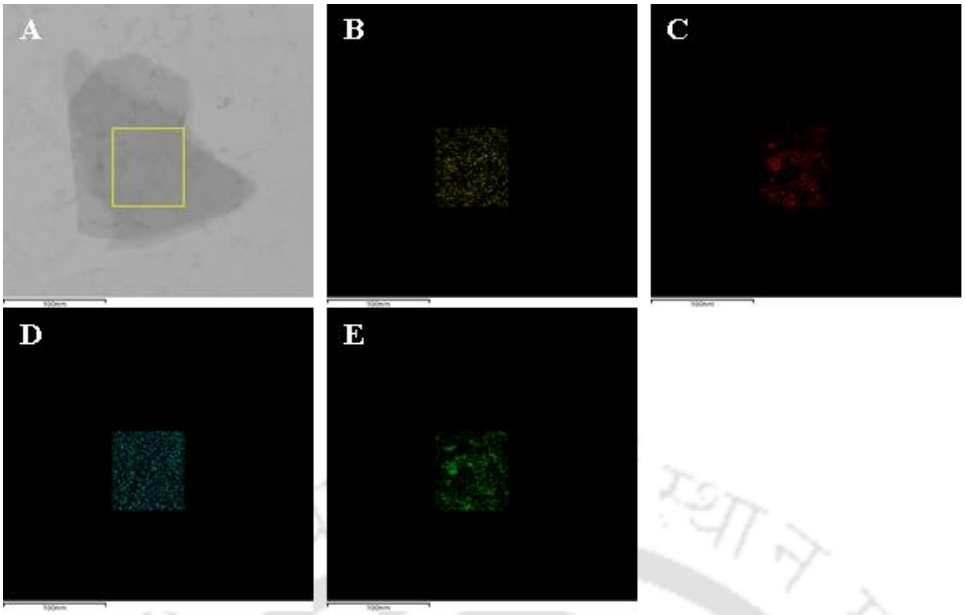

Fig A.3.10b. (**A**) Scanning transmission electron microscopy (STEM) image of the twisted nanosheets of Zn-CuNCs and elemental mapping of (**B**) Cu, (**C**) Zn, (**D**) O and (**E**) S on the selected rectangular area of that nanosheet performed using Ni grid.

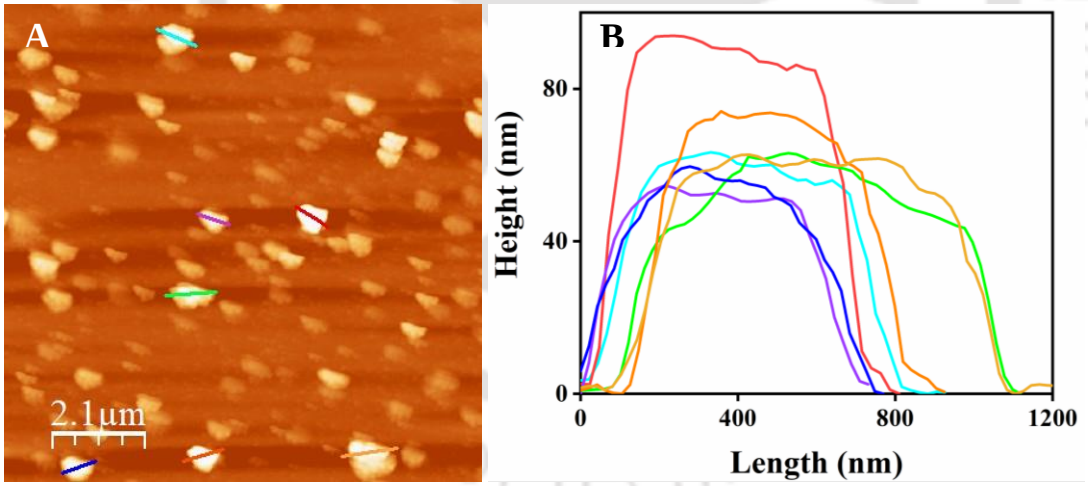

Fig. A.3.11. (**A**) Atomic force microscopy (AFM) image of twisted Zn–CuNCs featuring the presence of 2D nanosheets. (**B**) Corresponding height profiles of the same as obtained from part **A**.

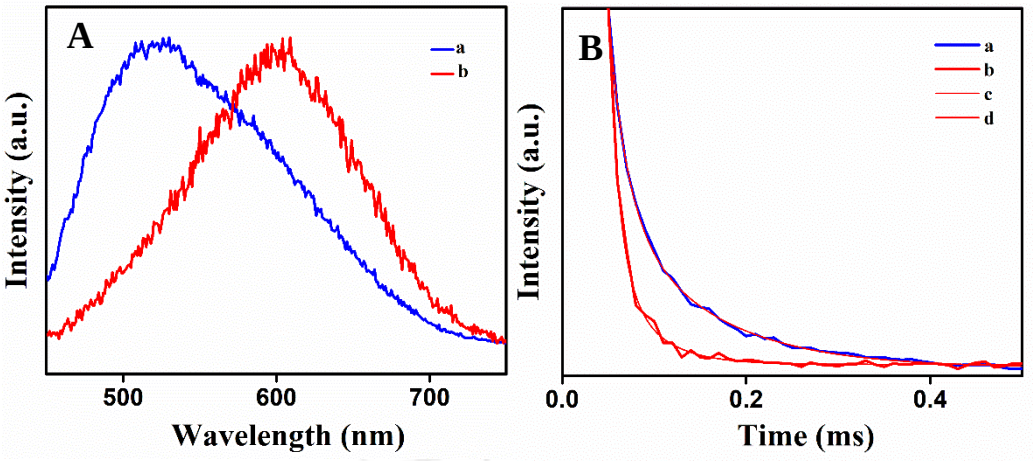

Fig A.3.12: (A) Normalized delayed photoluminescence spectra of (**a**) twisted quasiperiodic and (**b**) hexagonal nanosheets of Zn-CuNCs, (**B**) typical time resolved delayed photoluminescence decay profiles of (**a**) twisted quasiperiodic and (**b**) hexagonal Zn-CuNCs and (**c, d**) corresponding fitted lines.

Table A.3.3: Calculated parameters as-obtained from time-resolved delayed photoluminescence study of hexagonal and twisted quasiperiodic nanosheets of Zn-CuNCs.

Sample	Hexagonal Zn-CuNCs			Twisted Quasiperiodic Zn-CuNCs		
Experiment no	1	2	3	1	2	3
χ^2	0.99	0.99	0.99	0.99	0.99	0.99
First component α_1 (%)	7.14×10^5	7.77×10^5	1.01×10^6	2.81×10^6	2.56×10^6	3.40×10^6
First component lifetime τ_1 (ms)	0.011	0.010	0.013	0.106	0.11	0.10
Second component α_2 (%)	3.16×10^5	3.40×10^5	2.53×10^5	3.93×10^6	3.68×10^6	4.23×10^6
Second component lifetime τ_2 (ms)	0.041	0.035	0.038	0.023	0.023	0.019
Average lifetime τ_{av} (ms)	0.030	0.025	0.023	0.087	0.090	0.085
Average lifetime with error bar τ_{av} (μs)	26.0 ± 3.6			87.3 ± 2.5		

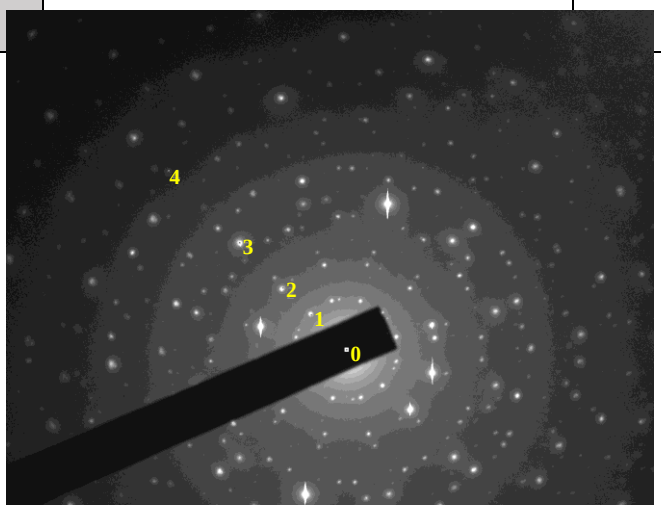

Fig A.3.13. Selected area electron diffraction pattern (SAED) image (obtained at the same spot with different contrast as in Fig. 3.2C in Chapter 3) depicting spots following Fibonacci sequence .

Table A.3.4: Parameters for average τ value calculation (as calculated from using Fig. A.3.13).

Spot	d-spacing (nm)	Reciprocal Position (nm)	Ratio of the spot distances from the origin (τ)	Average ratio with error bar
1	0.46	2.18	$\frac{01}{02} = 1.76$	1.71 ±
2	0.26	3.90	$\frac{02}{03} = 1.73$	
3	0.15	6.65	$\frac{03}{04} = 1.66$	
4	0.9	11.12		

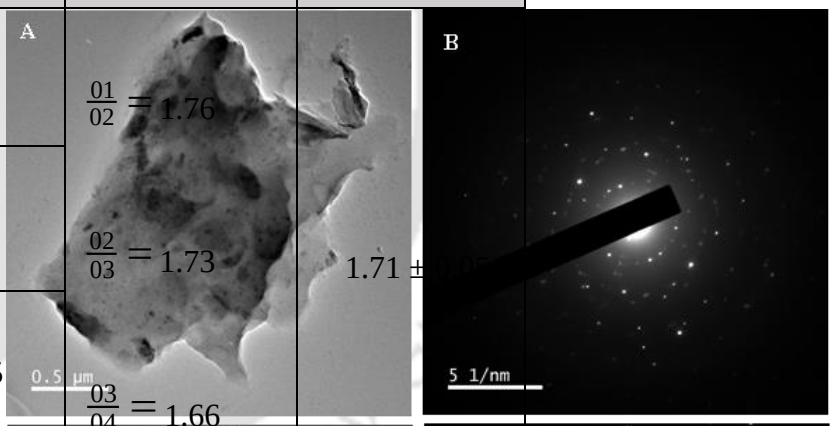

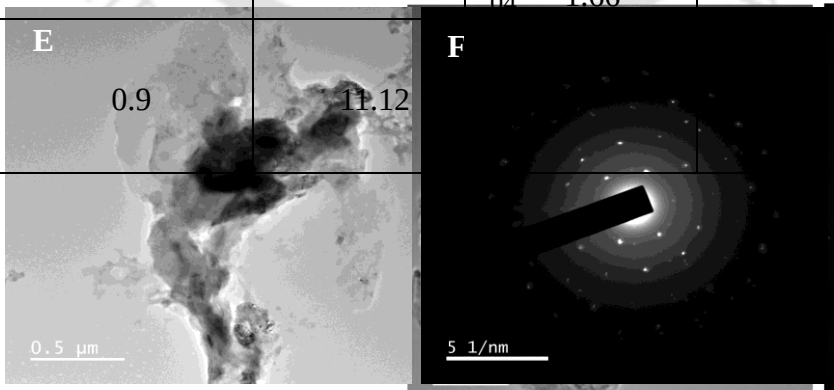

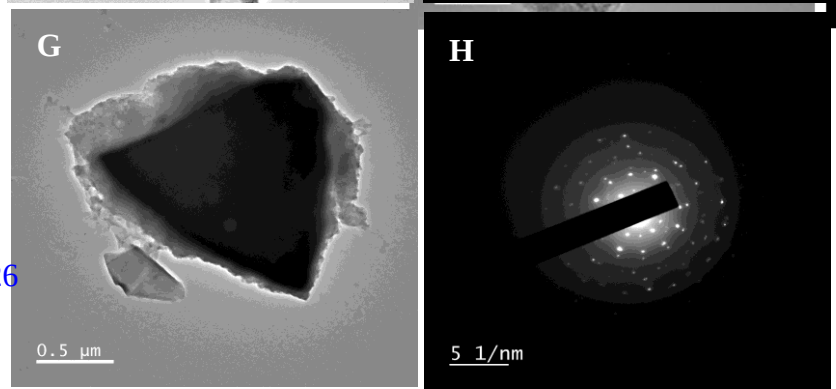

Fig A.3.14. Transmission electron microscopy images and corresponding selected area electron diffraction pattern images of Zn-CuNC nanosheets having twisted stacking at different molar ratio of Cu and Zn – (**A-B**) 1:3, (**C-D**) 1:6, (**E-F**) 1:21 and (**G-H**) 1:60.

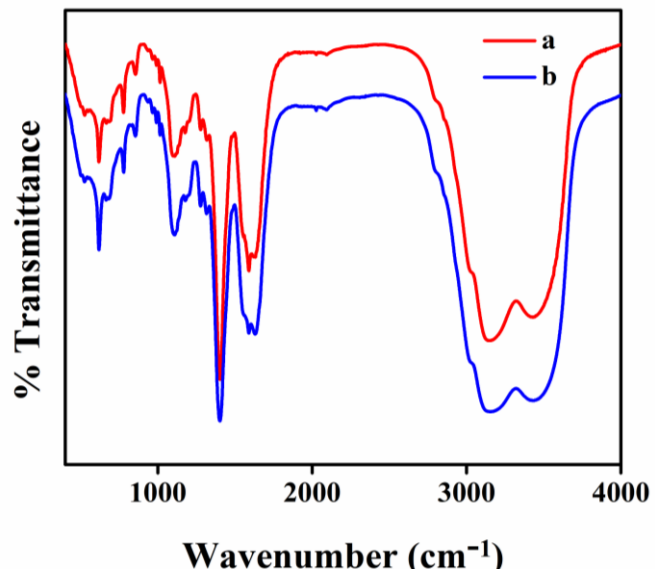

Fig A.3.15. Fourier-transform infrared spectra of (**a**) hexagonal and (**b**) twisted quasiperiodic nanosheets of Zn-CuNCs.

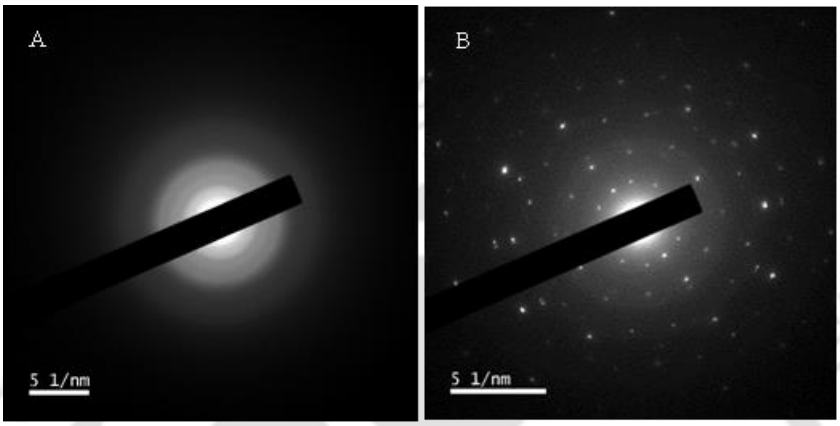

Fig. A.3.16. Selected area electron diffraction (SAED) pattern images of (**A**) hexagonal and (**B**) twisted quasiperiodic nanosheets of Zn-CuNCs after addition of 0.42 mM of I_2.

References:

1. Das, P.; Chattopadhyay, A. Delayed Dual Emission of Two- Dimensional Copper Nanocluster Assembly. *J. Phys. Chem. C* **2022**, *126* (2), 997-1005.

Chapter 4

Moiré superlattices of Two-dimensional Copper Nanocluster Assemblies with Tuneable Twin Emissions from Hierarchical Components Leading to White Light Emission

4.1 Abstract:

Chemically programmed angular stacking of two-dimensional (2D) assembly into interactive superstructures – such as moiré superlattices – may bring novel physical and chemical properties purely due to interlayer interactions. Herein, we report the formation of moiré superlattices through supramolecular chemical reaction of 2D crystalline copper nanocluster assemblies of hexagonal lattices with triphenylphosphine in the liquid medium, having an association constant of $(5.8 \pm 2.0) \times 10^4\ M^{-1}$. Transmission electron microscopic analysis confirmed the angles of twist of the nanosheets producing large moiré periodicity below 5°. The so-formed moiré superlattices with large periodicities generated a new quantum emissive state owing to the cuprophilic interactions amongst the neighbouring clusters of the adjacent layers. The retention of the red emission of the constituent 2D nanosheets and the tuneable new emission due to the now closely spaced clusters in the twisted super-stacking resulted in near white light photoluminescence. Moreover, the super-structures exhibited enhanced delayed photoluminescence with an increased lifetime that was on the order of 0.1 ms.

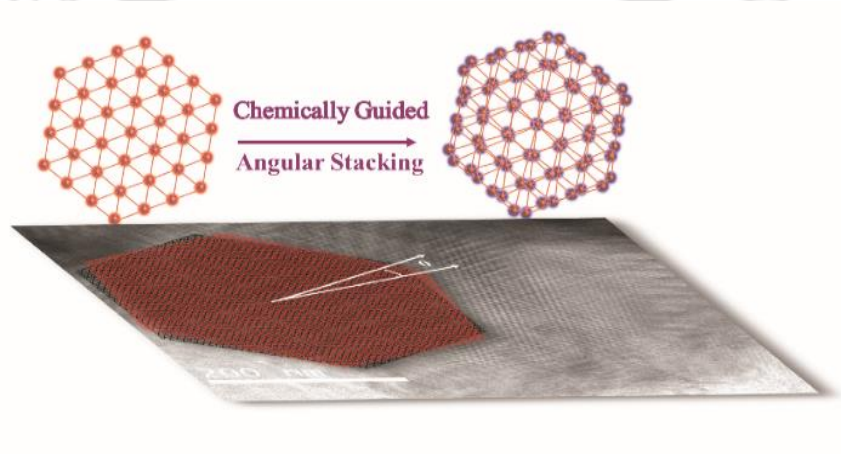

* [Das et al. *Journal of Materials Chemistry C* **2023,** *11* (35), 12029-12036] - Reproduced by permission from the Royal Society of Chemistry.

4.2 Introduction:

Realization of novel physical and chemical properties through programmed assembly of two-dimensional (2D) materials into higher order stacked structures has recently received extraordinary attention. The primary proposition is that with the chosen alignment of 2D atomic layers, the electronic band structure of the intervening layers can be tuned and thus new electronic properties due to the assembled structure would arise.[1-4] The results have been especially prominent for layers aligned at low twisted angles.[5,6] For example, the discovery of the superconductivity in graphene bilayers when twisted at a magic angle of 1.1° has initiated special interest in pursuing angular stacking of 2D layers.[7,8] Other examples include photonic crystals in twisted graphene superlattices,[9] moiré excitons in transition metal dichalcogenide heterostructures,[10–12] interfacial ferroelectricity in twisted stacking of transition metal dichalcogenides,[13] atomic reconstructions in twisted bilayer graphene and MoS_2 bilayers[14,15] and Mott-like insulator states due to the localization of electrons in the moiré superlattices of magic angle twisted bilayer graphene.[16,17] The early results involving well-established 2D systems make the nascent field poised for new breakthroughs.

The primary challenge lies in finding suitable techniques to stack 2D layers at desired angles. Popular conventional physical methods of assembling 2D layers involve mechanical stacking of exfoliated single layers oriented at particular angles. While these techniques may be ideal for pursuing physical properties of such twisted structures, scaling for a large number of devices may become prohibitive. On the other hand, fabrication of similar twisted structures in a liquid medium – based on principles of chemical bonding – may help address the issue of scaling. In addition, the well-defined chemical bonding between two such layers may provide additional options of tuning their properties. The principles of chemistry may also be applied for further modification of such twisted bilayers through additional functionalization as deemed necessary for versatile applications.

On the other hand, recent success of the chemical reaction based 2D assembly formation of atomic clusters in liquid media inspires pursuing more complex forms of organization such as the ones mentioned above. For example, crystallization 2D hexagonal assembly of Au or Cu nanoclusters (AuNCs or CuNCs) in liquid media has been made possible, using complexation reaction of the ligands stabilizing the clusters and Zn^{2+} ions (Zn–AuNCs or Zn–CuNCs). The so assembled 2D crystalline films were found to exhibit superior physical and chemical properties such as near white light fluorescence and delayed

fluorescence and storage and sensing of O_2 and CO_2 gases.[18–21] In addition, the targeted cancer theranostic potential of the assembly appeared promising.[22] Importantly, results also suggest that based on similar reaction conditions – as above – *in situ* stacking of such 2D crystalline assembly of nanoclusters is possible by carefully controlling the concentration of the Zn^{2+} ions in the medium.[23] Thus, stacking of assemblies of CuNCs at 30° in this way resulted in superstructures with superior delayed photoluminescence and chemical stability against treatment with iodine. However, there is still a need for methods for chemical organization of such 2D assemblies stacked at chosen angles to each other. This would provide important opportunities in facile organization of 2D materials in liquid media where the repertoire of chemistry could be utilized.

It is also established that the small angular orientation of two identical layers can generate moiré superlattices of larger periods due to the lattice mismatch. The additional periodicity, attained from strong electron correlations in moiré superlattices and also due to atomic alignments with symmetry different from the intrinsic layers, confers anomalous properties to the system. For example, the emergence of chiral phonons at the moiré wavelength occurs due to the disruption of C_{2z} symmetry in the van der Waals heterostructures.[24] Furthermore, symmetry breaking in the double-moiré superlattice domains of twisted tri-layer graphene results in anomalous electrical conductivity.[25] Additionally, the breaking of the C3 rotational symmetry of the WS_2 layers in the super-twisted spiral structure results in magnified interlayer strain through asymmetric charge densities in the moiré superlattice.[26] Such arrangements of 2D lattices into superstructures using the principles of chemistry in liquid medium may provide new ways of attaining moiré structures based on chemical bonding between the intervening layers. Importantly, metallophilic interactions between the atomic clusters of Au or Cu, when placed at short distances through interlayer separations at low angles, may bring new properties that are not available in ordinary 2D assemblies of the same.

We report that it has been possible to organize the 2D Zn–CuNC nanosheets hierarchically at smaller twist angles and form super-stacked nanosheets by a chemical reaction of the hexagonal nanosheets with triphenyl phosphine (TPP). In addition, for the first time, we report the formation of moiré superlattices from two dimensional CuNC assembly through a chemical reaction. The moiré superlattices so formed were also correlated with the appearance of a new photoluminescence at shorter wavelengths due to cuprophilic interactions among the CuNCs of the intervening layers – in comparison to the red emission

of the hexagonal Zn–CuNCs. Moreover, the extent of the moiré lattices was tuneable with the change in the concentration of the TPP added during the reaction. Supramolecular assembly of molecular materials, based on reaction conditions and bonding, gives rise to novel chemical and physical properties. We have combined the principle of chemistry and supramolecular organization to arrive at moiré superlattices of crystalline two-dimensional assembly of Zn–CuNCs, which gave rise to new optical properties. The tunability of the moiré superlattice induced emission with the simultaneous presence of the unaltered emission of the constituent nanosheets led to near white light emission. The reported moiré superlattices of NCs formed due to chemical bonding between two crystalline hexagonal Zn–CuNC lattices that can be controlled by reaction conditions, thus established a new route for such angular superstructure formation in the liquid medium.

4.3 Experimental Section:

4.3.1 Materials. Copper(ii) nitrate trihydrate (Sigma-Aldrich), 3-mercaptopropionic acid (MPA, Sigma-Aldrich), 4-mercaptobenzoic acid (MBA, Sigma-Aldrich), zinc acetate dihydrate (Merck), *N*,*N*-dimethylformamide (DMF, Merck) and triphenylphosphine (TPP, Sigma-Aldrich) were purchased and used without further purification. Elixgrade water from a Milli-Q purification system was used for the experiments.

4.3.2 Synthesis of CuNCs. Copper nanoclusters were synthesized at 0 °C in a round bottom flask containing 20 mL of DMF as solvent, in which 2.4 mL of 10 mM copper nitrate solution and 1.6 mL of 0.11 M MPA solution were added and stirred for 5 min, followed by addition of 6 mg of MBA and the mixture solution was kept stirring for another 30 min. The obtained pale yellow coloured CuNCs solution was stored at 4 °C for further experiments.

4.3.3 Synthesis of hexagonal Zn–CuNCs. 1.5 mL of as-prepared CuNCs solution was added to 1.5 mL of H_2O followed by addition of 350 μL of 100 mM zinc acetate solution resulting in a white dispersion. The white pellet was then collected by centrifugation of the dispersion at 10 000 rpm for 10 min and then dispersed in water for further experiments.

4.3.4 Synthesis of TPP added moiré Zn–CuNCs. A stock solution of 5 mM TPP was prepared in acetone. A set of 2 mL dispersions of the Zn–CuNCs (with concentration of Cu metal of about 0.5 mM) were taken in separate vials and were reacted with different concentrations (0.12 mM, 0.23 mM, 0.29 mM, 0.35 mM, 0.45 mM and 0.55 mM) of TPP by adding 50 μL, 100 μL, 125 μL, 150 μL, 200 μL, and 250 μL of the TPP solution to the vials

separately. Then, the reactant mixtures were kept for 10 min at room temperature, which was followed by centrifugation at 15 000 rpm for 15 min and the centrifuged products were collected for further experiments.

4.3.5 Optical measurements. Photoluminescence spectra for all the samples were recorded using an Agilent Cary 100 UV-vis spectrophotometer and a HORIBA FluoroMax-4 spectrofluorometer, respectively. Fourier-transform infrared spectroscopy (FTIR) analyses were performed using the PerkinElmer (Spectrum Two) FTIR spectrometer. The pellets used for FTIR spectral recording were prepared by adding the evaporated dry sample to the heat dried KBr.

4.3.6 Transmission electron microscopic (TEM) analysis and selected area electron diffraction (SAED) analysis. TEM and SAED of CuNCs, hexagonal Zn–CuNCs and TPP added moiré Zn–CuNCs were performed in JEOL JEM 2100 and JEOL JEM 2100 F at a maximum accelerating voltage of 200 kV. TEM samples were prepared by diluting the above-mentioned samples to appropriately ten times and thereafter drop-casting the same on carbon-coated copper grids.

4.4 Results and Discussion:

Red luminescent CuNCs, stabilized by mercaptopropionic acid (MPA) and mercaptobenzoic acid (MBA), were synthesized according to a reported procedure.[18] The as-synthesized pale yellow colored CuNC dispersion exhibited red luminescence with emission maximum at 615 nm when excited at 405 nm (Fig. A.4.1A, Appendix).UV-Vis spectrum and TEM results further supported the formation of the small sized NCs in the synthesized medium (Fig. A.4.1(B-D), Appendix). Thereafter, a simple inorganic complexation reaction was pursued between the as-synthesized CuNCs and Zn^{2+} ions at room temperature, which resulted in white dispersion with enhanced photoluminescence intensity having emission maximum at 600 nm (Fig. A.4.2A, Appendix). The transmission electron microscopy (TEM) image of the complexed product confirmed the formation of two-dimensional nanosheets with a hexagonal diffraction pattern observed on selected area electron diffraction (SAED) analysis of the same (Fig. A.4.2(B-C), Appendix). The lattice parameter of the crystalline diffraction pattern was measured to be 4.7 ± 0.2 Å, which matched well with the previously reported lattice parameter of the hexagonal Zn–CuNC nanosheets.[18] The structure of the

nanosheets was thus assumed to be a hexagonal array of CuNCs with one CuNC at the centre of the hexagon. The significant increment of the photoluminescence intensity – in comparison to the constituent CuNCs – resulted from the restricted intramolecular motions due to the crystalline organization of the NCs in 2D arrays.[18]

The white dispersions of the Zn–CuNCs were then reacted with different concentrations of TPP solution (0.1 mM–0.9 mM) at room temperature. The photoluminescence measurements of the obtained products, collected after centrifugation at 15 000 rpm, exhibited a new emission peak ranging from 480–490 nm. The intensity of the peak was observed to have increased with the rise in TPP concentration until saturation at 0.9 mM of TPP (Fig. 4.1A). Deconvolution of the emission spectrum (Fig. 4.1A(b)) resulted in two major components – one with emission maximum at 490 nm and the other at 600 nm (Fig. 4.1B). This suggested the formation of a product with a new emissive energy state at 490 nm, the concentration of which was dependent on the concentration of TPP. At the same time, the simultaneous presence of the emission from the parent hexagonal Zn–CuNC nanosheets at 600 nm was also evident. Moreover, when the typical trends in changes of the emission peak intensities at 490 nm and 600 nm were examined upon increasing the concentration of TPP, it was observed that the intensity at 600 nm did not change significantly, while the intensity at 490 nm continued to increase (Fig. 4.1C). A control experiment was also pursued by reacting TPP with zinc-acetate solution without the presence of CuNCs, which did not generate the emission curve with maximum near 490 nm (Fig. A.4.3, Appendix). The results indicated that the new product might be a complex structure comprising of intact Zn–CuNC hexagonal layers with their original intrinsic photoluminescence property unaltered, in addition to the appearance of a new emissive state. In the Fourier transform infrared (FTIR) spectral analysis, Zn-coordinated carboxylate group stretching frequencies of both the parent hexagonal Zn–CuNC nanosheets and TPP added product (occurring at 1658 and 1587 cm^{-1}, and 1660 and 1587 cm^{-1}, respectively) also suggested no change in bonding between Zn and the carboxylate group of the ligands (Fig. A.4.4, Appendix). This also indicated

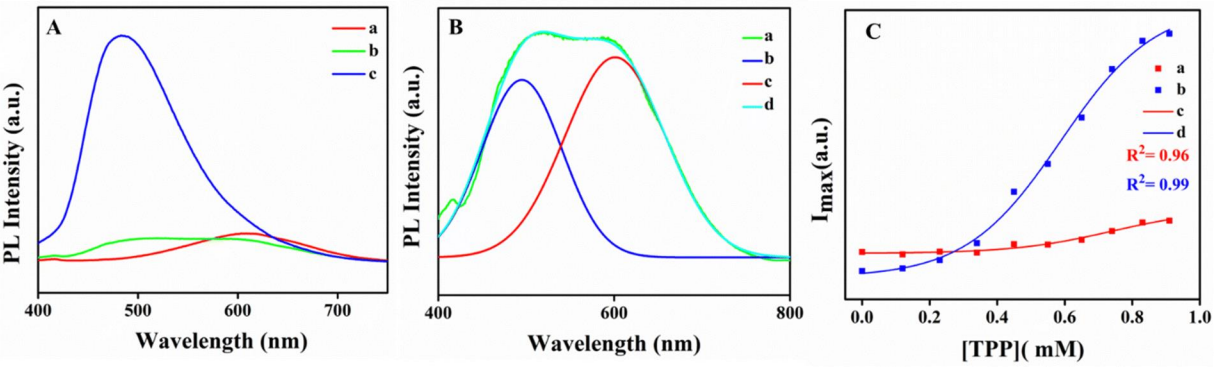

Fig. 4.1 (**A**) Photoluminescence spectra of (**a**) Zn–CuNC nanosheets and of those upon reaction with (**b**) 0.29 mM, and (**c**) 0.65 mM triphenylphosphine (TPP). (B) (**a**) The same photoluminescence spectrum as given in A(**b**), (**b**) and (**c**) two Gaussian components obtained on deconvolution of the broad spectrum in trace a and (**d**) cumulative fitted curve. (**C**) Intensity *vs*. TPP concentration plots at (**a**) 600 nm and (**b**) 490 nm wavelengths, and (**c**) and (**d**) fitted curve of a and b, respectively.

that the reaction of the Zn–CuNC nanosheets with TPP did not result in the loss of the crystalline assembly of the individual nanosheets. Also, X-ray photoelectron spectroscopic (XPS) measurements of the as-synthesized CuNCs, Zn–CuNCs with a hexagonal lattice and TPP added multi-twisted Zn–CuNCs confirmed no change in the oxidation state of the Cu (0) of the original CuNCs (Fig. A.4.5, Appendix). Furthermore, the changes in the new emission peak intensity at 490 nm with increased concentration of TPP represented a sigmoidal curve, indicating an isodesmic supramolecular reaction[27,28] (Fig. 4.1C). Now, since even after the reaction, the photoluminescent properties of the hexagonal crystalline Zn–CuNC nanosheets remained unaltered and since both the reactants, Zn–CuNCs and TPP comprised aromatic rings, there might be a strong possibility of π–π supramolecular interactions among them. This might have led to the vertical assembly of hexagonal Zn–CuNC nanosheets connected through TPP molecules. The association constant (*K*) according to the conventional method of isodesmic supramolecular reaction was obtained by plotting the degree of stacking-assembly (calculated from the variable photoluminescence intensities at 490 nm with respect to concentration) Vs concentration of TPP and was found to be $(5.8 \pm 2.0) \times 10^4\ M^{-1}$ (details are given in Fig. A.4.6, Appendix).[29] In simple supramolecular π–π interaction-based reaction, no new covalent bond is formed, which implies that the new emission at 490 nm could not be the result of any newly formed complex luminophore in the assembly. In other

words, the emission at 490 nm might originate from the interactions of the component luminophores in the assembly.

It has been reported that the photoluminescence emission wavelength of metal nanoclusters in an assembly depends on the inter-nanocluster metallophilic interactions.[30–32] The emission wavelength is dependent on the inter-cluster metal–metal distances, with shorter distances resulting in higher blue shifts. In the TPP added Zn–CuNC assemblies, two adjacent nanosheets might have been chemically bonded through supramolecular π–π interactions with TPP. As a result, the short inter-nanocluster distances between the stacked layers gave rise to strong cuprophilic interactions, thus causing the blue-shifted emission. From the comparison of the normalized XPS results given in Fig. A.4.7 (refer to Appendix) of the CuNCs, hexagonal Zn–CuNCs and TPP added multi-twisted Zn–CuNCs, broadening of the peaks in the case of TPP added multi-twisted Zn–CuNCs can be more clearly observed than for the other two. It is reported that the broadening of a peak in the XPS spectrum may occur due to the different charge state of the surface, which matched well with our proposal of multi-twisted Zn–CuNCs having Cu–Cu inter nanocluster interactions (which were absent in hexagonal Zn–CuNCs).

The TPP added multi-twisted Zn–CuNCs exhibited nearly the same photoluminescence spectrum in the solid form as in the dispersed medium (Fig. A.4.8A, Appendix). On the other hand, the photoluminescence spectrum of the hexagonal Zn–CuNC nanosheets in the solid form was blue shifted by 50 nm as compared to that in the liquid dispersion (Fig. A.8B, Appendix). This could be due to stacking of the nanosheets at large angles when dried.[23]

TEM images of the resultant product revealed the formation of multi-stacked twisted nanosheets with moiré patterns of large periodicity (Fig. 4.2A and Fig. A.4.9, Appendix). Moiré fringes in 2D materials are known to form due to the overlaying of two layers of different lattice constants or of the same lattice constant with relative twist. SAED pattern analysis (Fig. 4.2B) of the depicted rectangular area of super-stacked nanosheets on Fig. 4.2A exhibited a ring like pattern with a six-fold symmetric set of defined bright diffraction spots, which might be assumed to have resulted from overlaying multiple hexagonal lattices with relative twist. Overlaying of the hexagonal lattices should ideally contain the set of planes with the hexagonal unit cell lattice parameter of 4.7 ± 0.2 Å in the electron diffraction. However, as shown in Fig. 4.2B, diffraction spots corresponding to a cell parameter of 2.1 ±

0.1 Å could only be observed. However, tilting of the specimen at 17° angle – with respect to the axis of the holder – resulted in a diffraction pattern with the lattice planes of 4.2 Å (Fig. A.4.10, Appendix) confirming that the multi-twisted nanosheets had resulted from the overlaying of component hexagonal Zn–CuNC layers. Also, diffraction spots having distances of 4.7 Å and 2.6 Å from the origin (0A and 0B, respectively) in Fig. 4.2C (*i.e.*, corresponding to the two planar distances of Zn–CuNC nanosheets) indicated that the diffraction pattern might be due to the lattices of the complex, with the basic hexagonal lattice unit of Zn–CuNC nanosheets. The expected diffraction planes of hexagonal lattices, along with the marking of the planes obtained in the SAED image of the assembly, are depicted on an experimentally obtained diffraction pattern image in the appendix (Fig. A.4.11, Appendix). The TEM results also indicated that the nanosheets in the assembled product were in closer vicinity with relative orientation against each other to have strong interlayer interaction and to have given rise to additional periodicities. The results are consistent with the conclusions made from the results of the photoluminescence measurements that TPP mediated π–π supramolecular interaction between the hexagonal Zn–CuNC nanosheets brought the layers close enough to activate metallophilic interactions. Moreover, the twist angles of two consecutive nanosheets (as measured from the angular separation of the neighbouring diffraction spots) were calculated to be below 5° (Fig. 4.2C). The smallness of the angles resulted in large moiré diffractions and strong interlayer cuprophilic interactions. Additional TEM images of the moiré Zn–CuNCs of different sizes have been provided in the appendix (Fig. A.4.12, Appendix). The results indicated that moiré structures of the stacked nanosheets were formed notwithstanding their sizes.

Now, considering the complex diffraction pattern resulted from the multi-layer rotated hexagonal Zn–CuNCs of lattice constant 4.7 Å, possible moiré periodicities corresponding to all the measured twist angles were calculated using the following equation of conventional rotational moiré model and are presented in tabular form with angular notation in the Appendix (Table A.4.1)

$$\boldsymbol{a/2D = \mathrm{Sin}(\theta/2)} \quad \text{.....(1)}$$

where a = basal lattice constant (the lattice constant for the hexagonal array of CuNCs, *i.e.*, 4.7 Å), D = period of moiré lattice, and θ = twisted angle.

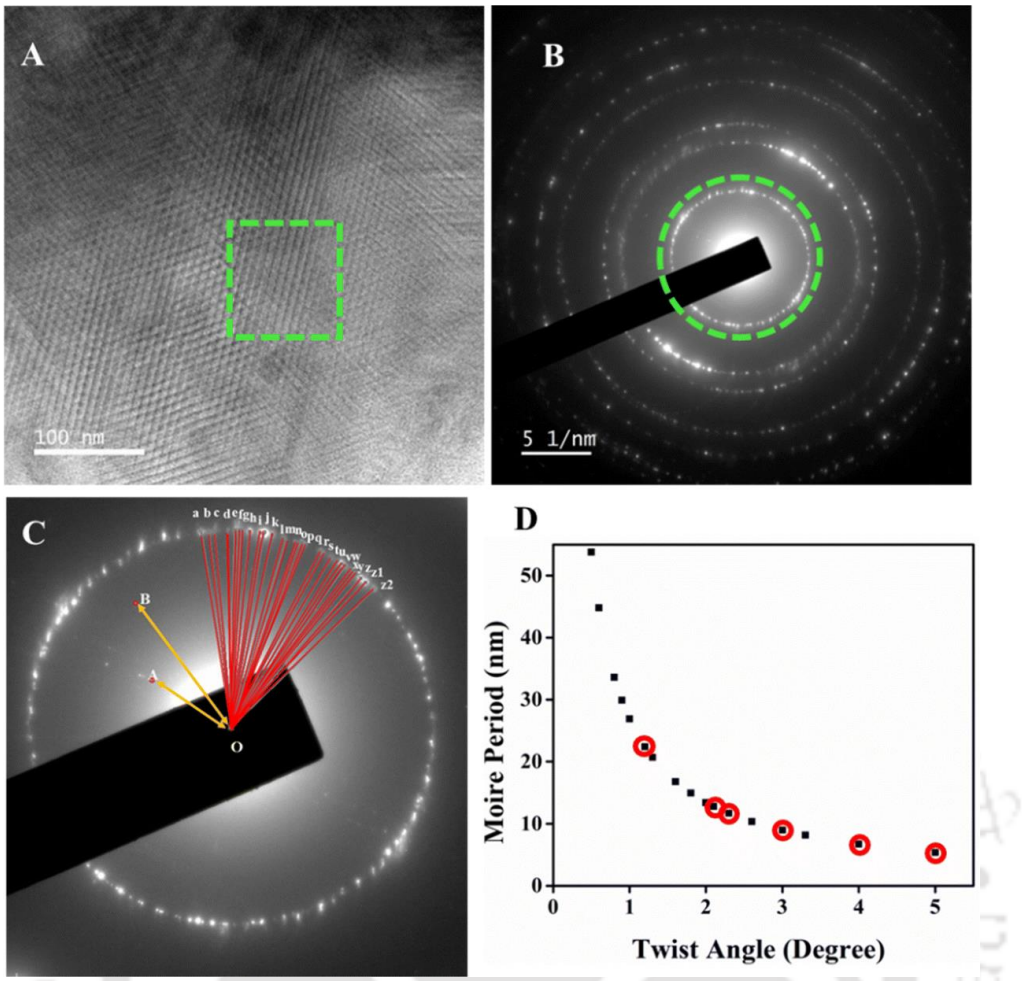

Fig. 4.2 (**A**) Transmission electron microscopy (TEM) image of the TPP added Zn–CuNC nanosheets depicting moiré lattices, (**B**) corresponding selected area electron diffraction (SAED) pattern image, (**C**) enlarged view of the encircled part of image B depicting the twist angles, and (**D**) plot of the possible moiré periods *versus* the twist angles obtained from image C (with the periods marked in red circles matching perfectly with the experimentally observed moiré image parameters).

Interestingly, the experimentally observed moiré periods, of values 5.4 nm, 7.1 nm, 11.2 nm, 8.7 nm, 12.9 nm, and 21.5 nm in Fig. 4.2A, matched with some of the values calculated for low twist angle (measured from Fig. 4.2C) superpositions of hexagonal lattices using eqn (1). Fig. 4.2D represents the calculated possible moiré periods corresponding to the measured twist angles with those encircled in red matched with the experimentally observed lattices. Since the calculated moiré periods were from single stacked sheets of hexagonal lattices of lattice constant (4.7 ± 0.2) Å, it can be concluded that the experimentally observed

periodicities were the result of multiple stacking of hexagonal Zn–CuNC nanosheets at smaller twist angles (≤ 5^0). Although moiré superlattices of van der Waals heterostructures consisting of graphene, metal dichalcogenides and boron nitride have been reported recently, the current work may be considered as a first report of such a structure generated based on hierarchical assemblies of metal nanoclusters by using chemical means in a liquid medium.[33–36] The precise positionings of CuNCs at short distances led to photoluminescence that originated from pairwise cuprophilic interactions of the neighbouring clusters. The results portend a bright future of programmed chemical assembly of moiré superlattices of function-specific and interactive nanostructures. A pictorial view of the formation of multi-twisted stacking of hexagonal lattices with small angular rotations (<5°), through chemical reaction of the hexagonal nanosheets with TPP molecules and with its corresponding electron diffraction lattices are shown in Scheme 4.1A. Here each set of two consecutive layers (colored in black and red) in the multi-twisted stacked nanosheets are responsible for the generation of moiré patterns by strong interlayer interactions of CuNC lattices. The simulated figure of one of the sets with twisting angle of 4° is presented in Scheme 4.1B, where the two hexagonal layers with a lattice parameter of "*a*" were found to generate an additional moiré periodicity of lattice parameter "*b*" (*b* ≫ *a*) upon stacking at the mentioned twist angle.

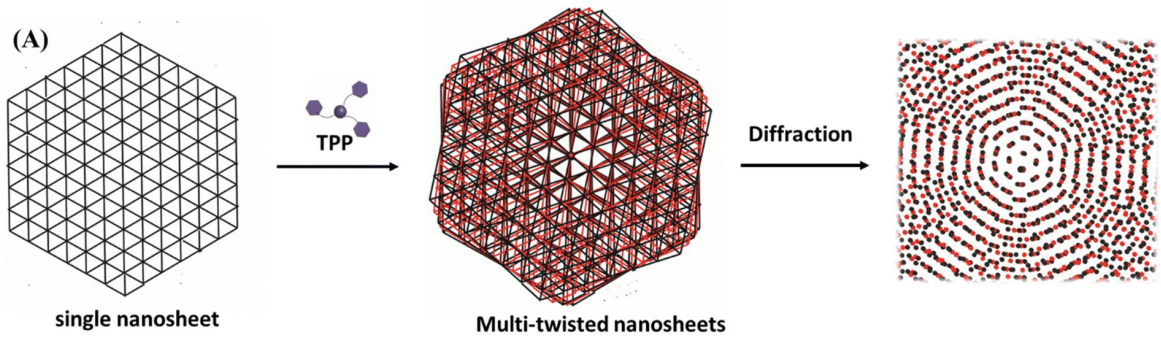

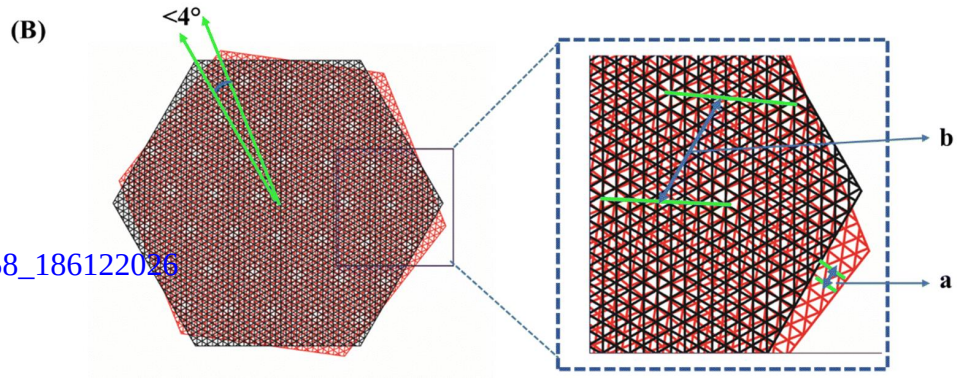

Scheme 4.1 (**A**) Schematic view of the reaction of two-dimensional Zn–CuNC nanosheets of hexagonal lattices with the TPP molecule, giving rise to a product with multi-twisted stacked layers along with its corresponding electron diffraction lattice. (**B**) Simulated structure of two hexagonal lattices rotated at a relative angle of 4° and thus generating higher ordered moiré periodicity.

The so-formed moiré superlattices of Zn–CuNC 2D assemblies were found to have superior optical properties in comparison with the parent nanosheets. The photoluminescence quantum yield of 0.9 mM TPP added Zn–CuNC moiré nanosheets was calculated to be (0.54 ± 0.04) % in the relative method, which was five times higher than that of the constituent hexagonal Zn–CuNC nanosheets (0.10 ± 0.03%) (Table A.4.2, Appendix). The absolute quantum yield measurements using an integrating sphere were also performed (Table A.4.3, Appendix), where the moiré Zn–CuNCs showed higher quantum yield values than the hexagonal Zn–CuNCs with the quantum yield values of (12.04 ± 1.36) % in the dispersion medium and (4.57 ± 0.64) % in the solid state. The moiré superlattices also exhibited delayed emission at around 480 nm with a significant enhancement in emission intensity as compared to the hexagonal Zn–CuNCs (Fig. 4.3A). The recorded lifetimes of time resolved delayed photoluminescence of the moiré and hexagonal nanosheets at their emission maxima were (116.4 ± 7.2) μs and (26.0 ± 6.2) μs, respectively (Fig. 4.3B and Table A.4.4, Appendix). The intense and long delayed photoluminescence at 480 nm that originated due to cuprophilic interactions established novel emission properties of twisted superlattices of the CuNC assemblies hitherto unknown.

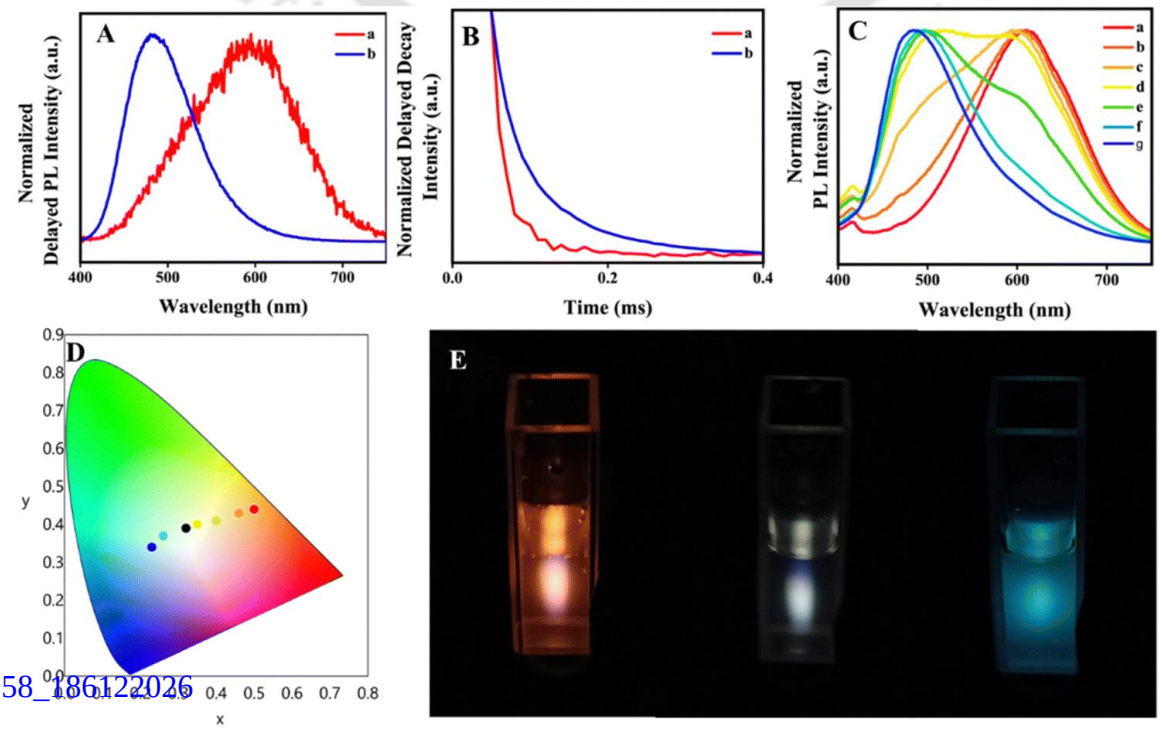

Fig. 4.3. (**A**) Normalized delayed photoluminescence spectra, (**B**) normalized time-resolved delayed photoluminescence decay profiles of (a) Zn–CuNC nanosheets, and (b) 0.9 mM triphenylphosphine (TPP) added Zn–CuNC nanosheets. (**C**) Normalized photoluminescence spectra of (a) Zn–CuNC nanosheets and that recorded upon addition of (b) 0.12 mM, (c) 0.23 mM, (d) 0.29 mM, (e) 0.35 mM, (f) 0.45 mM and (g) 0.55 mM of TPP and (**D**) corresponding chromaticity color coordinates in the CIE diagram. (**E**) Digital photographs of the liquid dispersions of hexagonal Zn–CuNC, and 0.35 mM and 0.9 mM TPP added Zn–CuNC nanosheets under UV light excitation of 365 nm.

As mentioned above, the moiré stacking of 2D assemblies of Cu nanoclusters generated a new emission at 490 nm due to interactions between clusters of intervening layers, in addition to the retention of the original emission at 600 nm owing to the clusters in the original assemblies. In other words, the photoluminescence properties that consist of both prompt and delayed luminescence, of the moiré superlattices had two components in the visible region of wavelengths – one at longer wavelength (red) while the other appeared at shorter wavelength (blue). In addition, the extent of supramolecular assembly – resulting in superlattice formations – could be controlled by the concentration of TPP, thus providing a chemical handle in tuning the emission properties of the assemblies. Specifically, the emission intensity ratios at 490 nm to that 600 nm could be tuned by the solution concentration of TPP. The photoluminescence spectra of (a) hexagonal Zn–CuNC nanosheets and those recorded upon addition of (b) 0.12 mM, (c) 0.23 mM, (d) 0.29 mM, (e) 0.35 mM, (f) 0.45 mM and (g) 0.55 mM of TPP solution are depicted in Fig. 4.3C. The corresponding chromaticity color coordinates with values (0.48, 0.43), (0.44, 0.42), (0.39, 0.41), (0.35, 0.40), (0.32, 0.39), (0.26, 0.37) and (0.23, 0.34), respectively, have been shown through the CIE diagram in Fig. 4.3D. Interestingly, the 0.35 mM TPP added Zn–CuNC moiré nanosheets gave near white light emission with the chromaticity index value of (0.32, 0.39), correlated color temperature (CCT) value of 5848 K and color rendering index (CRI) of 84. Digital photographs of red luminescent Zn–CuNCs and TPP added moiré Zn–CuNCs with white and blue emission are presented in Fig. 4.3E and their corresponding photoluminescence spectra with time are also presented in the Appendix (Fig. A.4.13). The results indicated substantial stabilities of the assembled products in the dispersion medium. Thus, the results demonstrated metallophilic interaction-based tuneable photoluminescence – especially near while light emission – from moiré superlattices of 2D Zn–CuNC assemblies. Such an achievement of

chemically twisted assemblies of interactive metal NCs or similar moieties giving rise to novel optical properties may have bright future prospects for practical applications.

4.5 Conclusion:

In summary, we have shown directed synthesis of moiré superlattices starting from small ligand stabilized red luminescent CuNCs first by assembling them into crystalline 2D nanosheets using complexation reaction. That was followed by the formation of an isodesmic super-stacked assembly of the crystalline nanosheets with small relative twist angles induced by supramolecular π–π interaction with the TPP molecule. The so-formed moiré superlattices not only introduced additional periodicity to the system but also an additional emissive energy state (with emission maximum at 480–490 nm) resulting in superior prompt and delayed photoluminescence. Moreover, depending on the population of the moiré superlattice, it has been possible to tune the emission color of the super-assembly and generate white light with a chromaticity index value of (0.32, 0.39). This discovery thus opens a path in engineering nanoparticle-based 2D moiré superlattices with novel physical properties, based on the principle of molecular chemistry, especially supramolecular interactions.

4.6 Bibliography:

1. Liu, W.; Kraemer, S.; Sarkar, D.; Li, H.; Ajayan, P. M.; Banerjee, K., Controllable and Rapid Synthesis of High-Quality and Large-Area Bernal Stacked Bilayer Graphene Using Chemical Vapor Deposition. *Chem. Mater.* **2014,** *26* (2), 907-915.

2. Sharma, M.; Ajayan, P. M.; Deb, P., Quantum Energy Storage in 2D Heterointerfaces. *Adv. Mater. Interfaces* **2023,** *10* (11), 2202058.

3. Motala, M. J.; Zhang, X.; Kumar, P.; Oliveira, E. F.; Benton, A.; Miesle, P.; Rao, R.; Stevenson, P. R.; Moore, D.; Alfieri, A.; Lynch, J.; Austin, D.; Post, S.; Gao, G.; Ma, S.; Zhu, H.; Wang, Z.; Petrov, I.; Stach, E. A.; Kennedy, W. J.; Vangala, S.; Tour, J. M.; Galvao, D. S.; Jariwala, D.; Muratore, C.; Snure, M.; Ajayan, P. M.; Glavin, N. R., Synthesis of two-dimensional van der waals superlattices, heterostructures, and alloys from conversion of sequentially layered sub-nanometer metal films. *Mater. Today Nano* **2023,** *22*, 100319.

4. Kim, G.; Song, S.; Jariwala, D., Spatially controlled two-dimensional quantum heterostructures. *Mater. Res. Lett* **2023,** *11* (5), 327-346.

5. Song, Z.; Sun, X.; Wang, L., Switchable Asymmetric Moiré Patterns with Strongly Localized States. *J. Phys. Chem. Lett.* **2020,** *11* (21), 9224-9229.

6. Yang, Q.; Wu, M.; Li, J., Origin of Two-Dimensional Vertical Ferroelectricity in WTe2 Bilayer and Multilayer. *J. Phys. Chem. Lett.* **2018,** *9* (24), 7160-7164.

7. Cao, Y.; Fatemi, V.; Fang, S.; Watanabe, K.; Taniguchi, T.; Kaxiras, E.; Jarillo-Herrero, P., Unconventional superconductivity in magic-angle graphene superlattices. *Nature* **2018,** *556* (7699), 43-50.

8. Fischer, A.; Goodwin, Z. A. H.; Mostofi, A. A.; Lischner, J.; Kennes, D. M.; Klebl, L., Unconventional superconductivity in magic-angle twisted trilayer graphene. *npj Quantum Mater.* **2022,** *7* (1), 5.

9. Sunku, S. S.; Ni, G. X.; Jiang, B. Y.; Yoo, H.; Sternbach, A.; McLeod, A. S.; Stauber, T.; Xiong, L.; Taniguchi, T.; Watanabe, K.; Kim, P.; Fogler, M. M.; Basov, D. N., Photonic crystals for nano-light in moiré graphene superlattices. *Sci.* **2018,** *362* (6419), 1153-1156.

10. Tran, K.; Moody, G.; Wu, F.; Lu, X.; Choi, J.; Kim, K.; Rai, A.; Sanchez, D. A.; Quan, J.; Singh, A.; Embley, J.; Zepeda, A.; Campbell, M.; Autry, T.; Taniguchi, T.; Watanabe, K.; Lu, N.; Banerjee, S. K.; Silverman, K. L.; Kim, S.; Tutuc, E.; Yang, L.; MacDonald, A. H.; Li, X., Evidence for moiré excitons in van der Waals heterostructures. *Nature* **2019,** *567* (7746), 71-75.

11. Jin, C.; Regan, E. C.; Yan, A.; Iqbal Bakti Utama, M.; Wang, D.; Zhao, S.; Qin, Y.; Yang, S.; Zheng, Z.; Shi, S.; Watanabe, K.; Taniguchi, T.; Tongay, S.; Zettl, A.; Wang,

F., Observation of moiré excitons in WSe2/WS2 heterostructure superlattices. *Nature* **2019,** *567* (7746), 76-80.

12. Alexeev, E. M.; Ruiz-Tijerina, D. A.; Danovich, M.; Hamer, M. J.; Terry, D. J.; Nayak, P. K.; Ahn, S.; Pak, S.; Lee, J.; Sohn, J. I.; Molas, M. R.; Koperski, M.; Watanabe, K.; Taniguchi, T.; Novoselov, K. S.; Gorbachev, R. V.; Shin, H. S.; Fal'ko, V. I.; Tartakovskii, A. I., Resonantly hybridized excitons in moiré superlattices in van der Waals heterostructures. *Nature* **2019,** *567* (7746), 81-86.

13. Wang, X.; Yasuda, K.; Zhang, Y.; Liu, S.; Watanabe, K.; Taniguchi, T.; Hone, J.; Fu, L.; Jarillo-Herrero, P., Interfacial ferroelectricity in rhombohedral-stacked bilayer transition metal dichalcogenides. *Nat. Nanotechnol.* **2022,** *17* (4), 367-371.

14. Yoo, H.; Engelke, R.; Carr, S.; Fang, S.; Zhang, K.; Cazeaux, P.; Sung, S. H.; Hovden, R.; Tsen, A. W.; Taniguchi, T.; Watanabe, K.; Yi, G.-C.; Kim, M.; Luskin, M.; Tadmor, E. B.; Kaxiras, E.; Kim, P., Atomic and electronic reconstruction at the van der Waals interface in twisted bilayer graphene. *Nat. Mater.* **2019,** *18* (5), 448-453.

15. Quan, J.; Linhart, L.; Lin, M.-L.; Lee, D.; Zhu, J.; Wang, C.-Y.; Hsu, W.-T.; Choi, J.; Embley, J.; Young, C.; Taniguchi, T.; Watanabe, K.; Shih, C.-K.; Lai, K.; MacDonald, A. H.; Tan, P.-H.; Libisch, F.; Li, X., Phonon renormalization in reconstructed MoS2 moiré superlattices. *Nat. Mater.* **2021,** *20* (8), 1100-1105.

16. Lee, J. Y.; Khalaf, E.; Liu, S.; Liu, X.; Hao, Z.; Kim, P.; Vishwanath, A., Theory of correlated insulating behaviour and spin-triplet superconductivity in twisted double bilayer graphene. *Nat. Commun.* **2019,** *10* (1), 5333.

17. Cao, Y.; Fatemi, V.; Demir, A.; Fang, S.; Tomarken, S. L.; Luo, J. Y.; Sanchez-Yamagishi, J. D.; Watanabe, K.; Taniguchi, T.; Kaxiras, E.; Ashoori, R. C.; Jarillo-

Herrero, P., Correlated insulator behaviour at half-filling in magic-angle graphene superlattices. *Nature* **2018,** *556* (7699), 80-84

18. Das, P.; Chattopadhyay, A., Delayed Dual Emission of Two-Dimensional Copper Nanocluster Assembly. *J. Phys. Chem. C* **2022,** *126* (2), 997-1005.

19. Basu, S.; Chattopadhyay, A., Room-Temperature Delayed Fluorescence of Gold Nanoclusters in Zinc-Mediated Two-Dimensional Crystalline Assembly. *Langmuir* **2019,** *35* (15), 5264-5270.

20. Paul, M.; Basu, S.; Chattopadhyay, A., Complexation Reaction-Based Two-Dimensional Luminescent Crystalline Assembly of Atomic Clusters for Recyclable Storage of Oxygen. *Langmuir* **2020,** *36* (3), 754-759.

21. Basu, S.; Bhandari, S.; Pan, U. N.; Paul, A.; Chattopadhyay, A., Crystalline nanoscale assembly of gold clusters for reversible storage and sensing of CO2via modulation of photoluminescence intermittency. *J. Mater. Chem. C* **2018,** *6* (30), 8205-8211.

22. Basu, S.; Goswami, U.; Paul, A.; Chattopadhyay, A., Crystalline assembly of gold nanoclusters for mitochondria targeted cancer theranostics. *J. Mater. Chem. B* **2018,** *6* (11), 1650-1657.

23. Das, P.; Chattopadhyay, A., Enhanced Chemical Stability in the Twisted Dodecagonal Stacking of Two-Dimensional Copper Nanocluster Assemblies. *J. Phys. Chem. Lett.* **2022,** *13* (37), 8793-8800.

24. Suri, N.; Wang, C.; Zhang, Y.; Xiao, D., Chiral Phonons in Moiré Superlattices. *Nano Lett.* **2021,** *21* (23), 10026-10031.

25. Li, Y.; Xue, M.; Fan, H.; Gao, C.-F.; Shi, Y.; Liu, Y.; Watanabe, K.; Tanguchi, T.; Zhao, Y.; Wu, F.; Wang, X.; Shi, Y.; Guo, W.; Zhang, Z.; Fei, Z.; Li, J., Symmetry Breaking and Anomalous Conductivity in a Double-Moiré Superlattice. *Nano Lett.* **2022,** *22* (15), 6215-6222.

26. Ci, P.; Zhao, Y.; Sun, M.; Rho, Y.; Chen, Y.; Grigoropoulos, C. P.; Jin, S.; Li, X.; Wu, J., Breaking Rotational Symmetry in Supertwisted WS2 Spirals via Moiré Magnification of Intrinsic Heterostrain. *Nano Lett.* **2022,** *22* (22), 9027-9035.

27. Rest, C.; Kandanelli, R.; Fernández, G., Strategies to create hierarchical self-assembled structures via cooperative non-covalent interactions. *Chem. Soc. Rev.* **2015,** *44* (8), 2543-2572.

28. Dhiman, S.; Sarkar, A.; George, S. J., Bioinspired temporal supramolecular polymerization. *RSC Adv.* **2018,** *8* (34), 18913-18925.

29. Hartlieb, M.; Mansfield, E. D. H.; Perrier, S., A guide to supramolecular polymerizations. *Polym. Chem.* **2020,** *11* (6), 1083-1110.

30. Wu, Z.; Liu, J.; Gao, Y.; Liu, H.; Li, T.; Zou, H.; Wang, Z.; Zhang, K.; Wang, Y.; Zhang, H.; Yang, B., Assembly-Induced Enhancement of Cu Nanoclusters Luminescence with Mechanochromic Property. *J. Am, Chem. Soc.* **2015,** *137* (40), 12906-12913.

31. Wu, Z.; Liu, J.; Li, Y.; Cheng, Z.; Li, T.; Zhang, H.; Lu, Z.; Yang, B., Self-Assembly of Nanoclusters into Mono-, Few-, and Multilayered Sheets via Dipole-Induced Asymmetric van der Waals Attraction. *ACS Nano* **2015,** *9* (6), 6315-6323.

32. Liu, Y.; Yao, D.; Zhang, H., Self-Assembly *ACS Nano* Driven Aggregation-Induced Emission of Copper Nanoclusters: A Novel Technology for Lighting. *ACS Appl. Mater. Interfaces* **2018,** *10* (15), 12071-12080.

33. Carr, S.; Fang, S.; Kaxiras, E., Electronic-structure methods for twisted moiré layers. *Nat. Rev. Mater.* **2020,** *5* (10), 748-763.

34. Liu, Y.; Huang, Y.; Duan, X., Van der Waals integration before and beyond two-dimensional materials. *Nature* **2019,** *567* (7748), 323-333.

35. Sutter, P.; Wimer, S.; Sutter, E., Chiral twisted van der Waals nanowires. *Nature* **2019,** *570* (7761), 354-357.

36. Rhodes, D.; Chae, S. H.; Ribeiro-Palau, R.; Hone, J., Disorder in van der Waals heterostructures of 2D materials. *Nat. Mater.* **2019,** *18* (6), 541-549

Appendix

A4 Chapter 4

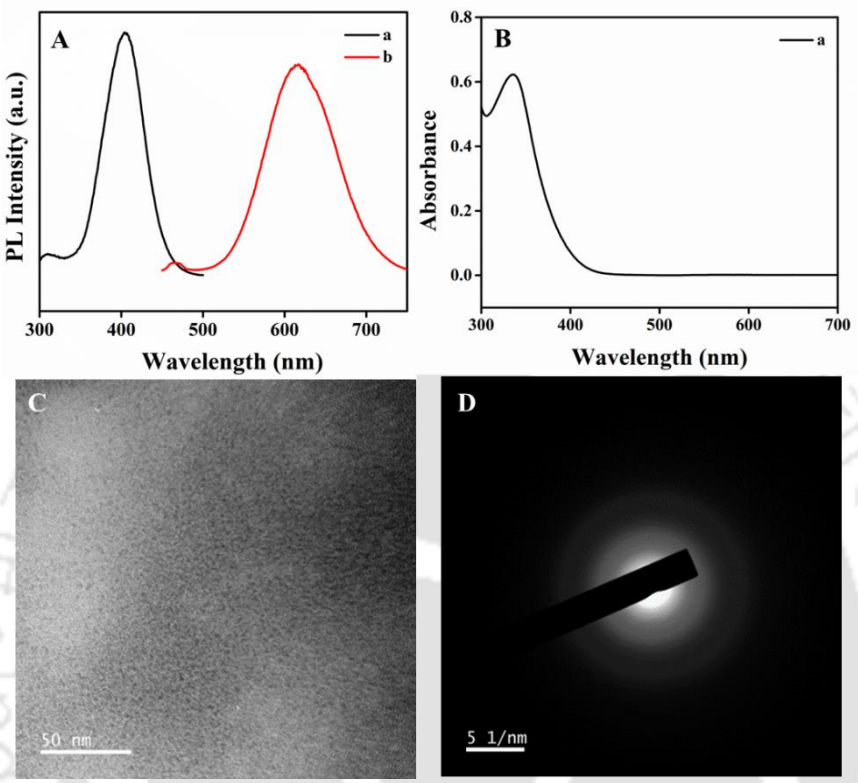

Fig. A.4.1. (**A**) (**a**) Excitation spectrum (emission wavelength was set at 615 nm) and (**b**) emission spectrum (excitation wavelength was set at 405 nm) of the as-synthesized Cu nanoclusters (CuNCs). (**B**) UV-Vis spectrum of the CuNCs. (**C**) Transmission electron microscopy (TEM) image of the as synthesized CuNCs and (**D**) selected area electron diffraction (SAED) pattern acquired on a typical area shown in image C.

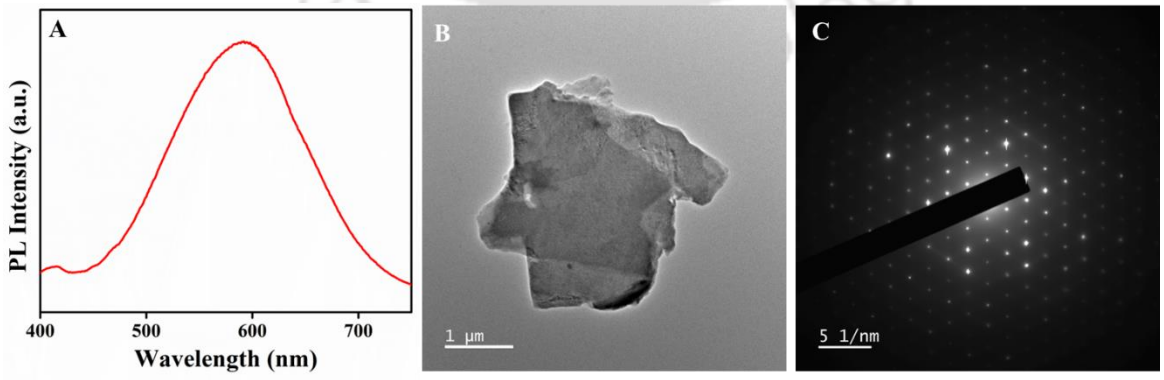

Fig. A.4.2. (**A**) Photoluminescence emission spectrum of Zn-CuNCs (excitation maximum was set at 365 nm). (**B**) Transmission electron microscopy (TEM) image of Zn-CuNC nanosheet and (**C**) corresponding selected area electron diffraction (SAED) pattern image.

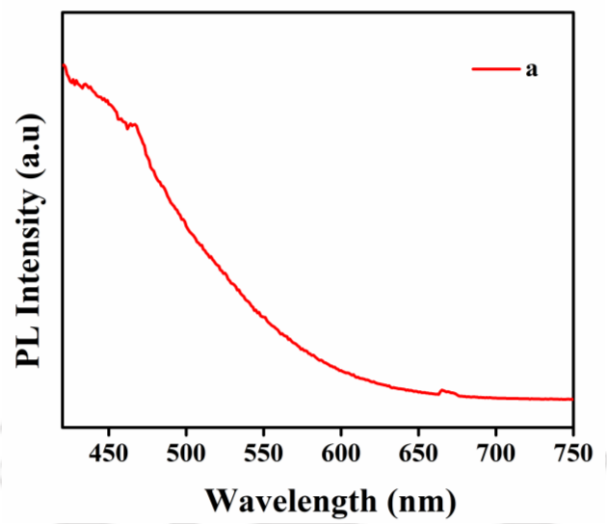

Fig. A.4.3. (**a**) Photoluminescence emission spectrum of triphenylphosphine (TPP) added zinc acetate solution (excitation wavelength was set at 365 nm).

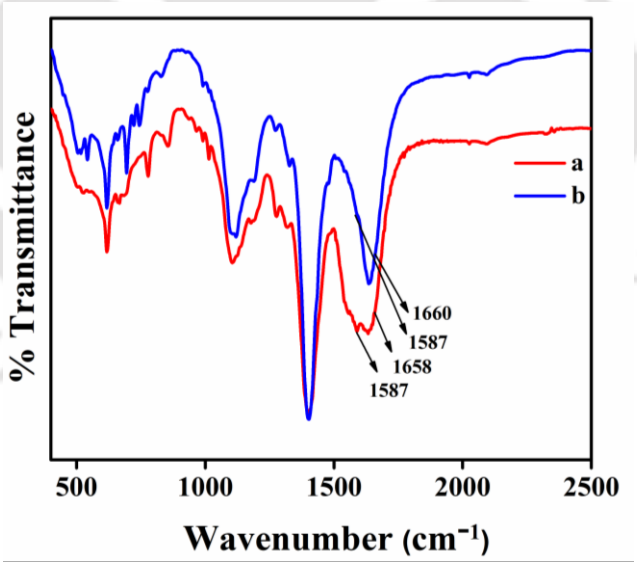

Fig. A.4.4. Fourier-transform infrared spectra of (a) Zn-CuNCs and (b) 0.9mM TPP added Zn-CuNCs.

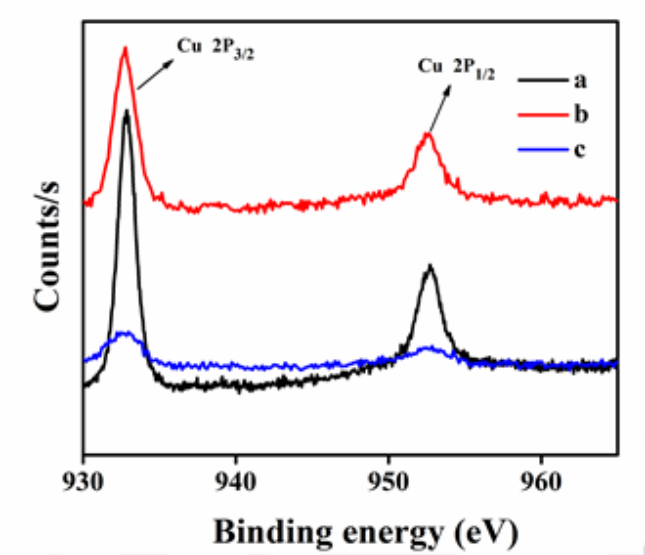

Fig. A.4.5. X-ray photoelectron spectra of (a) as synthesized CuNCs, (b) Zn-CuNCs, and (c) . TPP added multi-twited Zn-CuNCs.

Calculation of association constant for supramolecular stacking process:

The degree of stacking-assembly was calculated with the following equation

$$\alpha = (I_C - I_H) / (I_S - I_H) \quad \text{.....Equation A.4.1}$$

where, I_C = Photoluminescence intensity of the medium containing Zn-CuNCs at any given concentration of TPP,

I_H = Photoluminescence intensity of the medium containing component hexagonal Zn-CuNCs only (without any twisted stacking assembly), and

I_S = Photoluminescence intensity of the medium containing completely twisted-stacked nanosheets at the highest concentration of TPP.

Plot of α vs concentration of TPP resulted in the curve below with sigmoidal nature (characteristic of an isodesmic supramolecular reaction). [S1] The fitting of the curve with Hill equation using Origin software gave the association constant value of $(5.8 \pm 2.0) \times 10^4\ M^{-1}$.

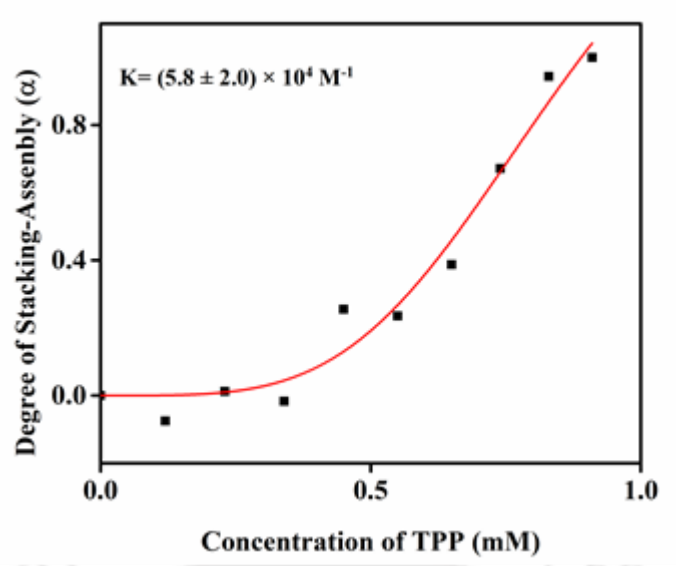

Fig. A.4.6. Plot of degree of stacking assembly versus concentration of TPP.

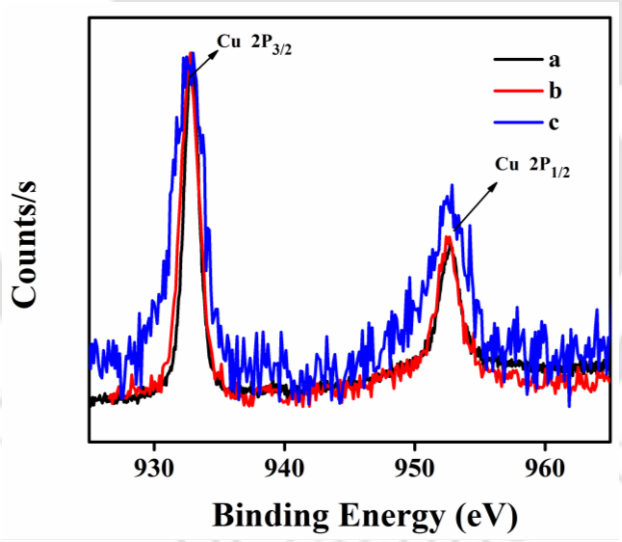

Fig A.4.7. Normalized x-ray photoelectron spectra of (a) as synthesized CuNCs, (b) Zn-CuNCs, and (c) TPP added multi-twisted Zn-CuNCs.

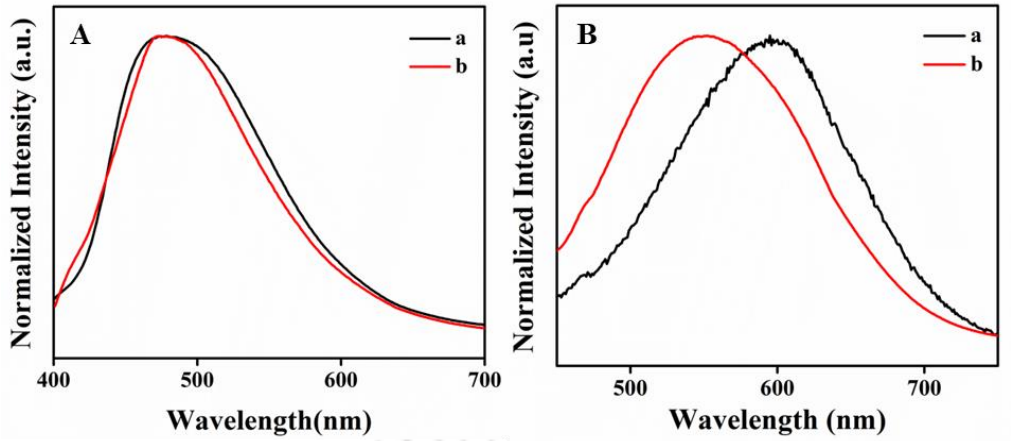

Fig. A.4.8: (**A**) Photoluminescence spectra of 0.9mM TPP added Zn-CuNCs in (**a**) the dispersion medium and (**b**) solid state. (**B**) Photoluminescence spectra of hexagonal Zn-CuNCs in (**a**) the dispersion medium and (**b**) solid state.

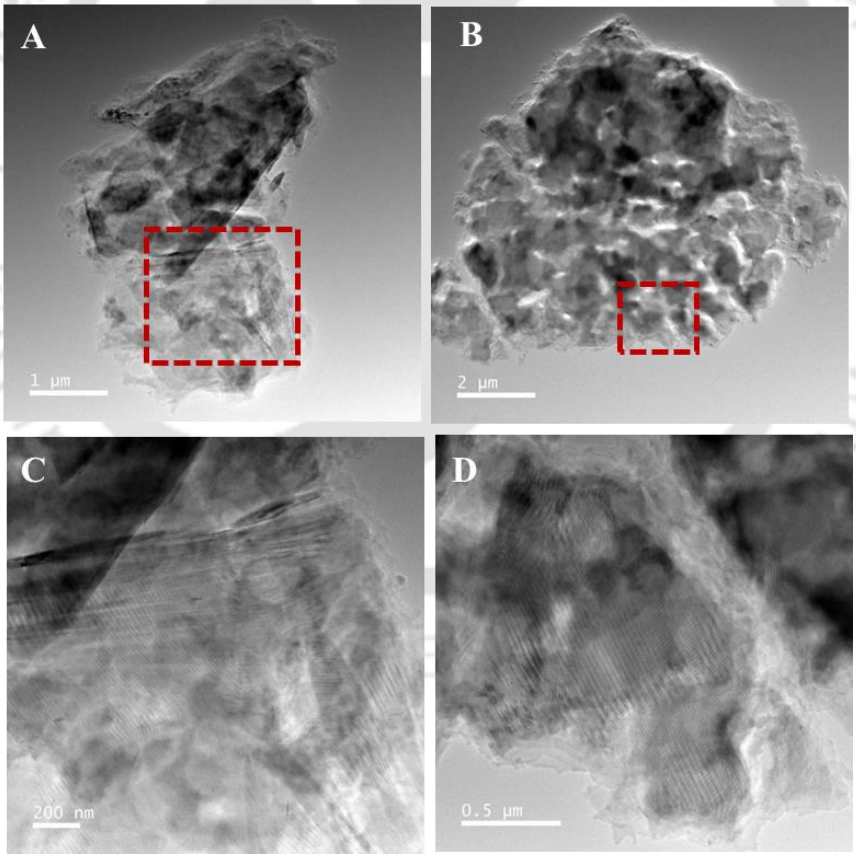

Fig. A.4.9. (A, B) Transmission electron microscopy (TEM) images of TPP added Zn-CuNC moiré nanosheets and (**C, D**) enlarged views of the marked areas showing moiré lattices in the images A and C, respectively.

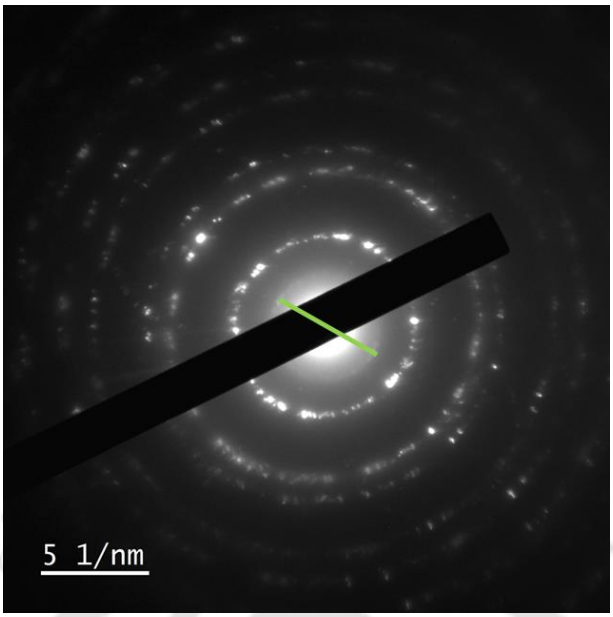

Fig. A.4.10. Selected area electron diffraction (SAED) pattern image of the TPP added Zn-CuNC nanosheet given in Fig. S9C recorded through rotation of the sample holder at an angle of 17° (having marked the plane with lattice parameter of 4.2 Å).

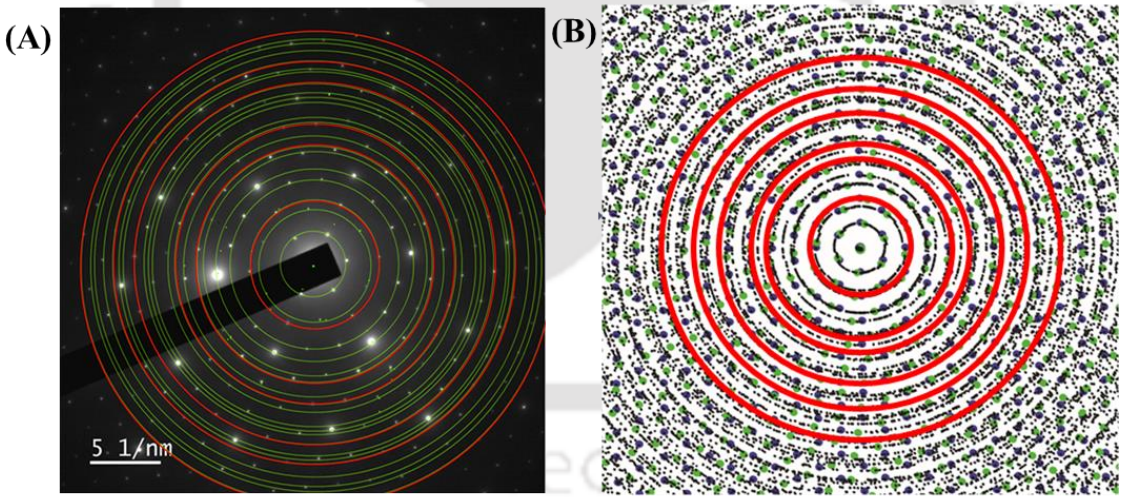

Fig. A.4.11. (**A**) Experimentally obtained selected area electron diffraction (SAED) pattern image of a typical Zn-CuNC nanosheet with hexagonal diffraction lattices marking all the planes in green and the observed planes in the moiré nanosheet in red. (**B**) Simulated image of multiple twisted hexagonal lattices (with twist angles measured from **Fig.** 2C) with the experimentally obtained diffraction planes in red circles.

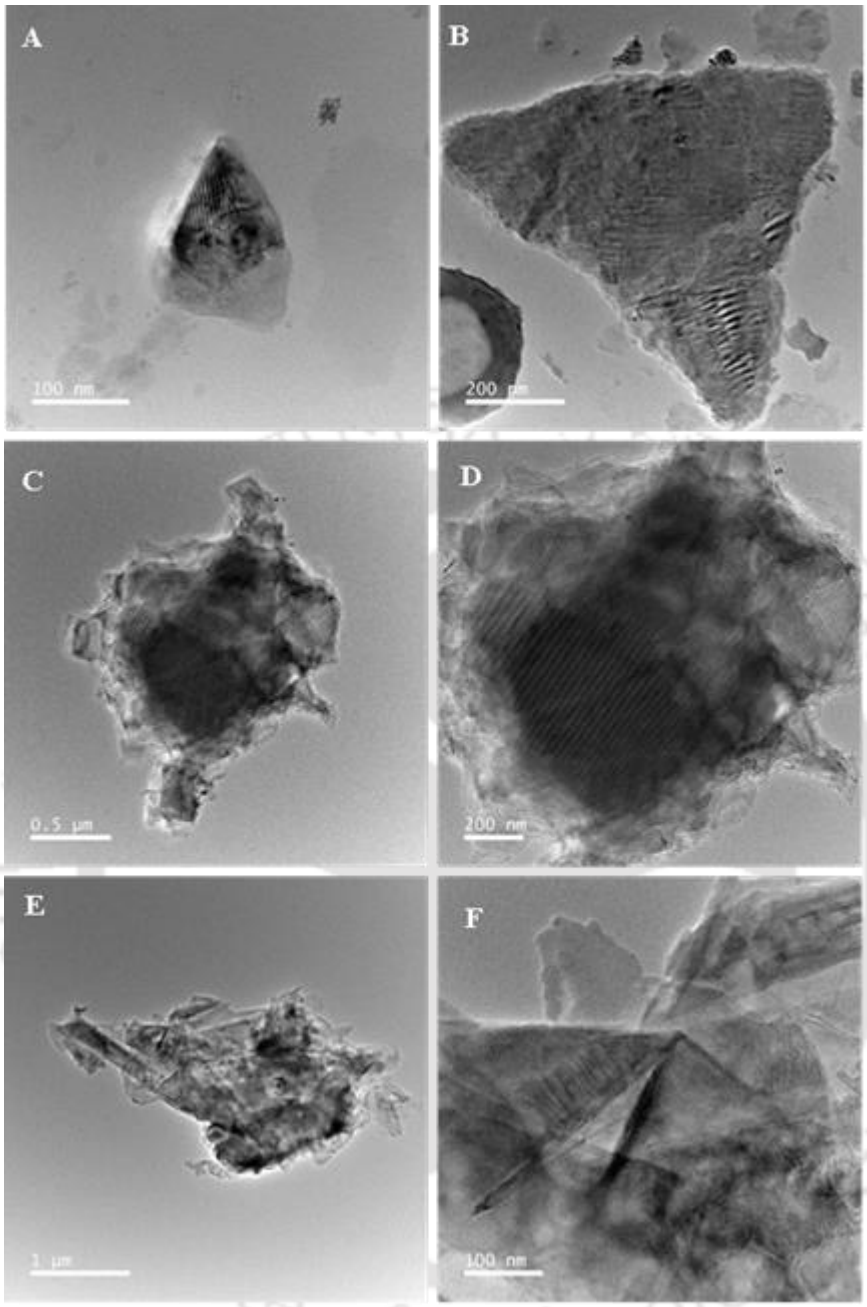

Fig. A.4.12. (**A, B, C, E**) Additional transmission electron microscopy (TEM) images of moiré-Zn-CuNC nanosheets and (**D** and **F**) TEM images at different scales of those in C and E, respectively.

Table A.4.1. All the relative twisted angles measured from the SAED image in the **Fig.** 2C and the calculated values of the corresponding moiré periods.

	Angle notation	Angles, **θ** (Degree)	Moire Period, **D** (nm)
1	<a0b, <j0k	2.3	**11.7**
2	<b0c, <o0p	1.6	16.8
3	<c0d	4	**6.7**
4	<d0e, <t0u	2.1	**12.8**
5	<e0f, <m0n, <p0q	0.5	53.8
6	<f0g, <i0j	1	26.9
7	<g0h	2.6	10.4
8	<h0i, <k0l	3.3	8.1
9	<l0m	0.6	44.8
10	<q0r, <s0t	0.9	29.9
11	<r0s	5	**5.4**
12	<t0u, <w0x	2	13.4
13	<u0v, <x0y	1.3	20.7
14	<v0w	1.2	**22.4**
15	<y0z	0.8	33.6
16	<z0z1, <z10z2	1.8	14.9
17	<n0o	3	**8.9**

Quantum yield calculation (based on relative method):

Photoluminescence quantum yield was measured with respect to quinine sulphate in 0.1 M H_2SO_4 with reported quantum yield of 54% using the following equation-

$$\varphi_S = \varphi_R \times \frac{I_S}{I_R} \times \frac{A_R}{A_S} \times \frac{\eta_S^2}{\eta_R^2} \quad \text{..... Equation S2}$$

Here, φ_S = quantum yield of the sample; φ_R = quantum yield of the reference; I_S = area under the emission spectrum of the sample; I_R = area under the emission spectrum of reference; A_R = absorbance of reference; A_S = absorbance of the sample; η_S = refractive index of the sample solution; η_R = refractive index of reference. Refractive index of water = 1.33, QY of quinine sulphate=0.54

Table 2. Parameters for quantum yield measurements (based on relative method).

Sample	Experi-ment No	Area under the PL curve of QS excited at 365 nm (a.u.) (I_R)	Area under the PL curve of sample excited at 365 nm (a.u.) (I_S)	Absorbance of QS at 365 nm (A_R)	Absorbance of the sample at 365 nm (A_S)	Quantum yield (Q.Y.) (%)	Average quantum yield with error bar (%)
Hexagonal Zn-CuNCs	1	4.4×10^8	1.37×10^6	0.1074	0.1254	0.14	0.10±0.03
	2	5.5×10^8	1.12×10^6	0.1003	0.1367	0.08	
	3	5.5×10^8	1.04×10^6	0.1003	0.1131	0.09	
Moiré Zn-CuNCs	1	4.4×10^8	5.07×10^6	0.1074	0.1241	0.54	0.54±0.04
	2	4.4×10^8	3.87×10^6	0.1074	0.1037	0.49	
	3	4.4×10^8	4.66×10^6	0.1074	0.1054	0.58	

Table A.4.3. Absolute quantum yield values (using an integrating sphere) of hexagonal Zn-CuNCs and moiré Zn-CuNCs in the dispersed medium and solid state.

Sample		Dispersed medium		Solid state (thin film)	
	Experiment No.	Absolute quantum yield (%)	Average absolute quantum yield (%)	Absolute quantum yield (%)	Average absolute quantum yield (%)
Hexagonal Zn-CuNCs	1	0.50	1.35±0.6	1.90	2.28±0.29
	2	1.60		2.62	
	3	1.95		2.34	
Moiré Zn-CuNCs	1	10.84	12.04±1.36	3.68	4.57±0.64
	2	11.34		4.85	
	3	13.95		5.19	

Table A.4.4. Calculated parameters as-obtained from time resolved delayed photoluminescence decay study of Zn-CuNCs and TPP added moiré Zn-CuNCs in sub-millisecond range.

Sample	Hexagonal Zn-CuNCs			Moiré Zn-CuNCs		
Experiment no	1	2	3	1	2	3
$\chi 2$	0.99	0.99	0.99	0.99	0.99	0.99
First component α_1 (%)	6.37×10^5	6.52×10^5	4.71×10^5	9.33×10^7	1.54×10^7	1.95×10^7
First component lifetime τ_1 (ms)	0.027	0.023	0.070	0.040	0.036	0.033
Second component α_2 (%)	3.76×10^6	5.12×10^5	4.29×10^6	8.31×10^7	1.46×10^7	1.49×10^7
Second component lifetime τ_2 (ms)	7.0×10^{-4}	0.003	0.016	0.152	0.131	0.129
Average lifetime τ_{av} (ms)	0.024	0.021	0.033	0.1265	0.1096	0.1133
Average lifetime with error bar τ_{av} (μs)	26.0 ± 6.2			116.4 ± 7.2		

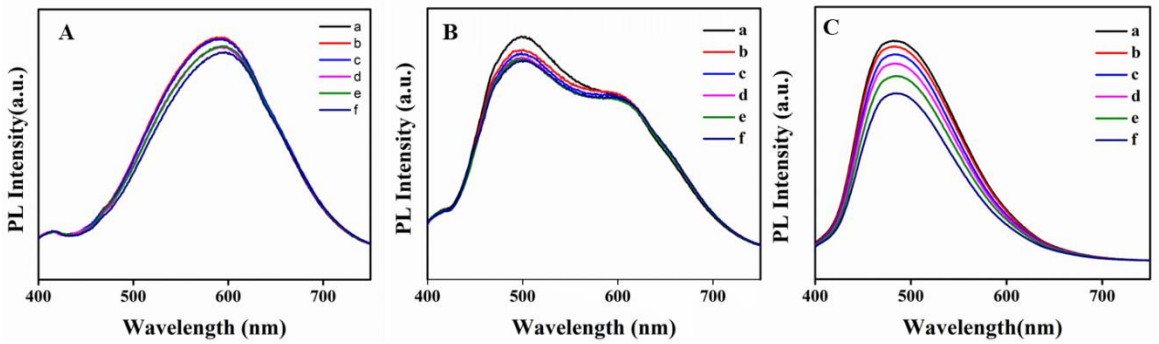

Fig. A.4.13. (**A-C**) Photoluminescence spectra recorded in (**a**) 0min, (**b**) 30 min, (**c**) 60 min, (**d**) 90 min, (**e**) 120 min and (**f**) 270 min of three compounds having red, white and blue luminescence respectively, digital images of which are shown in the Fig. 3E of the manuscript.

Reference:

A.4.1. Hartlieb, M.; Mansfield, E. D. H.; Perrier, S., A guide to supramolecular polymerizations. *Polymer Chemistry* **2020,** *11* (6), 1083-1110.

Chapter 5

Summary and Future Prospects

5.1 Summary:

The current thesis describes the stabilization of weak red luminescent copper nanoclusters (CuNCs) through two-dimensional (2D) single-crystalline assembly followed by super-assembly formation via angular stacking for novel properties. 2D crystalline assembly of the CuNCs showed a huge enhancement in the photoluminescence intensity with the generation of delayed emission with exceptionally higher quantum yield in delayed photoluminescence. Surface functionalization of the nanosheets with 8-hydroxyquinoline created another emitting channel, providing a dual-emitting, single-component nano-compound. The specific ratio of the two luminophores in the same compound produced near-white light emission in both prompt and delayed photoluminescence. During the complexation reaction for nanosheet formation, it was discovered that optimizing the concentration of Zn metal ions in conjunction with CuNCs resulted in hexagonal Zn-CuNCs with a 30° twisted stacking pattern, exhibiting dodecagonal quasiperiodic lattices in the electron diffraction pattern. Moreover, the new quasiperiodic crystal of CuNCs showed improved chemical stability compared to the constituent hexagonal nanosheets when reacted with molecular iodine. Additionally, we demonstrated a supramolecular reaction between triphenylphosphine (TPP) and Zn-CuNC nanosheets resulting in a lower angular twisted stacking and the formation of large moiré superlattices. Interestingly, the additional moiré periodicities in the compound generated an additional quantum emissive state through Cu-Cu inter-nanocluster metallophilic interactions of interactive layers. The moiré superlattices not only enhanced the photoluminescence properties but also generated white light emission with a chromaticity index value of (0.32, 0.39).

5.2 Future Prospects:

This thesis proposes a strategy for stabilizing small ligand-stabilized CuNCs through crystalline assembly formation while preserving the inherent properties of the clusters. This will enable researchers to fully utilize the potential of areal-sensitive CuNCs in various applications. Thereafter, 2D assembly formation and the surface functionalization of the 2D assembly to create a single component dual emitting nanomaterial with enhanced lifetime and white light emission have paved the way for potential future developments in creating white phosphorescent or delayed emitting nanomaterials using photoluminescent metal NCs. This could be highly advantageous in replacing toxic materials in light-emitting diodes. The work of synthesizing 30° twisted stacking of 2D assembly of CuNCs into quasicrystalline structure provides the hope to generate materials with anisotropic properties through deterministic chemical twisting of 2D materials. Moreover, the successful achievement of moiré superlattice formation in liquid medium through chemical interactions holds promise to enhance our comprehension and implementation of twisted electronics in nanoscience based on chemical principles.

For example, we have discovered a potential application of triphenylphosphine (TPP) mediated formation of moiré superlattices of Zn complexed CuNCs (TPP-Zn-CuNCs) in therapeutic activity on cancerous HeLa cells by inducing damage to their mitochondrial membrane potential with greater efficiency in comparison to the constituent 2D Zn-CuNCs or individual CuNCs. The half-maximal inhibitory concentration (IC50) value for the moiré superlattices was determined to be 10.15±2.5 μM (with respect to Cu) through the cytotoxicity results (Fig 5.1). Additionally, the mean membrane destabilization in cells treated with the moiré superlattices was found to be 73.0%) showing a significant efficacy in cancer cell treatment (Fig 5.2).

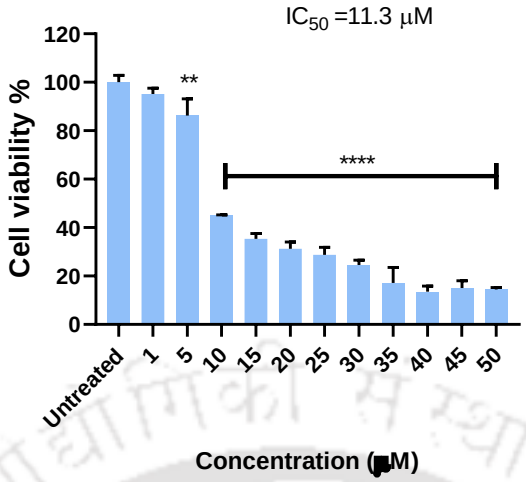

Fig 5.1: A typical cell viability analysis of HeLa cells treated with moiré TPP-Zn-CuNCs.

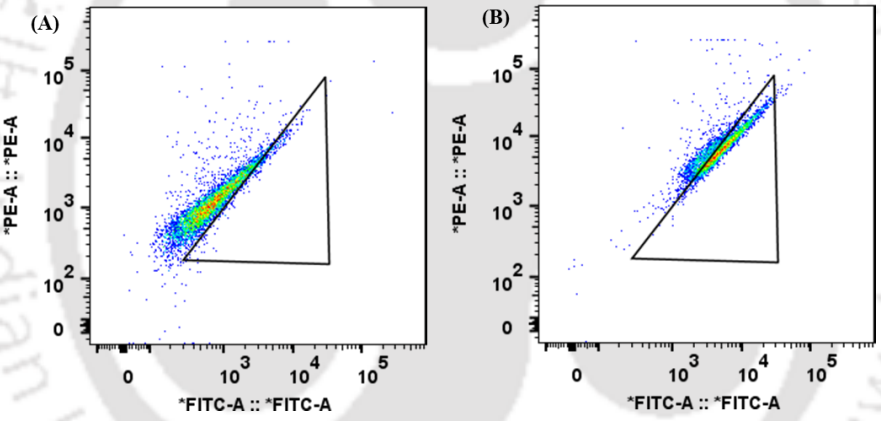

Fig 5.2: Flow cytometry diagram of JC 1 dye-treated (**A**) HeLa cells and (**B**) that treated with moiré-Zn-CuNCs.

*Note: All the biological experiments related to this chapter were performed by Dr. Debashree Debasmita and Ms. Sawna Roy.

List of Publications

1. **Das, P**.; Chattopadhyay, A. Delayed Dual Emission of Two-Dimensional Copper Nanocluster Assembly. *J. Phys. Chem. C* **2022**, *126* (2), 997– 1005, DOI: 10.1021/acs.jpcc.1c07839.

2. **Das, P**.; Chattopadhyay, A. Enhanced Chemical Stability in the Twisted Dodecagonal Stacking of Two-Dimensional Copper Nanocluster Assemblies. *J. Phys. Chem. Lett.* **2022**, *13(37),* 8793–8800, DOI: 10.1021/acs.jpclett.2c02300.

3. **Das, P**.; Chattopadhyay, A. Moiré superlattices of two-dimensional copper nanocluster assemblies with tuneable twin emissions from hierarchical components leading to white light emission. *J. Mater. Chem. C*, **2023**. DOI: 10.1039/d3tc02193a.

4. Sumit Singha, S.; Manna, M.; **Das, P**.; Pramanik Pramanik, S.; Bhandari, S. Surfactant mediated enhanced FRET from quantum-dot complex for ratiometric sensing of food colorants, *Chem. Commun.* **2023,** DOI: 10.1039/D3CC04104B

Permissions

Marketplace

Order Date	16-Oct-2023	Type of Use	Republish in a thesis/dissertation
Order License ID	1406851-1		
ISSN	2050-7496	Publisher	Royal Society of Chemistry
		Portion	Image/photo/illustration

LICENSED CONTENT

Publication Title	Journal of materials chemistry. A, Materials for energy and sustainability	Publication Type	e-Journal
		Start Page	11188
Article Title	Ultra-small and highly crystallized ZnFe2O4 nanoparticles within double graphene networks for super-long life lithium-ion batteries	End Page	11196
		Issue	22
		Volume	5
		URL	http://pubs.rsc.org/en/journals/journalissues/ta
Author/Editor	Royal Society of Chemistry (Great Britain)		
Date	01/01/2013		
Language	English		
Country	United Kingdom of Great Britain and Northern Ireland		
Rightsholder	Royal Society of Chemistry		

REQUEST DETAILS

Portion Type	Image/photo/illustration	Distribution	Worldwide
Number of Images / Photos / Illustrations	1	Translation	Original language of publication
Format (select all that apply)	Print, Electronic	Copies for the Disabled?	No
		Minor Editing Privileges?	No
Who Will Republish the Content?	Not-for-profit entity	Incidental Promotional Use?	No
Duration of Use	Life of current edition	Currency	USD
Lifetime Unit Quantity	Up to 499		
Rights Requested	Main product		

NEW WORK DETAILS

Title	Chemically twisted superlattices of two-dimensional assembly of copper nanocluster	Institution Name	IIT Guwahati
		Expected Presentation Date	2023-12-21
Instructor Name	Priya Das		

TH-3358_186122026

ADDITIONAL DETAILS

Order Reference Number	N/A	**The Requesting Person / Organization to Appear on the License**	Priya Das

REQUESTED CONTENT DETAILS

Title, Description or Numeric Reference of the Portion(s)	Figure 1	**Title of the Article / Chapter the Portion Is From**	Ultra-small and highly crystallized ZnFe2O4 nanoparticles within double graphene networks for super-long life lithium-ion batteries
Editor of Portion(s)	Zhang, Longhai; Wei, Tong; Yue, Jingming; Sheng, Lizhi; Jiang, Zimu; Yang, Deren; Yuan, Libo; Fan, Zhuangjun	**Author of Portion(s)**	Zhang, Longhai; Wei, Tong; Yue, Jingming; Sheng, Lizhi; Jiang, Zimu; Yang, Deren; Yuan, Libo; Fan, Zhuangjun
Volume / Edition	5	**Issue, if Republishing an Article From a Serial**	22
Page or Page Range of Portion	11188-11196	**Publication Date of Portion**	2017-06-14

Marketplace Permissions General Terms and Conditions

The following terms and conditions ("General Terms"), together with any applicable Publisher Terms and Conditions, govern User's use of Works pursuant to the Licenses granted by Copyright Clearance Center, Inc. ("CCC") on behalf of the applicable Rightsholders of such Works through CCC's applicable Marketplace transactional licensing services (each, a "Service").

1) **Definitions.** For purposes of these General Terms, the following definitions apply:

"License" is the licensed use the User obtains via the Marketplace platform in a particular licensing transaction, as set forth in the Order Confirmation.

"Order Confirmation" is the confirmation CCC provides to the User at the conclusion of each Marketplace transaction. "Order Confirmation Terms" are additional terms set forth on specific Order Confirmations not set forth in the General Terms that can include terms applicable to a particular CCC transactional licensing service and/or any Rightsholder-specific terms.

"Rightsholder(s)" are the holders of copyright rights in the Works for which a User obtains licenses via the Marketplace platform, which are displayed on specific Order Confirmations.

"Terms" means the terms and conditions set forth in these General Terms and any additional Order Confirmation Terms collectively.

"User" or "you" is the person or entity making the use granted under the relevant License. Where the person accepting the Terms on behalf of a User is a freelancer or other third party who the User authorized to accept the General Terms on the User's behalf, such person shall be deemed jointly a User for purposes of such Terms.

"Work(s)" are the copyright protected works described in relevant Order Confirmations.

2) **Description of Service.** CCC's Marketplace enables Users to obtain Licenses to use one or more Works in accordance with all relevant Terms. CCC grants Licenses as an agent on behalf of the copyright rightsholder identified in the relevant Order Confirmation.

3) **Applicability of Terms.** The Terms govern User's use of Works in connection with the relevant License. In the event of any conflict between General Terms and Order Confirmation Terms, the latter shall govern. User acknowledges that Rightsholders have complete discretion whether to grant any permission, and whether to place any limitations on any grant, and that CCC has no right to supersede or to modify any such discretionary act by a Rightsholder.

4) **Representations; Acceptance.** By using the Service, User represents and warrants that User has been duly authorized by the User to accept, and hereby does accept, all Terms.

5) **Scope of License; Limitations and Obligations.** All Works and all rights therein, including copyright rights, remain the sole and exclusive property of the Rightsholder. The License provides only those rights expressly set forth in the terms and conveys no other rights in any Works

6) **General Payment Terms.** User may pay at time of checkout by credit card or choose to be invoiced. If the User chooses to be invoiced, the User shall: (i) remit payments in the manner identified on specific invoices, (ii) unless otherwise specifically stated in an Order Confirmation or separate written agreement, Users shall remit payments upon receipt of the relevant invoice from CCC, either by delivery or notification of availability of the invoice via the Marketplace platform, and (iii) if the User does not pay the invoice within 30 days of receipt, the User may incur a service charge of 1.5% per month or the maximum rate allowed by applicable law, whichever is less. While User may exercise the rights in the License immediately upon receiving the Order Confirmation, the License is automatically revoked and is null and void, as if it had never been issued, if CCC does not receive complete payment on a timely basis.

7) **General Limits on Use.** Unless otherwise provided in the Order Confirmation, any grant of rights to User (i) involves only the rights set forth in the Terms and does not include subsequent or additional uses, (ii) is non-exclusive and non-transferable, and (iii) is subject to any and all limitations and restrictions (such as, but not limited to, limitations on duration of use or circulation) included in the Terms. Upon completion of the licensed use as set forth in the Order Confirmation, User shall either secure a new permission for further use of the Work(s) or immediately cease any new use of the Work(s) and shall render inaccessible (such as by deleting or by removing or severing links or other locators) any further copies of the Work. User may only make alterations to the Work if and as expressly set forth in the Order Confirmation. No Work may be used in any way that is unlawful, including without limitation if such use would violate applicable sanctions laws or regulations, would be defamatory, violate the rights of third parties (including such third parties' rights of copyright, privacy, publicity, or other tangible or intangible property), or is otherwise illegal, sexually explicit, or obscene. In addition, User may not conjoin a Work with any other material that may result in damage to the reputation of the Rightsholder. Any unlawful use will render any licenses hereunder null and void. User agrees to inform CCC if it becomes aware of any infringement of any rights in a Work and to cooperate with any reasonable request of CCC or the Rightsholder in connection therewith.

8) **Third Party Materials.** In the event that the material for which a License is sought includes third party materials (such as photographs, illustrations, graphs, inserts and similar materials) that are identified in such material as having been used by permission (or a similar indicator), User is responsible for identifying, and seeking separate licenses (under this Service, if available, or otherwise) for any of such third party materials; without a separate license, User may not use such third party materials via the License.

9) **Copyright Notice.** Use of proper copyright notice for a Work is required as a condition of any License granted under the Service. Unless otherwise provided in the Order Confirmation, a proper copyright notice will read substantially as follows: "Used with permission of [Rightsholder's name], from [Work's title, author, volume, edition number and year of copyright]; permission conveyed through Copyright Clearance Center, Inc." Such notice must be provided in a reasonably legible font size and must be placed either on a cover page or in another location that any person, upon gaining access to the material which is the subject of a permission, shall see, or in the case of republication Licenses, immediately adjacent to the Work as used (for example, as part of a by-line or footnote) or in the place where substantially all other credits or notices for the new work containing the republished Work are located. Failure to include the required notice results in loss to the Rightsholder and CCC, and the User shall be liable to pay liquidated damages for each such failure equal to twice the use fee specified in the Order Confirmation, in addition to the use fee itself and any other fees and charges specified.

10) **Indemnity.** User hereby indemnifies and agrees to defend the Rightsholder and CCC, and their respective employees and directors, against all claims, liability, damages, costs, and expenses, including legal fees and expenses, arising out of any use of a Work beyond the scope of the rights granted herein and in the Order Confirmation, or any use of a Work which has been altered in any unauthorized way by User, including claims of defamation or infringement of rights of copyright, publicity, privacy, or other tangible or intangible property.

11) **Limitation of Liability.** UNDER NO CIRCUMSTANCES WILL CCC OR THE RIGHTSHOLDER BE LIABLE FOR ANY DIRECT, INDIRECT, CONSEQUENTIAL, OR INCIDENTAL DAMAGES (INCLUDING WITHOUT LIMITATION DAMAGES FOR LOSS OF BUSINESS PROFITS OR INFORMATION, OR FOR BUSINESS INTERRUPTION) ARISING OUT OF THE USE OR INABILITY TO USE A WORK, EVEN IF ONE OR BOTH OF THEM HAS BEEN ADVISED OF THE POSSIBILITY OF SUCH DAMAGES. In any event, the total liability of the Rightsholder and CCC (including their respective employees and directors) shall not exceed the total amount actually paid by User for the relevant License. User assumes full liability for the actions and omissions of its principals, employees, agents, affiliates, successors, and assigns.

12) **Limited Warranties.** THE WORK(S) AND RIGHT(S) ARE PROVIDED "AS IS." CCC HAS THE RIGHT TO GRANT TO USER THE RIGHTS GRANTED IN THE ORDER CONFIRMATION DOCUMENT. CCC AND THE RIGHTSHOLDER DISCLAIM ALL OTHER WARRANTIES RELATING TO THE WORK(S) AND RIGHT(S), EITHER EXPRESS OR IMPLIED, INCLUDING WITHOUT LIMITATION IMPLIED WARRANTIES OF MERCHANTABILITY OR FITNESS FOR A PARTICULAR PURPOSE. ADDITIONAL RIGHTS MAY BE REQUIRED TO USE ILLUSTRATIONS, GRAPHS, PHOTOGRAPHS, ABSTRACTS, INSERTS, OR OTHER PORTIONS OF THE WORK

TH-3358_186122026

(AS OPPOSED TO THE ENTIRE WORK) IN A MANNER CONTEMPLATED BY USER; USER UNDERSTANDS AND AGREES THAT NEITHER CCC NOR THE RIGHTSHOLDER MAY HAVE SUCH ADDITIONAL RIGHTS TO GRANT.

13) **Effect of Breach.** Any failure by User to pay any amount when due, or any use by User of a Work beyond the scope of the License set forth in the Order Confirmation and/or the Terms, shall be a material breach of such License. Any breach not cured within 10 days of written notice thereof shall result in immediate termination of such License without further notice. Any unauthorized (but licensable) use of a Work that is terminated immediately upon notice thereof may be liquidated by payment of the Rightsholder's ordinary license price therefor; any unauthorized (and unlicensable) use that is not terminated immediately for any reason (including, for example, because materials containing the Work cannot reasonably be recalled) will be subject to all remedies available at law or in equity, but in no event to a payment of less than three times the Rightsholder's ordinary license price for the most closely analogous licensable use plus Rightsholder's and/or CCC's costs and expenses incurred in collecting such payment.

14) **Additional Terms for Specific Products and Services.** If a User is making one of the uses described in this Section 14, the additional terms and conditions apply:

a) ***Print Uses of Academic Course Content and Materials (photocopies for academic coursepacks or classroom handouts).*** For photocopies for academic coursepacks or classroom handouts the following additional terms apply:

i) The copies and anthologies created under this License may be made and assembled by faculty members individually or at their request by on-campus bookstores or copy centers, or by off-campus copy shops and other similar entities.

ii) No License granted shall in any way: (i) include any right by User to create a substantively non-identical copy of the Work or to edit or in any other way modify the Work (except by means of deleting material immediately preceding or following the entire portion of the Work copied) (ii) permit "publishing ventures" where any particular anthology would be systematically marketed at multiple institutions.

iii) Subject to any Publisher Terms (and notwithstanding any apparent contradiction in the Order Confirmation arising from data provided by User), any use authorized under the academic pay-per-use service is limited as follows:

A) any License granted shall apply to only one class (bearing a unique identifier as assigned by the institution, and thereby including all sections or other subparts of the class) at one institution;

B) use is limited to not more than 25% of the text of a book or of the items in a published collection of essays, poems or articles;

C) use is limited to no more than the greater of (a) 25% of the text of an issue of a journal or other periodical or (b) two articles from such an issue;

D) no User may sell or distribute any particular anthology, whether photocopied or electronic, at more than one institution of learning;

E) in the case of a photocopy permission, no materials may be entered into electronic memory by User except in order to produce an identical copy of a Work before or during the academic term (or analogous period) as to which any particular permission is granted. In the event that User shall choose to retain materials that are the subject of a photocopy permission in electronic memory for purposes of producing identical copies more than one day after such retention (but still within the scope of any permission granted), User must notify CCC of such fact in the applicable permission request and such retention shall constitute one copy actually sold for purposes of calculating permission fees due; and

F) any permission granted shall expire at the end of the class. No permission granted shall in any way include any right by User to create a substantively non-identical copy of the Work or to edit or in any other way modify the Work (except by means of deleting material immediately preceding or following the entire portion of the Work copied).

iv) Books and Records; Right to Audit. As to each permission granted under the academic pay-per-use Service, User shall maintain for at least four full calendar years books and records sufficient for CCC to determine the numbers of copies made by User under such permission. CCC and any representatives it may designate shall have the right to audit such books and records at any time during User's ordinary business hours, upon two days' prior notice. If any such audit shall determine that User shall have underpaid for, or underreported, any photocopies sold or by three percent (3%) or more, then User shall bear all the costs of any such audit; otherwise, CCC shall bear the costs of any such audit. Any amount determined by such audit to have been underpaid by User shall immediately be paid to CCC by User, together with interest thereon at the rate of 10% per annum from the date such amount was originally due. The provisions of this paragraph shall survive the termination of this License for any reason.

TH-3358_186122026

b) ***Digital Pay-Per-Uses of Academic Course Content and Materials (e-coursepacks, electronic reserves, learning management systems, academic institution intranets).*** For uses in e-coursepacks, posts in electronic reserves, posts in learning management systems, or posts on academic institution intranets, the following additional terms apply:

i) The pay-per-uses subject to this Section 14(b) include:

A) **Posting e-reserves, course management systems, e-coursepacks for text-based content,** which grants authorizations to import requested material in electronic format, and allows electronic access to this material to members of a designated college or university class, under the direction of an instructor designated by the college or university, accessible only under appropriate electronic controls (e.g., password);

B) **Posting e-reserves, course management systems, e-coursepacks for material consisting of photographs or other still images not embedded in text,** which grants not only the authorizations described in Section 14(b)(i)(A) above, but also the following authorization: to include the requested material in course materials for use consistent with Section 14(b)(i)(A) above, including any necessary resizing, reformatting or modification of the resolution of such requested material (provided that such modification does not alter the underlying editorial content or meaning of the requested material, and provided that the resulting modified content is used solely within the scope of, and in a manner consistent with, the particular authorization described in the Order Confirmation and the Terms), but not including any other form of manipulation, alteration or editing of the requested material;

C) **Posting e-reserves, course management systems, e-coursepacks or other academic distribution for audiovisual content,** which grants not only the authorizations described in Section 14(b)(i)(A) above, but also the following authorizations: (i) to include the requested material in course materials for use consistent with Section 14(b)(i)(A) above; (ii) to display and perform the requested material to such members of such class in the physical classroom or remotely by means of streaming media or other video formats; and (iii) to "clip" or reformat the requested material for purposes of time or content management or ease of delivery, provided that such "clipping" or reformatting does not alter the underlying editorial content or meaning of the requested material and that the resulting material is used solely within the scope of, and in a manner consistent with, the particular authorization described in the Order Confirmation and the Terms. Unless expressly set forth in the relevant Order Conformation, the License does not authorize any other form of manipulation, alteration or editing of the requested material.

ii) Unless expressly set forth in the relevant Order Confirmation, no License granted shall in any way: (i) include any right by User to create a substantively non-identical copy of the Work or to edit or in any other way modify the Work (except by means of deleting material immediately preceding or following the entire portion of the Work copied or, in the case of Works subject to Sections 14(b)(1)(B) or (C) above, as described in such Sections) (ii) permit "publishing ventures" where any particular course materials would be systematically marketed at multiple institutions.

iii) Subject to any further limitations determined in the Rightsholder Terms (and notwithstanding any apparent contradiction in the Order Confirmation arising from data provided by User), any use authorized under the electronic course content pay-per-use service is limited as follows:

A) any License granted shall apply to only one class (bearing a unique identifier as assigned by the institution, and thereby including all sections or other subparts of the class) at one institution;

B) use is limited to not more than 25% of the text of a book or of the items in a published collection of essays, poems or articles;

C) use is limited to not more than the greater of (a) 25% of the text of an issue of a journal or other periodical or (b) two articles from such an issue;

D) no User may sell or distribute any particular materials, whether photocopied or electronic, at more than one institution of learning;

E) electronic access to material which is the subject of an electronic-use permission must be limited by means of electronic password, student identification or other control permitting access solely to students and instructors in the class;

F) User must ensure (through use of an electronic cover page or other appropriate means) that any person, upon gaining electronic access to the material, which is the subject of a permission, shall see:

- a proper copyright notice, identifying the Rightsholder in whose name CCC has granted permission,
- a statement to the effect that such copy was made pursuant to permission,

TH-3358_186122026

- a statement identifying the class to which the material applies and notifying the reader that the material has been made available electronically solely for use in the class, and

- a statement to the effect that the material may not be further distributed to any person outside the class, whether by copying or by transmission and whether electronically or in paper form, and User must also ensure that such cover page or other means will print out in the event that the person accessing the material chooses to print out the material or any part thereof.

G) any permission granted shall expire at the end of the class and, absent some other form of authorization, User is thereupon required to delete the applicable material from any electronic storage or to block electronic access to the applicable material.

iv) Uses of separate portions of a Work, even if they are to be included in the same course material or the same university or college class, require separate permissions under the electronic course content pay-per-use Service. Unless otherwise provided in the Order Confirmation, any grant of rights to User is limited to use completed no later than the end of the academic term (or analogous period) as to which any particular permission is granted.

v) Books and Records; Right to Audit. As to each permission granted under the electronic course content Service, User shall maintain for at least four full calendar years books and records sufficient for CCC to determine the numbers of copies made by User under such permission. CCC and any representatives it may designate shall have the right to audit such books and records at any time during User's ordinary business hours, upon two days' prior notice. If any such audit shall determine that User shall have underpaid for, or underreported, any electronic copies used by three percent (3%) or more, then User shall bear all the costs of any such audit; otherwise, CCC shall bear the costs of any such audit. Any amount determined by such audit to have been underpaid by User shall immediately be paid to CCC by User, together with interest thereon at the rate of 10% per annum from the date such amount was originally due. The provisions of this paragraph shall survive the termination of this license for any reason.

c) ***Pay-Per-Use Permissions for Certain Reproductions (Academic photocopies for library reserves and interlibrary loan reporting) (Non-academic internal/external business uses and commercial document delivery).*** The License expressly excludes the uses listed in Section (c)(i)-(v) below (which must be subject to separate license from the applicable Rightsholder) for: academic photocopies for library reserves and interlibrary loan reporting; and non-academic internal/external business uses and commercial document delivery.

i) electronic storage of any reproduction (whether in plain-text, PDF, or any other format) other than on a transitory basis;

ii) the input of Works or reproductions thereof into any computerized database;

iii) reproduction of an entire Work (cover-to-cover copying) except where the Work is a single article;

iv) reproduction for resale to anyone other than a specific customer of User;

v) republication in any different form. Please obtain authorizations for these uses through other CCC services or directly from the rightsholder.

Any license granted is further limited as set forth in any restrictions included in the Order Confirmation and/or in these Terms.

d) ***Electronic Reproductions in Online Environments (Non-Academic-email, intranet, internet and extranet).*** For "electronic reproductions", which generally includes e-mail use (including instant messaging or other electronic transmission to a defined group of recipients) or posting on an intranet, extranet or Intranet site (including any display or performance incidental thereto), the following additional terms apply:

i) Unless otherwise set forth in the Order Confirmation, the License is limited to use completed within 30 days for any use on the Internet, 60 days for any use on an intranet or extranet and one year for any other use, all as measured from the "republication date" as identified in the Order Confirmation, if any, and otherwise from the date of the Order Confirmation.

ii) User may not make or permit any alterations to the Work, unless expressly set forth in the Order Confirmation (after request by User and approval by Rightsholder); provided, however, that a Work consisting of photographs or other still images not embedded in text may, if necessary, be resized, reformatted or have its resolution modified without additional express permission, and a Work consisting of audiovisual content may, if necessary, be "clipped" or reformatted for purposes of time or content management or ease of delivery (provided that any such resizing, reformatting, resolution modification or "clipping" does not alter the underlying editorial content or meaning of the Work used, and that the resulting material is used solely within the scope of, and in a manner consistent with, the particular License described in the Order Confirmation and the Terms.

TH-3358_186122026

15) **Miscellaneous.**

a) User acknowledges that CCC may, from time to time, make changes or additions to the Service or to the Terms, and that Rightsholder may make changes or additions to the Rightsholder Terms. Such updated Terms will replace the prior terms and conditions in the order workflow and shall be effective as to any subsequent Licenses but shall not apply to Licenses already granted and paid for under a prior set of terms.

b) Use of User-related information collected through the Service is governed by CCC's privacy policy, available online at www.copyright.com/about/privacy-policy/.

c) The License is personal to User. Therefore, User may not assign or transfer to any other person (whether a natural person or an organization of any kind) the License or any rights granted thereunder; provided, however, that, where applicable, User may assign such License in its entirety on written notice to CCC in the event of a transfer of all or substantially all of User's rights in any new material which includes the Work(s) licensed under this Service.

d) No amendment or waiver of any Terms is binding unless set forth in writing and signed by the appropriate parties, including, where applicable, the Rightsholder. The Rightsholder and CCC hereby object to any terms contained in any writing prepared by or on behalf of the User or its principals, employees, agents or affiliates and purporting to govern or otherwise relate to the License described in the Order Confirmation, which terms are in any way inconsistent with any Terms set forth in the Order Confirmation, and/or in CCC's standard operating procedures, whether such writing is prepared prior to, simultaneously with or subsequent to the Order Confirmation, and whether such writing appears on a copy of the Order Confirmation or in a separate instrument.

e) The License described in the Order Confirmation shall be governed by and construed under the law of the State of New York, USA, without regard to the principles thereof of conflicts of law. Any case, controversy, suit, action, or proceeding arising out of, in connection with, or related to such License shall be brought, at CCC's sole discretion, in any federal or state court located in the County of New York, State of New York, USA, or in any federal or state court whose geographical jurisdiction covers the location of the Rightsholder set forth in the Order Confirmation. The parties expressly submit to the personal jurisdiction and venue of each such federal or state court.

Last updated October 2022

RightsLink

Iron-Cluster-Directed Synthesis of 2D/2D Fe–N–C/MXene Superlattice-like Heterostructure with Enhanced Oxygen Reduction Electrocatalysis

Author: Lili Jiang, Jingjing Duan, Junwu Zhu, et al
Publication: ACS Nano
Publisher: American Chemical Society
Date: Feb 1, 2020

PERMISSION/LICENSE IS GRANTED FOR YOUR ORDER AT NO CHARGE

This type of permission/license, instead of the standard Terms and Conditions, is sent to you because no fee is being charged for your order. Please note the following:

- Permission is granted for your request in both print and electronic formats, and translations.
- If figures and/or tables were requested, they may be adapted or used in part.
- Please print this page for your records and send a copy of it to your publisher/graduate school.
- Appropriate credit for the requested material should be given as follows: "Reprinted (adapted) with permission from {COMPLETE REFERENCE CITATION}. Copyright {YEAR} American Chemical Society." Insert appropriate information in place of the capitalized words.
- One-time permission is granted only for the use specified in your RightsLink request. No additional uses are granted (such as derivative works or other editions). For any uses, please submit a new request.

If credit is given to another source for the material you requested from RightsLink, permission must be obtained from that source.

BACK CLOSE WINDOW

Polycationic Polymer-Regulated Assembling of 2D MOF Nanosheets for High-Performance Nanofiltration

Author: Huixiang Ang, Liang Hong
Publication: Applied Materials
Publisher: American Chemical Society
Date: Aug 1, 2017

PERMISSION/LICENSE IS GRANTED FOR YOUR ORDER AT NO CHARGE

This type of permission/license, instead of the standard Terms and Conditions, is sent to you because no fee is being charged for your order. Please note the following:

- Permission is granted for your request in both print and electronic formats, and translations.
- If figures and/or tables were requested, they may be adapted or used in part.
- Please print this page for your records and send a copy of it to your publisher/graduate school.
- Appropriate credit for the requested material should be given as follows: "Reprinted (adapted) with permission from {COMPLETE REFERENCE CITATION}. Copyright {YEAR} American Chemical Society." Insert appropriate information in place of the capitalized words.
- One-time permission is granted only for the use specified in your RightsLink request. No additional uses are granted (such as derivative works or other editions). For any uses, please submit a new request.

If credit is given to another source for the material you requested from RightsLink, permission must be obtained from that source.

BACK CLOSE WINDOW

RightsLink

PD

Tuning Carrier Confinement in the MoS2/WS2 Lateral Heterostructure

Author: Jun Kang, Hasan Sahin, François M. Peeters
Publication: The Journal of Physical Chemistry C
Publisher: American Chemical Society
Date: Apr 1, 2015

PERMISSION/LICENSE IS GRANTED FOR YOUR ORDER AT NO CHARGE

This type of permission/license, instead of the standard Terms and Conditions, is sent to you because no fee is being charged for your order. Please note the following:

- Permission is granted for your request in both print and electronic formats, and translations.
- If figures and/or tables were requested, they may be adapted or used in part.
- Please print this page for your records and send a copy of it to your publisher/graduate school.
- Appropriate credit for the requested material should be given as follows: "Reprinted (adapted) with permission from {COMPLETE REFERENCE CITATION}. Copyright {YEAR} American Chemical Society." Insert appropriate information in place of the capitalized words.
- One-time permission is granted only for the use specified in your RightsLink request. No additional uses are granted (such as derivative works or other editions). For any uses, please submit a new request.

If credit is given to another source for the material you requested from RightsLink, permission must be obtained from that source.

BACK CLOSE WINDOW

RightsLink

Controlled Self-Assembly of Gold Nanotetrahedra into Quasicrystals and Complex Periodic Supracrystals

Author: Yi Wang, Jun Chen, Ruipeng Li, et al
Publication: Journal of the American Chemical Society
Publisher: American Chemical Society
Date: Aug 1, 2023

PERMISSION/LICENSE IS GRANTED FOR YOUR ORDER AT NO CHARGE

This type of permission/license, instead of the standard Terms and Conditions, is sent to you because no fee is being charged for your order. Please note the following:

- Permission is granted for your request in both print and electronic formats, and translations.
- If figures and/or tables were requested, they may be adapted or used in part.
- Please print this page for your records and send a copy of it to your publisher/graduate school.
- Appropriate credit for the requested material should be given as follows: "Reprinted (adapted) with permission from {COMPLETE REFERENCE CITATION}. Copyright {YEAR} American Chemical Society." Insert appropriate information in place of the capitalized words.
- One-time permission is granted only for the use specified in your RightsLink request. No additional uses are granted (such as derivative works or other editions). For any uses, please submit a new request.

If credit is given to another source for the material you requested from RightsLink, permission must be obtained from that source.

BACK CLOSE WINDOW

RightsLink

PD

Interlayer Decoupling in 30° Twisted Bilayer Graphene Quasicrystal

Author: Bing Deng, Binbin Wang, Ning Li, et al
Publication: ACS Nano
Publisher: American Chemical Society
Date: Feb 1, 2020

PERMISSION/LICENSE IS GRANTED FOR YOUR ORDER AT NO CHARGE

This type of permission/license, instead of the standard Terms and Conditions, is sent to you because no fee is being charged for your order. Please note the following:

- Permission is granted for your request in both print and electronic formats, and translations.
- If figures and/or tables were requested, they may be adapted or used in part.
- Please print this page for your records and send a copy of it to your publisher/graduate school.
- Appropriate credit for the requested material should be given as follows: "Reprinted (adapted) with permission from {COMPLETE REFERENCE CITATION}. Copyright {YEAR} American Chemical Society." Insert appropriate information in place of the capitalized words.
- One-time permission is granted only for the use specified in your RightsLink request. No additional uses are granted (such as derivative works or other editions). For any uses, please submit a new request.

If credit is given to another source for the material you requested from RightsLink, permission must be obtained from that source.

BACK CLOSE WINDOW

RightsLink

Delayed Dual Emission of Two-Dimensional Copper Nanocluster Assembly

Author: Priya Das, Arun Chattopadhyay
Publication: The Journal of Physical Chemistry C
Publisher: American Chemical Society
Date: Jan 1, 2022

PERMISSION/LICENSE IS GRANTED FOR YOUR ORDER AT NO CHARGE

This type of permission/license, instead of the standard Terms and Conditions, is sent to you because no fee is being charged for your order. Please note the following:

- Permission is granted for your request in both print and electronic formats, and translations.
- If figures and/or tables were requested, they may be adapted or used in part.
- Please print this page for your records and send a copy of it to your publisher/graduate school.
- Appropriate credit for the requested material should be given as follows: "Reprinted (adapted) with permission from {COMPLETE REFERENCE CITATION}. Copyright {YEAR} American Chemical Society." Insert appropriate information in place of the capitalized words.
- One-time permission is granted only for the use specified in your RightsLink request. No additional uses are granted (such as derivative works or other editions). For any uses, please submit a new request.

If credit is given to another source for the material you requested from RightsLink, permission must be obtained from that source.

BACK CLOSE WINDOW

Enhanced Chemical Stability in the Twisted Dodecagonal Stacking of Two-Dimensional Copper Nanocluster Assemblies

Author: Priya Das, Arun Chattopadhyay
Publication: Journal of Physical Chemistry Letters
Publisher: American Chemical Society
Date: Sep 1, 2022

PERMISSION/LICENSE IS GRANTED FOR YOUR ORDER AT NO CHARGE

This type of permission/license, instead of the standard Terms and Conditions, is sent to you because no fee is being charged for your order. Please note the following:

- Permission is granted for your request in both print and electronic formats, and translations.
- If figures and/or tables were requested, they may be adapted or used in part.
- Please print this page for your records and send a copy of it to your publisher/graduate school.
- Appropriate credit for the requested material should be given as follows: "Reprinted (adapted) with permission from {COMPLETE REFERENCE CITATION}. Copyright {YEAR} American Chemical Society." Insert appropriate information in place of the capitalized words.
- One-time permission is granted only for the use specified in your RightsLink request. No additional uses are granted (such as derivative works or other editions). For any uses, please submit a new request.

If credit is given to another source for the material you requested from RightsLink, permission must be obtained from that source.

BACK CLOSE WINDOW